İSTANBUL TECHNICAL UNIVERSITY ★ INSTITUTE OF SCIENCE AND TECHNOLOGY

REMOTE SENSING AND REGIONAL CLIMATE MODELING OF IMPACTS OF LAND COVER CHANGES ON THE CLIMATE OF THE MARMARA REGION OF TURKEY

Ph.D. Thesis by
Elif SERTEL, M.Sc.

Department : **Geodesy and Photogrammetry Engineering**
Programme: **Geomatic Engineering**

JANUARY 2008

İSTANBUL TECHNICAL UNIVERSITY ★ INSTITUTE OF SCIENCE AND TECHNOLOGY

REMOTE SENSING AND REGIONAL CLIMATE MODELING OF IMPACTS OF LAND COVER CHANGES ON THE CLIMATE OF THE MARMARA REGION OF TURKEY

Ph.D. Thesis by
Elif SERTEL, M.Sc.
(501032608)

Date of submission : 15 November 2007
Date of defence examination: 10 January 2008

Supervisor (Chairman): Prof. Dr. Cankut ÖRMECİ (İTÜ)
Members of the Examining Committee: Prof.Dr. Alan ROBOCK (Rutgers U.)
Prof.Dr. Mehmet KARACA (İTÜ)
Assoc. Prof. Dr. Cem GAZİOĞLU (İÜ)
Assist. Prof. Şinasi KAYA (İTÜ)

JANUARY 2008

ACKNOWLEDGEMENTS

I am grateful to Prof. Cankut Örmeci, my advisor, for all his continuous guidance and support during my academic research. He taught me great remote sensing classes where I decided to be an academician and reinforce and solidify my intense interest in scientific research. I would like to thank him and Prof. Muhammed Şahin for encouraging me to apply for the Fulbright Scholarship program, which then became an excellent opportunity for me to complete my research at Rutgers University, USA.

I wish to express deep gratitude to Prof. Alan Robock for the support, guidance, inspiration and encouragement he provided. I would like to thank him for giving me the opportunity to follow his courses and work for his project, where I gained great knowledge and experience about climate modeling. His suggestions did not only improve my research but also my personal life. I would like to also thank him for our regular weekly meetings, which improved my dissertation greatly.

I would like to thank Dr. Şinasi Kaya, Dr. Hande Demirel, Dr. Tayfun Kındap and Prof. Mehmet Karaca for their support during my research. I thank to Prof. Georgiy Stenchikov for his suggestions about climate modeling experiments. I thank my brother, Mustafa Kenan Saroğlu, for his effort to reprint my dissertation.

My deepest gratitude goes to my husband Tolga, who gave me constant support, patience and encouragement.

I would like to thank TUBITAK BIDEB for supporting me as a national Ph.D Scholar and Turkish Fulbright Commission for supporting me as a Ph.D. Scholar in U.S.

November, 2007 Elif SERTEL

TABLE OF CONTENTS **Page No**

ABBREVIATIONS

ARW : Advanced-Research Weather Research and Forecasting
AVHRR : Advanced Very High Resolution Radiometer
CFCs : Chlorofluorocarbons
DBMS : Database management system
DN : Digital number
ENSO : El Niño/Southern Oscillation
GCP : Ground Control Point
GIS : Geographic Information System
LAI : Leaf Area Index
Landsat ETM: Landsat Enhanced Thematic Mapper
Landsat MSS: Landsat Multispectral Scanner
Landsat TM : Landsat Thematic Mapper
LCC : Land cover change
LSM : Land surface model
MERIS : Medium Resolution Imaging Spectrometer
MM5 : Fifth-Generation NCAR/Penn State Mesoscale Model
MODIS : Moderate Resolution Imaging Spectroradiometer
NAO : North Atlantic Oscillation
NAOI : North Atlantic Oscillation index
NDVI : Normalized Difference Vegetation Index
NMM : Nonhydrostatic Mesoscale Model
RAMS : Regional Atmospheric Modeling System
RFM : Rational function model
SPOT : Satellite pour l'Observation de la Terre
SST : Sea surface temperature
UHI : Urban Heat Island
VOC : Volatile organic compounds
WPS : Weather Research and Forecasting Preprocessing System
WRF : Weather Research and Forecasting

TABLE LIST **Page No**

FIGURE LIST **Page No**

SYMBOL LIST

$\mathbf{R_n}$	**:** Net radiation
L↓	**:** Received infrared radiation
L↑	**:** Emitted infrared radiation
α	**:** Albedo
S↓	**:** Amount of energy reaches the Earth's surface
H	**:** Sensible heat flux
λE	**:** Latent heat flux
G	**:** Soil heat flux
F	**:** Chemical energy
P	**:** Available water
E	**:** Evaporation
R	**:** Runoff
ΔS	**:** Change in soil moisture storage
S	**:** Amount of solar radiation instantaneously incident at the planet
$\mathbf{T_e}$	**:** Effective blackbody radiating temperature of the Earth
$\mathbf{T_s}$	**:** Global mean surface temperature
$\mathbf{C_0}$, $\mathbf{C_1}$	**:** Offset and bias, respectively
DN	**:** Digital number
L	**:** Radiance
Lλ□	**:** Spectral radiance measured for the specific waveband
θ	**:** Solar zenith angle
ESUN	**:** Mean solar exoatmospheric irradiance
d	**:** Earth-sun distance in astronomical units
$\mathbf{a_{ik}}$, $\mathbf{b_{ik}}$	**:** Regression coefficients
$\mathbf{L_j}$	**:** Radiance of reference imagery J.
$\mathbf{L_i}$	**:** Radiance of any other images.
$\mathbf{a_0}$,$\mathbf{b_0}$	**:** Translations
$\mathbf{\omega_x}$, $\mathbf{\omega_y}$	**:** Rotations
$\mathbf{k_x}$, $\mathbf{k_y}$	**:** Scale factors
$\mathbf{Y_i^1}$, $\mathbf{X_i^1}$	**:** Coordinates of the point i in the image coordinate system
$\mathbf{Y_i^2}$, $\mathbf{X_i^2}$	**:** Coordinates of the point i in the reference coordinate system
v	**:** Residual vector
A	**:** Design matrix
l	**:** Vector of constant terms
$\mathbf{K_{xx}}$	**:** Transformation parameters
$\mathbf{Q_{xx}}$	**:** Variance-covariance matrix
$\mathbf{m_0}$	**:** Root mean squared error
q	**:** Number of classes error matrix
n	**:** Total number of observations in error matrix
$\mathbf{n_{ii}}$	**:** Major diagonal element for class i
$\mathbf{n_{i+}}$	**:** Total number of observations in row for class i (right margin)
$\mathbf{n_{+i}}$	**:** Total number of observations in column for class i (bottom margin)
γ(h)	**:** Semivariance

h	**:** Separation distance
s	**:** Sill
$\mathbf{A_0}$	**:** Range
$\mathbf{x_i}$	: Spatial location of observation i
$\mathbf{Z(x_i)}$	**:** Value of i at location x_i
$\boldsymbol{\lambda_i}$	: Weight value for $z(x_i)$ datum

TÜRKİYE'NİN MARMARA BÖLGESİNDEKİ ARAZİ ÖRTÜSÜ DEĞİŞİMLERİNİN İKLİM ÜZERİNDEKİ ETKİSİNİN UZAKTAN ALGILANMASI VE BÖLGESEL İKLİM MODELLENMESİ

ÖZET

Bu çalışmada arazi örtüsünde meydana gelen değişimleri belirlemek için kullanılabilecek uzaktan algılama yöntemleri, arazi örtüsünde meydana gelen değişimlerin Marmara Bölgesi yaz iklimi üzerindeki etkisi, Landsat görüntülerinin iklim modelleme için kullanılabilirliği ve iklim modellemede kullanılan arazi örtüsü verilerinin doğruluğu araştırılmıştır.

Bu amaçla endüstrileşme ve nüfus artışı sonucunda özellikle 1980 li yıllardan sonra arazi örtüsü değişimini meydana geldiği Marmara Bölgesi çalışma alanı olarak seçilmiştir. Marmara Bölgesine ait arazi kullanımı haritaları Landsat görüntüleri kullanılarak oluşturulmuştur. Çalışmanın ilk aşamasında, 1972-1975 tarihleri arasında elde edilen Landsat MSS ve 2001-2005 tarihleri arasında elde edilen Landsat ETM görüntüleri radyometrik ve atmosferik olarak düzeltilerek atmosferik parçacıklardan kaynaklanan bozulma etkileri ve sistematik hatalar elemine edilmiştir. Geometrik distorsiyonları elemine etmek, piksel bağıl konum hatalarını düzeltmek ve görüntüleri ortak bir koordinat sisteminde tanımlayabilmek amacıyla her bir görüntü geometrik olarak düzeltilmiştir. Bu çalışmada, yeni bir yaklaşım olarak semivariyogramların farkli arazi örtüsü tiplerini ayırt etmede kullanılması gereken bant kombinasyonlarını belirleme de kullanılabileceği, değişimin çok olduğu alanların değişen semivariyogram parametreleri ile yakalanabileceği ortaya konulmuştur. Ayrıca, mekansal profiller kullanılarak kıyı bölgelerde meydana gelen değişimlerin yönü ve büyüklüğü belirlenmiştir. Dijital görüntü işlemenin son aşamasında Landsat MSS ve Landsat ETM görüntüleri sınıflandırılarak, Marmara Bölgesi için 1975 ve 2005 tarihli arazi örtüsü haritaları türetilmiştir. Semivariyogram ve mekansal profillerle belirlenen değişimin çok olduğu pilot bölgeler ve spektral karışımın gözlendiği bölgeler ayrıca sınıflandırılmış ve sınıflandırmanın doğruluğu

arttırılmıştır. Sınıflandırma sonuçları 1 km mekansal çözünürlüğe örneklenip, karşılaştırma bu veriler üzerinden yapılmıştır. Yapılan değişim analizleri sonucunda, şehirleşme ile birlikte İstanbul, Bursa ve Adapazarı' nda tarım alanlarının yerleşim alanlarına dönüştürüldüğü, İstanbul Avrupa yakasının kıyı bölgelerinde yapılan açık maden çalışmaları sonucunda kıyının doldurularak kıyı şeridinin değiştirildiği ve bazı ormanlık alanlara açık alan ve seyrek bitkilik alanlara dönüştürüldüğü, Izmit gibi bazı bölgelerde ise açık alanların yerleşim alanlarına dönüştürüldüğü saptanmıştır.

Çalışmanın ikinci aşamasında, 2005 yılı arazi örtüsü haritası, iklim modellerinde kullanılan global arazi örtüsü verileri ile kıyaslanarak, bu verilerin Marmara Bölgesi için doğruluğu incelenmiştir. Yapılan karşılaştırmalar sonucunda, global arazi örtüsü verilerinin Marmara Bölgesinin bazı kısımlarını doğru ifade etmediği, özellikle yerleşim alanlarında problem olduğu, bazı veri setlerinin kıyı deniz sınırlarını doğru ifade edemediği tespit edilmiştir. Çalışmada kullanılan WRF modelleme sisteminin kullandığı arazi örtüsü verisi ile yapılan daha detaylı karşılaştırma sonucunda, bu verinin güncel olmadığı, yerleşim bölgelerini eksik ifade ettiği, kıyılarda meydana gelen değişimleri göstermediği ve İstanbul' ın kıyı bölgesindeki bazı ormanlık alanları tarla olarak gösterdiği bulunmuştur.

Çalışmanın üçüncü aşamasında, WRF modelleme sistemi ile farklı parametre alternatifleri kullanılarak çok sayıda deney yapılmış ve Marmara Bölgesi için en uygun model konfigürasyonu seçilmiştir. 27 km, 9 km ve 3 km yatay çözünürlükte bir ana ve iki iç çalışma alanı oluşturulmuştur. Belirlenen en uygun konfigürasyon, modeldeki arazi örtüsü ve NCEP/DOE Reanalysis II verisi başlangıç ve sınır şartı olarak kullanılıp Haziran-Ağustos 2004 dönemi için model çalıştırılarak kontrol simülasyonu elde edilmiştir. Sonraki adımda, 2005 yılı için üretilen arazi örtüsü verisi kullanılarak aynı periyot için ikinci bir simülasyon yapılmıştır. Kontrol simülasyonu ile yeni arazi modeli kullanılarak yapılan simülasyondan elde edilen sonuçlar, meteorolojik istasyonlardan elde edilen sonuçlarla kıyaslanmış ve minimum, maksimum ve ortalama sıcaklık değerlerinin yeni arazi örtüsü ile yapılan simülasyonlarda daha iyi sonuçlar verdiği bulunmuştur. Yağış için her iki simülasyonda benzer sonuçlar vermiş, yağışın genel yapısı bulunmasına karşın, miktarı ölçüm verilerinden daha düşük çıkmıştır.

Çalışmanın son aşamasında, 1975 yılı arazi örtüsü verisi ile simülasyon yapılıp, 2005 ile 1975 arazi örtüsü simülasyon sonuçları kıyaslanmış ve arazi örtüsü değişiminin Marmara Bölgesindeki yaz iklimine etkileri araştırılmıştır. Tarla ve boş alanların yerleşim alanlarına dönüştürülmesi ısınmaya, orman alanların boş ve seyrek bitkili alanlara dönüştürlümesi ısınmaya, tarlaların baraj çalışmalarıyla su alanlarına dönüştürülmesi soğumaya neden olmuştur. Isınma özellikle şehirleşmenin arttığı, İstanbul, Bursa ve Adapazarı illerinde gözlenmiştir. Öte yandan, İstanbul kıyı bölgelerindeki açık maden aktivitelerinin neden olduğu arazi kullanımı değişimi de ısınmaya neden olmuştur.

Bu çalışmanın sonucunda, arazi örtüzü verisinin iklim modelleme için önemli olduğu ve modeller içindeki verilerin bazı bölgelerde yanlış olduğu ve güncel olmadığı tespit edilmiştir. İklim modelleme için daha doğru arazi örtüsü verileri üretmek için Landsat görüntülerinin kullanılabileceği ve bu görüntülere uygulanması gereken dijital görüntü işleme prosedürleri gösterilmiştir. Ayrıca Marmara Bölgesinde meydana gelen arazi kullanımı değişimlerinin lokal iklimi etkilediği gösterilmiş ve sıcaklıkların lokal değişimlerden daha fazla etkilendiği ortaya konmuştur. Coğrafi Bilgi Sistemlerinin kullanılmasıyla tüm veriler ortak bir çatı altında toplanmış, tampon bölge analizleri yapılarak iklim üzerinde etkiye neden olan arazi kullanımı değişimleri ayrıntılı olarak incelenebilmiştir.

REMOTE SENSING AND REGIONAL CLIMATE MODELING OF IMPACTS OF LAND COVER CHANGES ON THE CLIMATE OF THE MARMARA REGION OF TURKEY

SUMMARY

This research investigated the usage of different remote sensing techniques to determine land cover change, impacts of land cover change on summer climate of the Marmara Region, the utilization of Landsat images in regional climate modeling and the accuracy of global land cover data sets used in climate modeling.

The Marmara Region, which experienced significant land cover changes as a result of rapid industrialization and population increase especially after 1980s, was selected as my study area. At the first stage of the research, Landsat MSS images obtained between 1972 and 1975 and Landsat ETM images obtained between 2001 and 2005 were used to derive multi-temporal land cover data of the Marmara Region. First, all images were atmospherically and radiometrically corrected to minimize contamination effects of atmospheric particles (scattering and absorption effects due to the atmosphere) and systematic errors. Then, geometric correction was performed for each image to eliminate geometric distortions, correct errors in the relative positions of pixels, and define images in a common coordinate system. A new approach, semivariograms, was introduced to select appropriate band combinations for studying different land cover classes and determine the regions having significant land cover changes. It was found that semivariograms can be used to determine spatial variations and significantly changed areas can be identified using the changes in semivariogram parameters. Spatial profiles were created and examined to find out significant land cover changes in pilot regions and to determine the location and the size of land cover changes occurred in coastal zones. Based on the information obtained from semivariograms and spatial profiles, several pilot areas were created and classification employed separately for each area to minimize the spectral mixing of various classes such as barren, crop and urban and increase the classification accuracy. The classification results were aggregated to 1 km and change detection

analysis, land cover data comparison and climate modeling were performed using this data set. Change detection analysis illustrated that, as a result of urbanization, crop areas were transformed into urban and built up areas in İstanbul, Bursa and Adapazarı. The coastal region of European side of İstanbul changed because of open mining activities and the coastline changed in this region. The Black Sea was filled with open mining residue and some forest areas were transformed into barren and sparsely vegetated areas in this region. In some parts of the Marmara Region like İzmit, barren and sparsely vegetated areas were transformed into urban and built up areas.

At the second stage of the research, 2005 land cover data obtained from Landsat images were compared with the global land cover data sets used in climate modeling to analyze the accuracy of these data sets for the Marmara Region. Comparisons showed that global land cover data sets, namely Global Land Cover Characterization, Global Land Cover 2000 and University of Maryland Land Cover, are not accurate for some parts of the Marmara Region, especially for the urban areas. One of the data sets also has problems to represent land and sea boundaries. Detailed analyses were conducted to determine the accuracy of land cover data used in the Weather Research and Forecasting (WRF) modeling system. These data are not up-to-date and do not represent urban areas accurately in İstanbul, Adapazarı, Bursa and İzmit. These data also had problems in the coastal part of the European side of İstanbul and showed some forest areas as crop areas. Therefore, it was important to derive more accurate land cover data of the study region, which was done with Landsat images in this research.

At the third stage of the research, several experiments with different parameter alternatives were tested in the WRF modeling system to find out the best model configuration for the Marmara Region. The experiments were conducted for the summer (June-July-August) season. One main and two nested domains were formed with 27 km, 9 km and 3 km horizontal resolution, respectively. The control run was employed with the best model configuration, model land cover data and initial and boundary conditions obtained from the National Centers for Environmental Prediction/Department of Energy Atmospheric Model Intercomparison Project-II Reanalysis. Another run was conducted similar to the control run but with new 2005 land cover data. The results of this new experiment were compared with those from

the control run for some meteorological stations and it is found out that minimum, maximum and average temperature values gave better results with new land cover data, especially for the changed region. Both runs gave similar results for precipitation. Although the general pattern of the precipitation can be captured, the precipitation amounts with model simulations were comparatively lower than the observations.

At the last stage of the research, 1975 land cover data were implemented in the WRF modeling system, simulation results obtained from 1975 and 2005 land cover data were compared, and the land cover change impact on summer climate of the Marmara Region was examined. Conversion of crop and barren and sparsely vegetated areas into urban areas caused warming, conversion of forest areas into barren and sparsely vegetated areas caused warming and conversion of sparsely vegetated to woodland around Bursa region caused cooling. Urban heat islands over İstanbul, Bursa and Adapazarı can be identified with the comparison of average temperatures obtained from 1975 and 2005 land cover data simulations. Also the results showed that warming occurred along the coastline regions of İstanbul as a result of open mining activities.

Overall results of this research suggest that land cover is an important determinant for regional climate modeling studies and global land cover data sets for the Marmara Region are not up-to-date and have some deficiencies. Landsat images can be used to derive more accurate land cover data for regional climate modeling and required digital image processing techniques that should be applied to these images were presented. Also, land cover change in the Marmara Region impacted the local climate and temperatures were more sensitive to local land cover changes than precipitation. Data from several sources were collected in a common frame with Geographic Information Systems and buffer zone analysis within the system showed detailed land cover change impacts on climate.

1. INTRODUCTION

Integrated usage of remote sensing and space technologies have been utilized for multidisciplinary applications by several scientists. Satellite sensor images provide rapid, economic, update information of earth surface characteristics, and can be used for various researches. Remote sensing accommodates accurate and reliable information to many researchers with high spatial, spectral and temporal resolution, synoptic view and very short data collection time. Land cover which is a fundamental variable impacting and linking many parts of the human and physical environments can be derived using remotely sensed data. Several different applications such as management of environmental and natural resources, sea and coastline studies, land use/cover changes in global and regional scales, weather forecasting and climate modeling can be conducted using the remote sensing technology **(Schweiger et al., 2005; Brivio et al., 2002; Ostir et al., 2002; Saroğlu, 2005; Ormeci and Ekercin, 2007).**

Global warming is one of the most important environmental problems that the world faces. Recent studies show that global average land-surface air temperature has been increasing and many natural systems are being affected because of the temperature increases. Changes in snow, ice and frozen ground cause enlargement and increase in numbers of glacial lakes and increase ground instability in permafrost regions, and rock avalanches in mountain regions. Global warming has effects on hydrological systems such as increased run-off and earlier spring peak discharge in many glacier- and snow-fed rivers and warming of lakes and rivers in many regions, with effects on thermal structure and water quality **(IPCC, 2007).**

Human beings, like other living organisms, have always influenced their environment. The impact of human activities has begun to extend to a much larger scale, continental or even global since the beginning of the Industrial Revolution, mid-18th century. As a result of human activities, in particular that involving the combustion of fossil fuels for industrial or domestic usage, and biomass burning, produce greenhouse gases and aerosols, the composition of the atmosphere has been

affected. The emission of chlorofluorocarbons (CFCs) and other chlorine and bromine compounds has impact on both the radiative forcing and depletion of the stratospheric ozone layer. Physical and biological properties of the Earth's surface have been affected as a result of land-use change, due to urbanization and human forestry and agricultural practices. Such effects change the radiative forcing and have a potential impact on regional and global climate **(IPCC, 2001)**.

Human activities such as urbanization, intensive agriculture, deforestation and forest management have considerably altered Earth's surface, especially during the last several hundred years **(Vitousek et al., 1997; Ramankutty and Foley, 1999)**. Local, regional, and global climate can be affected by such disturbance of because of the change of the energy balance on the Earth's surface and the chemical composition of the atmosphere **(Chase et al., 1999; Houghton et al., 1999; Pielke, 2001)**.

Land cover products used in most climate models were initially compiled from maps and ground surveys till the global scale land cover products generated from remote sensing images became avaible. These remotely sensed derived global land cover products like Global Land Cover Characteristics (GLCC), University of Maryland alnd cover classification (UMD) and Global Land Cover 2000 (GLC 2000) have been implemented into various land surface schemes and climate models. However, no land cover data set is 100% accurate, even if developed from the most advanced satellite images **(Mathews, 1983; Sellers et al., 1996a, 1996b; Walko et al., Friedl et al, 2002; Ge et al., 2007)**. **Ge et al. (2007)** investigated how the classification accuracy of a land cover data set employed in a land surface scheme affects simulated cumulative precipitation in a regional climate model .

Current land cover data available within the regional climate models such as Regional Atmospheric Modeling System (RAMS), the Fifth-Generation NCAR/Penn State Mesoscale Model (MM5) and Weather Research and Forecasting (WRF) was obtained from 1-km Advanced Very High Resolution Radiometer satellite images spanning April 1992 through March 1993 with an unsupervised classification technique. These data are not up-to-date and are not accurate for all regions and some land cover types such as urban areas. In this research, improved land cover data derived from Landsat images were implemented in a regional climate model. Using the improved land cover data produced for current and past conditions, land cover

change was determined and the impact of this land cover change on the local climate of study region was examined.

The objectives of the research are to investigate:

- land cover changes that occurred in the Marmara Region between 1975 and 2005 using Landsat images,
- utilization of digital image processing and geostatistical methods to determine land cover changes in the study area,
- the accuracy of global land cover databases used in climate modeling for the Marmara Region by comparing them to land cover data produced from Landsat images,
- contribution and utility of Landsat images to regional climate modeling,
- the performance of WRF on the Marmara Region
- the impacts of human induced land cover change on the regional summer climate of the research area,
- improvements that can be made in climate modeling using remote sensing and GIS.

Investigation of land cover change impact on climate requires accurate land cover data representing present, past and future. Much research has been conducted using the available land cover data within the model as current land cover and reconstructed past land cover from the topographic maps, vegetation databases or ecosystem models. Land cover data must be prepared based on a known classification scheme such as Biosphere Atmosphere Transfer Scheme (BATS), Simple Biosphere Model (SBM), United Stated Geological Survey (USGS) Land Use and Land Cover Classification Legend depending on the land surface or climate model that will be used in the research. There are some problems about past and current land cover data used in regional climate modeling. It is generally hard and not precise to reconstruct past land cover data from topographic maps and vegetation database since these data might not include the same classes with the classification scheme. On the other hand, current data in the regional climate models which are generally used to represent present land cover are not up to date and are not accurate for some classes. Since these data were derived from AVHRR vegetation indices,

they are not good at representing urban and built up areas. Accuracy of present land cover is not only important for determining land cover change but also important for simulating current climate precisely. Also, future projections of land cover are created based on past and present land cover, some scenarios and transformation models and accuracy of present and past land cover data would directly affect the accuracy of future projections. Therefore accurate representation of land cover is a key determinant for climate studies and being handled in this study.

In this research, remote sensing technology and Landsat satellite images were used to derive past and present land cover data of the Marmara Region and then introduced to WRF modeling system to analyze the impact of land cover change on local climate of the region. Current and past land cover data were created based on USGS scheme used in WRF modeling system. Several image processing techniques were conducted to remove atmospheric, radiometric and geometric distortions available in the images. Classification was supported with semivariograms and spatial profiles to derive the accurate land cover of the study region. Although classified images were resampled to 1 km same as AVHRR, classified images were including more details because of the higher spectral and spatial resolution of original data. Details of conducted image processing techniques are presented in following chapters.

Improved land cover data derived from satellite images were compared with global data sets used in regional climate models. Results illustrated that global data sets have deficiencies and inaccuries in some parts of the Marmara Region. Since global dataset used in WRF modeling system is not up-to-date, it is not convenient to use these data to simulate current climate especially for the regions faced with significant land cover changes. Besides, these data cannot represent urban classes correctly and in some parts of the Marmara there were spectral mixing problems between crops and forest types which lead misrepresentation of these classes. Comparison between the simulations conducted with improved land cover and model land cover illustrated that, current climate especially minimum, maximum and average temperatures can be more accurately simulated with new land cover. Comparison between current and past land cover simulations showed that there was a significant warming in the Marmara Region especially over the urban areas of İstanbul, Bursa and Adapazarı.

Overall results illustrated that Landsat images can be successfully used to derive past and present land cover of concerned regions. Implementing Landsat derived current

land cover to WRF modeling system improved the simulation of current climate. Implementing past land cover to modeling and comparing the results of current and past simulations pointed out the local climatic changes. Evaluating land cover data sets in GIS and employing buffer zone analysis emphasized the land cover change impact on local climate depending on the percentage of change land cover. These present and past land cover data will be an accurate source to project future land cover based on some scenarios and transformation models in future studies.

1.1 Warm season impacts of land cover change

Land surface characteristics have been changing as a result of human activities such as deforestation, urbanization, agricultural activities and modification of natural vegetation patterns. The way heat, moisture, momentum, dust, and pollutants move upward from the surface into the atmosphere have been effected the interaction between land surface and the overlying atmosphere **(Weaver and Avissar, 2001).**

The fundamental driving forces of atmospheric motions in the planetary boundary layer (PBL) are the fluxes of heat and moisture from the surface into the adjacent atmosphere **(Stull, 1988).** The response of the atmosphere to this forcing depends strongly on the scale of the land surface heterogeneity that determines the distribution of heat and moisture fluxes **(Weaver and Avissar, 2001).**

The impacts of land cover change on warm season climate over different spatial and temporal scales have been studied by **Dalu and Pielke (1993), Pielke et al. (1999), Pielke (2001), Weaver and Avissar, (2001) Wichansky et al. (2007), Baidya et al. (2003)**.

Pielke et al. (1999) investigated the possible impacts of 20th century land cover change on the Florida peninsula's summer time near-surface temperature and convective rainfall for the July-August period. Land cover data generated for 1900, 1973 and 1993 were implemented to the simulations. Replacement of 1900 land cover data with 1973 or 1993 dataset caused an increase in the average July-August near surface temperature. The simulations conducted with 1973 and 1993 land cover yielded a decrease in two-month total rainfall.

Pitman et al. (2003) used three high-resolution mesoscale model configurations forced at the boundaries to simulate July climates for each of natural and current land

cover. They obtained vegetation data from the Atlas of Australian Resources on Vegetation by the Australian Surveying and Land Information Group. They found that land cover change explained up to 50% of the observed warming in Western Australia. Simulated impacts of land cover change were caused by modification to the vegetation characteristics. Converting from trees to grass affected the partitioning of available water between runoff and evaporation, thereby affecting soil moisture and possibly rainfall. They also illustrated that land cover changes affected the partitioning of available energy between sensible and latent heat, affecting local air temperature and boundary layer structure.

Wang et al (2003) addressed the impact of observed land cover change on the June meteorology of China. They employed a historical land-cover data set, compiled with a time resolution of 50 years, from 1700 to 1990. Their results indicated warming of air temperature and ground temperature, and decrease of the specific humidity and the latent heat flux as a result of change from forest to short grass or crops. The changes in the model simulation when the land cover was altered from short grass to crops were quite different. The air and ground temperatures became cooler, latent heat increased and the atmosphere became moister. In both experiments, the changes in the latent heat flux were associated with the changes in surface parameters that land surface models are known to be sensitive to **(Pitman, 2003).**

Baidya Roy et al. (2003) used the Regional Atmospheric Modeling System (RAMS) model to investigate the possible impact of land cover change on the July climate of the coterminous United States. They estimated vegetation data using the Ecosystem Demography model. They found observed change in land cover leaded to a weak warming along the Atlantic coast and a strong cooling of more than 1 K over the Midwest and the Great Plains region but the precipitation signal was weaker.

Ezber et al. (2007) used statistical and numerical modeling tools to investigate the climatic effects of urbanization in İstanbul. Their statistical analysis showed that the largest impact of urbanization on the local climate is in the summer. Both statistical and modeling analyses indicated significant warming in the atmosphere over the urbanized areas of İstanbul. They also found out that the model uses a very old land cover/vegetation map that does not reflect the current urban boundaries in İstanbul. They made manual changes based on topographic maps to fix the land cover data.

Karaca et al. (1995a,b) studied the urban heat island (UHI) in İstanbul using long term temperature data (up to the year 1992) from stations within and around the city. They found out warming trends in the urban temperatures of southern İstanbul, which was the most densely populated part of the city.

Most of the studies conducted by other scientists have used land cover data available in the model or land cover data derived from topographic maps. In this research, I propose the usage of Landsat images as an alternative and reliable source to derive more accurate and up-to-date land cover data for climate modeling. Also, it is possible to derive past land cover data using achieve images. Several different digital image processing techniques, geostatistical methods and usage of spatial profiles were also proposed to derive accurate land cover map of the study area. Comparisons between global land cover data sets and Landsat derived data were made to analyze the accuracy of global data sets for the Marmara Region, which was not performed by any researcher previously.

As a result of rapid population increase and industrialization, human induced land cover changes occurred within the region like conversion of urban and barren areas into urban areas, conversion of forest areas into barren areas, conversion of sparsely vegetated areas into crop areas. Human induced land cover change due to population increase especially for the cities is a problem that developing countries faced with. Therefore, obtaining results for Marmara Region does not only provide information for Turkey but also for many counties since they have the similar problem. An important issue about the Marmara Region is its climate because it displays a transition between two different types of climate, namely Black Sea and Mediterranean. The results of study gave information about the land cover change impacts on two different climate regimes.

Simulations of the research were employed with WRF, which is a new and state-of-the-art modeling system, whereas most of the studies in literature were conducted with RAMS or MM5.

GIS was used to evaluate the relationships among climate model results, land cover data and other ancillary data in an integrated framework, where different source of data can be analyzed simultaneously and the results of analyses can support the decision-making mechanisms.

This research addressed the following scientific questions:

- Are global land cover data sets used in regional climate models representing the land surface accurately?
- Can Landsat satellite images be used to improve land surface data sets for regional climate models? Do these new land cover data produce improved climate simulations?
- How did land cover change in Marmara Region between 1975 and 2005 and how does these changes affect the local climate of the region? Are these local climate changes statistically significant or not?

2. CLIMATE, CLIMATE SYSTEM AND CLIMATE MODELING

2.1 Climate and Climate System

"The climate system is a complex, interactive system consisting of the atmosphere, land surface, snow and ice, oceans and other bodies of water, and living things" **(IPCC, 2007)**. Climate is most obviously characterized by the atmospheric component of the climate system. The mean and variability of temperature, precipitation and wind over a period of time, ranging from months to millions of years (the classical period is 30 years) are used to described climate which is often defined as "average weather". The climate system evolves in time under the influence of its own internal dynamics and due to changes in external forcing such as volcanic eruptions, solar variations and human-induced changes in atmospheric composition **(IPCC, 2007)**.

Temperature, precipitation, wind speed and direction, cloud type and amount, sunshine duration, atmospheric humidity, air pressure and visibility are physical elements make up the climate. Other elements may be equally, or more, important in particular situations. For example, radiant energy fluxes are important to understand atmospheric processes, pollutant concentration and the acidity of precipitation are of concern for human health while soil moisture, soil temperatures and evaporation are vital in agriculture **(Robinson and Henderson-Sellers, 1999)**.

There are many feedback mechanisms in the climate system that can either amplify ('positive feedback') or diminish ('negative feedback') the effects of a change in climate forcing **(IPCC, 2007)**. A feedback mechanism is an interaction in which an initially imposed change in a variable causes some other variable to change that then acts to modify the original change. An example for positive feedback is ice-albedo feedback. More snow is produced as a result of lower temperatures, which would increase the albedo of the system. The higher albedo causes less solar radiation to be absorbed by the system and causes cooling, producing even more snow **(Robock, 1985)**. Temperature-radiation feedback is an example for negative feedback.

Detecting, understanding and accurately quantifying climate feedbacks are important issues to clarify the relationships between climate components, external forcings, heat fluxes, and temperature **(Robock, 1985; IPCC, 2007)**.

Figure 2.1 shows the components of the climate system, their processes and interactions.

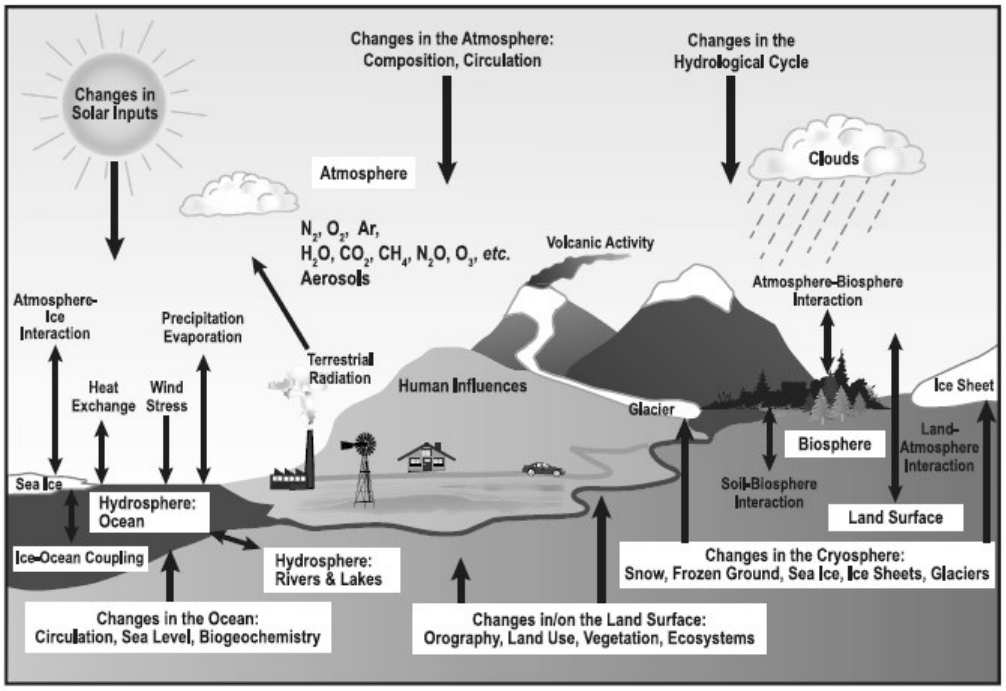

Figure 2.1: Components of the Climate System, Their Processes and Interactions **(IPCC, 2001)**

The energy exchanges provide the starting point and general framework for the climatology and any consideration of energy exchanges must incorporate surface effects. The vast majority of the solar radiation is absorbed at the surface forming the fundamental energy source for all atmospheric motions. Spatial variations in surface heating lead to large scale horizontal temperature gradients and local convective instability (Figure 2.2). Any air mass, heated from below (input), tends to rise, thus increase the available potential energy (uplift). Either this potential energy is released in convective activity or, through horizontal energy gradients, in large scale horizontal motions and synoptic-scale weather patterns. Shear instabilities and other boundary effects are rise by the small-scale irregularities on the surface as the resulting winds pass over the Earth's surface. All energy types are dissipated into

random molecular motions (output) at the final phase **(Robinson and Henderson-Sellers, 1999)**.

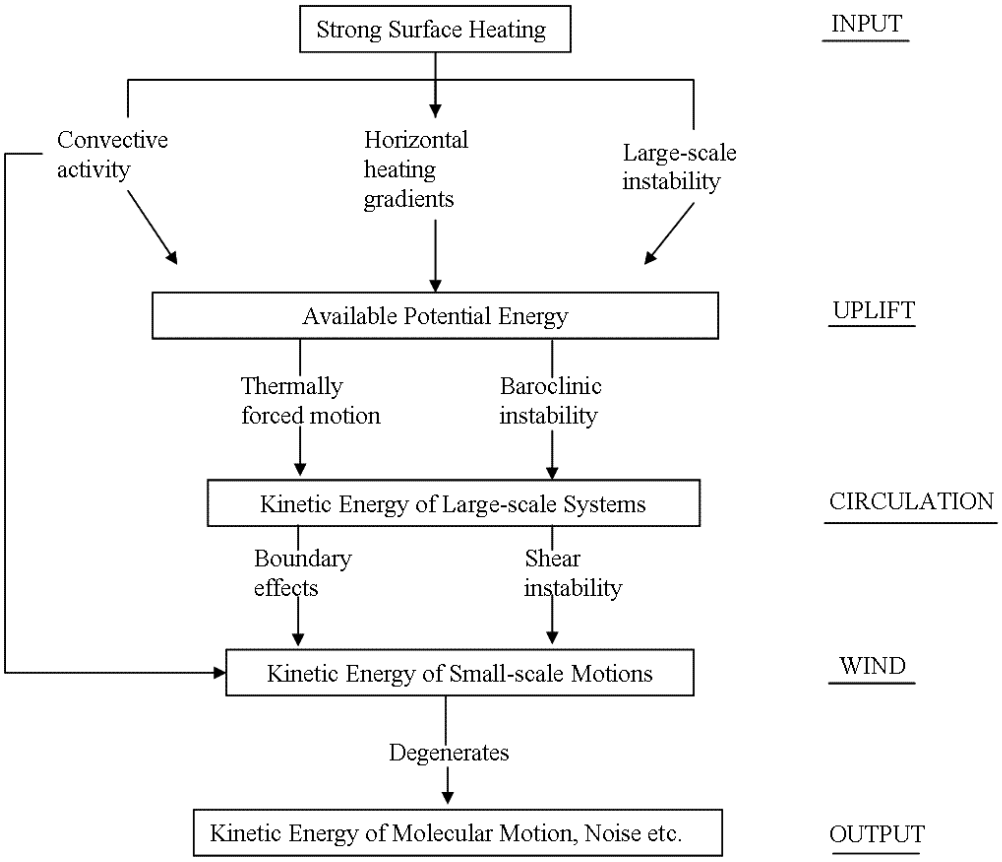

Figure 2.2: Atmospheric Transformation of Energy **(source: Robinson and Henderson-Sellers, 1999).**

2.1.1 Atmosphere

The Earth's atmosphere is composed of a mixture of dry air (several gases containing 78.08% nitrogen, 20.95% oxygen, 0.93% argon, 0.038% carbon dioxide, trace amounts of other gases), a variable amount (average around 1%) of water vapor, and aerosols. The interaction of atmospheric gases with radiant energy modulates the flow of energy through the climate system; therefore composition of the atmosphere is a key determinant of Earth's climate **(Hartmann, 1994).** The atmosphere exerts a pressure due to the effects of gravity since it is composed of material particles. Since the atmosphere is gaseous, the pressure decreases with height, so that the gas is most dense near the ground, with a sea level pressure of approximately 1013 mb, and the top of its density approaches to zero **(Washington and Parkinson, 2005)**.

The Temperature Structure of the Atmosphere

Vertical profile: The air temperature decreases with height in the lower part of the atmosphere, to a height of about 17 km at the equator and 6-9 km at the poles. This lower region termed as troposphere and it is the portion of the atmosphere in direct contact with the Earth's surface and is where most atmospheric processes take place. Above the troposphere, the temperature generally stays constant or increases with the height in the atmospheric region called the stratosphere. The division between troposphere and stratosphere, where the temperature often is near its minimum for the given vertical air column is the tropopause **(Washington and Parkinson, 2005)**.

In the tropics, atmospheric temperature profile is similar throughout the year, with a temperature near the ground of 27°C, decreasing to about -83°C at a height of about 17 km, and then increasing with height in the stratosphere. The polar regions experience the largest summer/winter tropospheric temperature contrast. In summer, polar temperatures are about 7°C near the ground and decrease to about -43°C at a height of 9 km, above which there is a general warming with height in the lower stratosphere. In winter, temperatures are about -38°C at the ground and increase rather than decrease with height for the first 1.5-2 km, above which the more tropospheric decrease with height occurs up to the tropopause at about 9 km **(Washington and Parkinson, 2005)**.

Radiation Budget of the Earth

Energy transfers and transformations within the climate system cause the winds, rain, clouds, humidity and temperature. The whole process starts with the arrival of energy from the Sun to the top of the atmosphere in the form of radiant energy. The Sun radiates energy approximately as a blackbody with a temperature of 6000 K; its radiation spectrum extends from the ultraviolet to the infrared, with a maximum in the visible range. The radiation striking the Earth's surface is depleted in portions of the spectrum because of the absorption of energy at specific wavelengths by gases in the Earth's atmosphere. In particular, oxygen and ozone in the lower stratosphere shield terrestrial biodata from much of the energy in the ultraviolet range, which is damaging to most forms of life. In the near infrared range, some of the sun's energy is absorbed by water vapor. Thus virtually all the Sun's energy arriving at the surface is at wavelengths smaller than 4 μm and this energy is referred as solar radiation or shortwave radiation **(Dingman, 2002)**.

The vertical flux of energy in the atmosphere is one of the most important climate processes. The radiative and nonradiative fluxes between the surface, the atmosphere, and space are key determinants of climate. The strength of greenhouse effect is determined by the solar radiation penetrating the atmosphere and terrestrial radiation transmitting through the atmosphere.

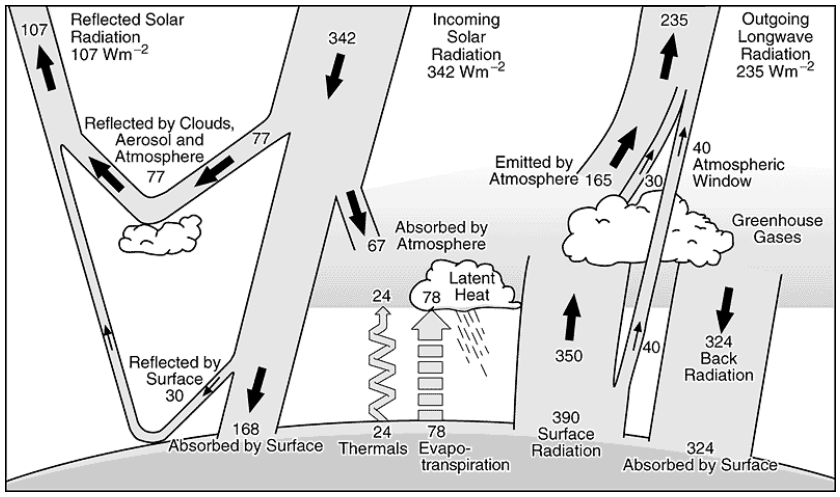

Figure 2.3: The Earth's Annual and Global Mean Energy Balance **(source: IPCC, 2001).**

The globally averaged available solar radiation at the top of the atmosphere is 342 Wm^{-2}, 31% of which is immediately reflected back into space by clouds, by the atmosphere, and by the Earth's surface. The remaining 235 Wm^{-2} is partly absorbed by the atmosphere but most (168 Wm^{-2}) warms the Earth's surface: the land and the ocean. The Earth's surface returns that heat to the atmosphere, partly as infrared radiation, partly as sensible heat and as water vapor which releases its heat when it condenses higher up in the atmosphere. This exchange of energy between surface and atmosphere maintains under present conditions a global mean temperature near the surface of 14°C, decreasing rapidly with height and reaching a mean temperature of –58°C at the top of the troposphere **(IPCC, 2001)**.

For a stable climate, a balance is required between incoming solar radiation and the outgoing longwave radiation. Therefore the climate system itself must radiate on average 235 Wm^{-2} back into space. Figure 2.3 shows the details of this energy balance, what happens with the incoming solar radiation is shown on the left hand side and how the atmosphere emits the outgoing infrared radiation is shown on the right side. Any physical object radiates energy of an amount and at wavelengths

typical for the temperature of the object: more energy is radiated at higher temperatures than at shorter wavelengths. For the Earth to radiate 235 Wm^{-2}, it should radiate at an effective emission temperature of -19°C with typical wavelengths in theinfrared part of the spectrum. This is 33°C lower than the average temperature of 14°C at the Earth's surface **(IPCC, 2001)**.

Several trace gases which absorb and emit infrared radiation are available in the atmosphere. These so-called greenhouse gases absorb infrared radiation, emitted by the Earth's surface, the atmosphere and clouds, except in the atmospheric window. They emit in turn infrared radiation in all directions including downward to the Earth's surface. Thus heat is trapped by the greenhouse gases within the atmosphere. This mechanism is called the natural greenhouse effect **(IPCC, 2001)**.

General Circulation of the Atmosphere

The unequal latitudinal distribution of absorbed and emitted radiation and latitudinal variations in the components of the atmospheric water system indicate that horizontal motions are necessary to maintain the present climate. The relative heating and cooling of different areas of the Earth's surface in large part drives local winds and large-scale atmospheric circulation. Characterisation of the general circulation of the atmosphere can be done with a three-cell model **(Hartmann, 1994; Robinson and Henderson-Sellers, 1999).**

The model was developed from the observation that there were zonal belts of low pressure around the equator and, in more diffuse form, around 60° latitude, whereas high pressure dominated around 30° and at the poles. Low pressure is associated with convergence and ascending air, and high pressure with descant and surface divergence which create the three cells namely, Hadley, Ferrell and Polar cells. The tropical Hadley and polar cells were being driven by the effects of surface heating and called "thermally direct", while the mid-latitude Ferrel cell one was a response to them and called "thermally indirect". Descent gives dry, cloudless conditions, while ascent creates clouds and precipitation **(Robinson and Henderson-Sellers, 1999).**

The rotation of the Earth causes moving air to be deflected to the right in the Northern Hemisphere and to the left in the Southern Hemisphere. This Coriolis deflection is a primary reason why the poleward-flowing upper air in the tropics does not travel from equator to pole and create a single-cell circulation pattern. Coriolis

deflection is the reason of easterly trade winds in low latitudes and westerly winds in mid-latitudes **(Washington and Parkinson, 2005).**

The tropical Hadley cell is driven by solar heating, causing rising motion near the equator, then by the release of latent heat as the rising air leads to precipitation in the upward branch of the cell. Following the seasonal shifts in the maximum intensity of solar heating, this upward branch of the Hadley cell moves north and south of the equator with season (Figure 2.4). The strength of the Hadley circulation varies with longitude and depends on the surface type (land or ocean). After rising near the equator, the air in the Hadley cell moves poleward in the upper region of the troposphere and sinks near 30°N and 30°S, generating a high pressure belt near 30°N and 30°S **(Washington and Parkinson, 2005).**

2.1.2 Hydrosphere, Cryosphere and Biosphere

The hydrosphere is the component comprising all liquid surface and subterranean water, both fresh water, including rivers, lakes and aquifers, and saline water of the oceans and seas. Fresh water runoff from the land returning to the oceans in rivers influences the ocean's composition and circulation. **(IPCC, 2001).**

Approximately 71% of the Earth' s surface area is occupied by seas and oceans. The water of the oceans transfers heat, nutrients, salt and momentum from one location to another. They store and transport a large amount of energy and dissolve and store great quantities of carbon dioxide. The three major oceans are Pacific, Atlantic and Indian oceans, covering 46%, 23% and 20%, respectively. A vital characteristic of the ocean is the large heat storage capacity it represents. Similar to the situation in the atmosphere, the bulk of the external heating of the oceans is due to solar insolation region of the tropics. Ocean circulations, driven by the wind and by density contrasts caused by salinity and thermal gradients (thermohaline circulation). Ocean currents then redistribute part of this energy to higher latitudes, where large amounts of energy are released to the atmosphere as latent and sensible heat and longwave radiation **(Robinson and Henderson-Sellers, 1999).**

Blowing of winds over the oceans causes momentum transfer. The kinetic energy in the wind is effectively transformed into the kinetic energy associated with ocean currents, which produce waves on a small scale. On a larger scale, when strong winds blow, the drag in the ocean surface is sufficient to permit movement of the

warm surface waters, which are then replaced by upwelling colder water from greater depth **(Robinson and Henderson-Sellers, 1999).**

Ice over land and sea and snow on continents form the Earth's cryosphere. The cryosphere occurs at high latitudes and high altitudes since its existence and persistence depend upon subfreezing temperatures. The perennial cryosphere covers approximately 8 % of the Earth's surface.

The cryospheric interaction with the overlaying air is primarily through the stabilizing effect that the cold surface creates. The extent of the cryosphere has an important effect on planetary albedo and planetary temperatures through the ice-albedo feedback **(Robinson and Henderson-Sellers, 1999).**

The atmosphere' s composition is affected by the marine and terrestrial biospheres. The biota influences the uptake and release of greenhouse gases. Significant amounts of carbon from carbon dioxide are stored by both marine and terrestrial plants (especially forests) through the photosynthetic process. Thus, the biosphere plays a central role in the carbon cycle, as well as in the budgets of many other gases, such as methane and nitrous oxide. Formation of atmospheric chemistry and aerosol formation might be affected by other biospheric emissions (so-called volatile organic compounds (VOC)) and these formations might affect climate. Feedbacks between climate change and atmospheric concentrations of trace gases can occur because the storage of carbon and the exchange of trace gases are influenced by climate **(IPCC, 2001).**

2.1.3 Land Surface

The climate over the land surface is extremely important to us since humans are land-dwelling creatures. Over the land surface, natural vegetation and the agricultural potential of the given area are determined by temperature and soil moisture. Vegetation, snow cover, and soil conditions also affect the local and global climate. Since 70% of Earth's land area is in the Northern Hemisphere, there are significant differences in the climates of the Northern and Southern Hemispheres. Climate in land areas are determined by the topography of the land surface and arrangement and orientation of mountain ranges **(Hartmann, 1994).**

Land surface controls the partitioning of available energy at the surface between sensible and latent heat, and it controls partitioning of available water between

evaporation and runoff. Coupling between land surface and atmosphere plays an important role in convection and precipitation distribution (Robock et al**., 2003)**

Human have altered a significant fraction of the Earth's surface as a result of deforestation, urbanization, agricultural activities etc. and caused land cover change (LCC).

Land Surface Scheme in Climate Models

The element simulating the initial effect of LCC in a climate model is the land surface model (LSM). The way that the Earth's surface interacts with the atmosphere, and the ways that this interaction changes as a result of human activities and natural processes must be represented to project the future climates. Similarly, to simulate the impacts of deforestation, reforestation or agricultural intensification using a climate model, the LSM must be representing the impact of these changes on surface-atmosphere interactions (**Pitman, 2003**). LSM is a key component to understand the carbon cycle of the Earth and how CO_2 increases in the atmosphere **(Prentice et al, 2001).**

The fundamental equations representing the key role of the surface in climate are the surface energy balance and the surface water balance.

The surface energy balance

The shortwave radiation emitted by the Sun is reflected, absorbed or transmitted by the atmosphere. An amount of energy S↓ reaches the Earth's surface and some is reflected (depending on the albedo α). As explained in section 2.1.1.3, 49% of incoming solar radiation is absorbed by the Earth surface. Infrared radiation is also received (L↓) and emitted (L↑) by the Earth's surface depending on the temperature and emissivity of the land and atmosphere. R_n, net radiation, is the net balance of incoming and reflected shortwave radiation, and the incoming and emitted longwave radiation at the earth's surface. It can be written as in the following equation.

$$R_n = S\downarrow.(1-\alpha) + L\downarrow - L\uparrow \qquad \textbf{(2.1)}$$

31% of incoming solar energy is exchanged as sensible and latent heat fluxes, where land surface significantly influences the way that this energy partitioned between sensible H and latent heat λE fluxes. R_n must be balanced by H, λE, the soil heat flux G and the chemical energy F stored during photosynthesis and releases by respiration

(which is negligible for the climate models as it amounts less that of 1% of absorbed insolation) **(Pitman, 2003):**

$$R_n = H + \lambda E + G + F \quad \textbf{(2.2)}$$

Changes in surface albedo affect net radiation therefore *H* and *λE.* Albedo changes naturally with solar insolation angle, seasonally with vegetation changes and stochastically with rain and snowfall. It can also be changed as a result of land cover change. Decrease in *λE* contributes less water vapor to the atmosphere and decreases cloudiness and precipitation, whereas decrease in H cools the planetary boundary layer and reduce convection **(Pitman, 2003).**

Changes in the actual vegetation cover alter the surface area of vegetation in contact with the atmosphere and the balance between fluxes from the soil and vegetation. Changes in the leaf area index (LAI) can influence the exchange of both *H* and *λE.* The amount of soil moisture available to plants to transpire is influenced by the changes in the distribution of roots **(Pitman, 2003).**

The surface water balance

Precipitation falling to the Earth's surface either intercepted by vegetation or reaches the soil surface directly. Intercepted precipitation either evaporates or drips to the surface, and the drip, combined with the rainfall reaching the surface directly, either infiltrates or runs across the soil surface. Infiltrating water may evaporate from the soil surface, drain through the soil, or be taken up by roots and transpired **(Pitman, 2003).**

A basic role of the land surface is to partition available water *(P)* between evaporation *(E)* and runoff *(R).*

$$P = E + R + \Delta S \quad \textbf{(2.3)}$$

R includes fast and slow component, *ΔS* is the change in soil moisture storage.

Changes in the characteristics of the land surface affect the surface water balance. Interception and transpiration are affected with the change in the nature of vegetation. Runoff and soil moisture content are affected with the changes in evapotranspiration, soil evaporation, re-evaporation of intercepted water.

NOAH Land Surface Model

NOAH is an abbreviation of following terms:

N: **N**ational Centers for Environmental Prediction (NCEP)

O: **O**regon State University (Dept. of Atmospheric Sciences)

A: **A**ir Force (both AFWA and AFRL - formerly AFGL, PL)

H: **H**ydrologic Research Lab - NWS (now Office of Hydrologic Dev. -- OHD)

NOAH is a 4-layer soil temperature and moisture model with canopy moisture and snow cover prediction. It includes root zone, evapotranspiration, soil drainage, and runoff, taking into account vegetation categories, monthly vegetation fraction, and soil texture. The Noah LSM provides surface sensible and latent heat fluxes, and surface skin temperature as lower boundary conditions **(Chen and Dudhia, 2001; Ek et al., 2004)**. It has single vegetation canopy layer and the following prognostic variables: soil moisture and temperature in the soil layers, water stored on the canopy, and snow stored on the ground. The Noah LSM additionally predicts soil ice, and fractional snow cover effects, has an improved urban treatment, and considers surface emissivity properties **(Skamarock et al, 2005; Chen and Dudhia, 2001).** Figure 2.4 illustrates the schema of NOAH land surface model.

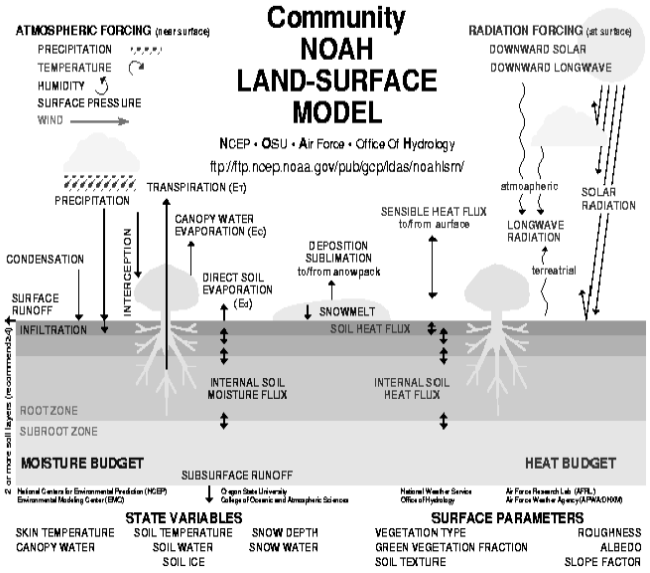

Figure 2.4: Schematic View NOAH Land Surface Model **(Source: Mitchell and Ek, 2006)**

2.2 Climate Models

A model is a simplified representation of reality yielding useful information about that reality. Principles of physics, chemistry, and biology are incorporated into a mathematical model of climate to better understand and predict climate and its variations. Climate models are tools employed to enhance understanding of the climate system and to aid prediction of future climates. L. F. Richardson was the first to publish the description of a method for constructing a weather forecast by means of numerical calculations **(Richardson, 1922)**. Climate models have been being used in several applications such as experiments of stratospheric processes, investigation of the deep ocean circulation and exploration of the impacts of human induced perturbations **(Hartmann, 1994; McGuffie and Henderson-Sellers, 2001).**

A climate model can range in complexity from the simple energy-balance models to very complex models. The equations of the simplest possible way of constructing a model of the Earth's climate by considering the radiative balance of the globe as a whole was given by **McGuffie and Henderson-Sellers (2001).** This is a zero dimensional model and the equations are as follow:

$$S.(1-\alpha)=\sigma.T_e^4 \qquad \textbf{(2.4)}$$

$$T_s = T_e + T_{greenhouse} \qquad \textbf{(2.5)}$$

where S is the amount of solar radiation instantaneously incident at the planet per unit area and has value of about Wm^{-2}. α is Earth's albedo and has a value of 0.3. T_e is the effective blackbody radiating temperature of the Earth and is found to be around 255 K. Whereas this value is lower than the current global mean surface temperature, T_s, of 288 K. The difference, about 33 K is the result of the greenhouse effect, $T_{greenhouse}$ **(McGuffie and Henderson-Sellers, 2001)**.

The component parts of a global climate model and development of climate models are shown in figure 2.5.

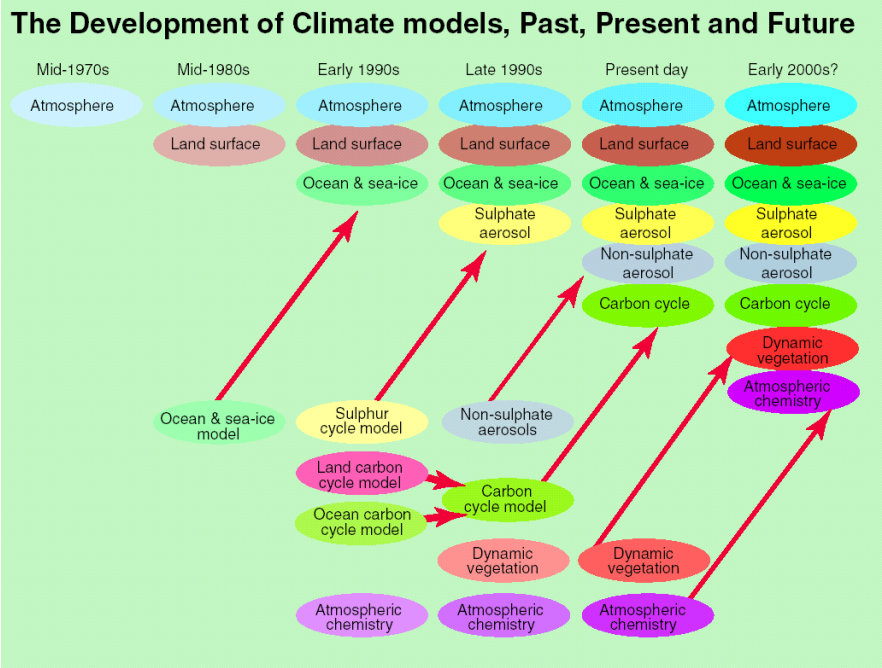

Figure 2.5: The Development of Climate Models, Past, Present and Future (IPCC, 2007)

General circulation models (GCMs) treat the full three-dimensional nature of the atmosphere and the full range of climatic elements and processes. This requires the solution of a series of equations that describe the movement of energy and momentum and the conservation of mass and water vapor as shown in Table 2.1 **(Robinson and Henderson-Sellers, 1999)**.

Table 2.1: Fundamental equations solved in GCMs (source: **Robinson and Henderson-Sellers, 1999**)

Equation name	Equation
Conservation of momentum	Force = mass x acceleration ($F=m.a$)
Conservation of mass	Sum of the gradient of (ρv) in three dimensional direction is zero.
Conservation of energy	Input energy = increase in internal energy + work done
Ideal gas law	(pressure x volume)/absolute temperature = gas constant ($P.V/T=R$)

The basic framework of a numerical model of the atmosphere or ocean is spatial grid work on which the equations of physics are presented. To efficiently solve the equations of motion, spectral methods are used wherein the field of velocity, temperature, and pressure are presented with continuous functions. Accurate

calculations of the derivatives needed for following the flow of heat and momentum are performed using these equations. The globe is always divided into geographic regions, whose sides often correspond to lines of latitude and longitude **(Hartmann, 1994).**

Vertical resolution is also important for the quality of an atmospheric simulation. Vertical resolution is identified by the number of vertical levels. The levels are not equally spaced in height or pressure, but tend to be most closely spaced near the lower boundary and tropopause **(Hartmann, 1994).**

The sources and sinks of momentum and heat are associated with phenomena occurring on much smaller scales than grid resolution. These are called sub-grid-scale phenomena, and their effect must be specified from knowledge of the state of the atmosphere at grid scale. To include all the processes in a climate model which are of a scale smaller than is resolved by the model, they must be parameterized. Key parameterizations in atmospheric models are radiation, convection and cloud and planetary boundary layer parameterization, also land surface parameterization is very important for the land component of the climate model **(Hartmann, 1994).** Brief descriptions of these parameterizations are presented in the following paragraphs.

Radiation Parameterization: The basic drive of the climate system is radiative heating from the sun and infrared cooling to space. Atmospheric heating due to radiative flux divergence and surface downward longwave and shortwave radiation for the ground heat budget are provided by the radiation schemes. Infrared or thermal radiation absorbed and emitted by gases and surface are longwave radiation. The surface emissivity that in turn depends upon land-use type, as well as the ground (skin) temperature determines the upward longwave radiative flux from the ground. Shortwave radiation includes visible and surrounding wavelengths that make up the solar spectrum. Hence, the only source is the Sun, but processes include absorption, reflection, and scattering in the atmosphere and at surfaces. The upward flux is the reflection due to surface albedo for shortwave radiation. The radiation responds to model-predicted cloud and water vapor distributions within the atmosphere **(Skamarock et al, 2005).**

Convection and Cloud Parameterization: Clouds affect radiative transfer, and convective motions associated with clouds produce important fluxes of mass, heat and moisture. The spatial scales at which cloud properties are determined are

generally much smaller than the grid size. Convection and cloud parameterization schemes are responsible for the sub-grid-scale effects of convective and/or shallow clouds. The schemes are intended to represent vertical fluxes due to unresolved updrafts and downdrafts and compensating motion outside the clouds **(Skamarock et al, 2005; Hartmann, 1994).**

Planetary Boundary Layer Parameterization:

In the atmospheric boundary layer, the fluxes of heat, momentum and moisture between the surface and the atmosphere is determined by the rapidly fluctuating phenomena with vertical and horizontal space scales much smaller than the grid spacing of climate models. These phenomena include turbulence, gravity waves, and rolls or other coherent structures that can not be resolved by climate models and must therefore parameterized **(Hartmann, 1994).**

Land Surface Parameterization: Detail information about LSM is given in section 2.1.5.1**.** Land component of a climate model must contain the surface heat balance equations and a surface moisture equation **(Hartmann, 1994).** Land surface fluxes provide a lower boundary condition for the vertical transport.

2.2.1 Weather Research and Forecasting (WRF) Modeling System

The WRF model is designed to be a flexible, state-of-the-art, portable code that is efficient in a massively parallel computing environment. It is suitable for use in a broad spectrum of applications across scales ranging from meters to thousands of kilometers. Such applications include research and operational numerical weather prediction (NWP), data assimilation and parameterized-physics research, downscaling climate simulations, driving air quality models, atmosphere-ocean coupling, and idealized simulations (e.g., boundary-layer eddies, convection, baroclinic waves) **(Skamarock et al, 2005).**

The WRF Advanced-Research WRF (ARW) core is based on an Eulerian solver for the fully compressible non-hydrostatic equations, cast in flux (conservative) form, using a mass (hydrostatic pressure) vertical coordinate. Prognostic variables for this solver are column mass of dry air (mu), velocities u, v and w (vertical velocity), potential temperature, and geopotential. Non-conserved variables (e.g., temperature, pressure, density) are diagnosed from the conserved prognostic variables. The solver uses a third-order Runge-Kutta time-integration scheme coupled with a split-explicit

2nd-order time integration scheme for the acoustic and gravity-wave modes. 5th-order upwind-biased advection operators are used in the fully conservative flux divergence integration; 2nd-6th order schemes are run-time selectable **(Skamarock et al, 2005).**

The model has terrain-following hydrostatic-pressure, with vertical grid stretching permitted. Top of the model is a constant pressure surface. It has Arakawa C-grid staggering horizontal grid. Initial conditions can be three dimensional for real-data, and one-, two- and three-dimensional using idealized data. Polar stereographic, Lambert-conformal, and Mercator projections are supported for real-data simulation. One-way, two-way, and moving nesting options are available within the model **(Skamarock et al, 2005).**

Radiation parameterization alternatives in WRF are as in the table 2.2:

Table 2.2: Radiation schemes

Scheme	Longwave/Shortwave	Spectral Bands	CO_2, O_3 ,clouds
RRTM	LW	16	CO_2, O_3 ,clouds
GFDL LW	LW	14	CO_2, O_3 ,clouds
GFDL SW	SW	12	CO_2, O_3 ,clouds
MM5 SW	SW	1	Clouds
Goddard	SW	11	CO_2, O_3 ,clouds

Kain-Fritsch, Betts-Miller-Janjic, Grell-Devenyi schemes can be used for Convection and Cloud Parameterization.

Medium Range Forecast Model (MRF), Yonsei University (YSU) and Mellor-Yamada-Janjic (MYJ) can be used to parameterize planetary boundary layer (PBL).

5-layer thermal diffusion, Noah LSM and Rapid Update Cycle (RUC) Model LSM can be employed for land surface parameterization.

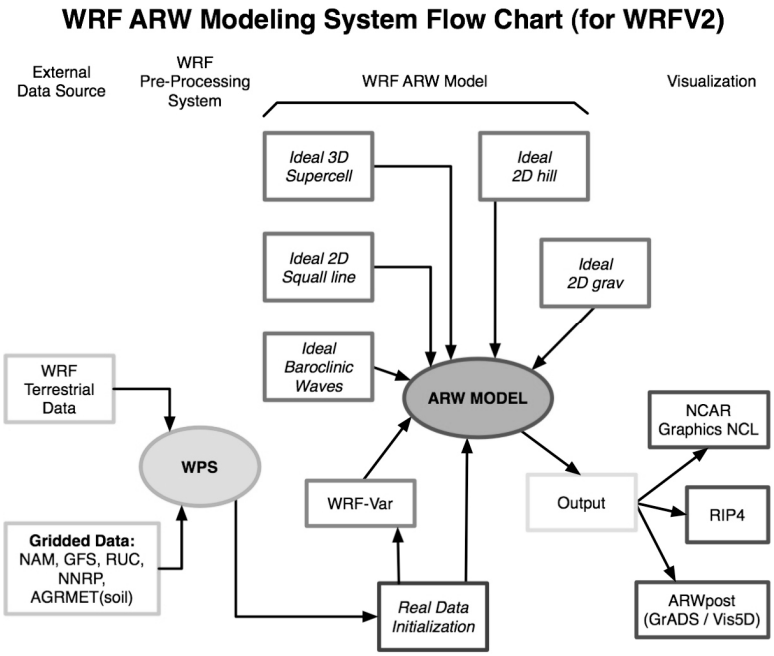

Figure 2.6: WRF ARW Modeling System

Figure 2.6 shows the flowchart for the WRF Modeling System. The WRF Modeling System consists of four major programs:

- The WRF Preprocessing System (WPS)
- WRF-Var
- ARW solver
- Post-processing graphics tools

The WPS is used primarily for real data simulations. It has three functions: 1) defining simulation domains; 2) interpolating terrestrial data (such as terrain, land use, and soil types) to the simulation domain; and 3) degribbing and interpolating meteorological data from another model to this simulation domain.

WRF-Var is used to ingest observations into the interpolated analyses created by WPS.

ARW Solver is the key component of the modeling system, and used to conduct idealized and real-data simulations.

Several visualization programs can be used for post processing. In this research GrADS was used for visualization of model results.

3. REMOTE SENSING, GEOSTATISTICS AND GEOGRAPHIC INFORMATION SYSTEMS

3.1 Remote Sensing

Determining the impacts of land-use and land-cover change on the Earth system has been studied by many researchers. Utilization of digital image processing techniques to remotely sensed images can produce accurate land use or/and land cover maps of related region for the past and present time which are valuable source of information for environmental, disaster, planning and climate studies. The image processing techniques conducted in this research to obtain past and present land cover map of the study area were explained in the following sections. Using the produced land cover maps, land cover changes in the area were determined and the interactions between land cover change and climate were investigated.

3.1.1 Radiometric and Atmospheric Correction

The electromagnetic radiation signals collected by satellites are modified by scattering and absorption by gases and aerosols while traveling through the atmosphere from the Earth surface to the sensor. Changes in scene illumination, atmospheric conditions, viewing geometry and instrument response cause radiometric distortions over satellite image. Therefore, satellite sensor images are radiometrically and atmospherically corrected to eliminate system errors and to minimize contamination effects of atmospheric particles through absorption and scattering of the radiation from the earth surface **(Liang, 2004; Song et al, 2001, Teilet, 1986).**

The objective of radiometric correction is to recover the "true" radiance and/or reflectance of the target of interest **(Lathrop, 1988).** In some cases, destriping, line drop or bit errors had been occurred and they should be corrected in the radiometric correction phase. Units of electromagnetic radiation namely irradiance, radiance and reflectance should be considered since they will be used in radiometric and atmospheric correction procedure.

- *Irradiance* - radiant flux incident on a receiving surface from all directions, per unit surface area, W m^{-2}
- *Radiance* - radiant flux emitted or scattered by a unit area of surface as measured through a solid angle, W m-2 sr-1
- *Reflectance* - fraction of the incident flux that is reflected by a medium

Conversion from radiance (analog signal) to Digital Number (DN) was conducted by a calibrated radiometric response function that is unique for channel. Inverse relationship can be used to convert from DN back to radiance. Calibration parameters such as gain and offset are available in published sources and image header files.

The following equation is used for the calculation of radiance values from DN values:

$$L = C_0 + C_1 * DN \quad \textbf{(3.1)}$$

where C_0 is offset (also known as bias) and C_1 is gain values in mW cm^{-2} sr^{-1} μm^{-1} units.

Table 3.1 illustrates the offset and bias parameters for Landsat ETM sensor.

Table 3.1: Offset and Bias Parameters for Landsat ETM [mW cm^{-2} sr^{-1} μm^{-1}]

Band	Gain	Bias
1	0.7756863	-6.1999969
2	0.7956862	-6.3999939
3	0.6192157	-5.0000000
4	0.6372549	-5.1000061
5	0.1257255	-0.9999981
6	0.0437255	-0.3500004

To further correct for scene-to-scene differences in solar illumination, it is useful to obtain at-satellite reflectance. The term "at-satellite" refers to the fact that this conversion does not account for atmospheric influences **(Lathrop, 1988).** At-Satellite Reflectance , p_λ;

$p_\lambda = (\pi L_\lambda d^2)/\square\square\square(ESUN_\lambda\square.\cos.\theta)$

(3.2)

Where,

L_λ = spectral radiance measured for the specific waveband

θ = solar zenith angle

$ESUN_\lambda$ = mean solar exoatmospheric irradiance (W m^{-2} μm^{-1}), specific to the particular wavelength interval for each waveband

d = Earth-sun distance in astronomical units.

Solar spectral irradiances for Landsat ETM is given in the following table.

Table 3.2: Solar Spectral Irradiances for Landsat ETM Sensor

Band No.	W m^{-2} μm^{-1}
Band 1	1969.0
Band 2	1840.0
Band 3	1551.0
Band 4	1044.0
Band 5	225.70
Band 7	82.07
Band 8	1368.0

Atmospheric correction procedures are designed to minimize scattering and absorption effects due to the atmosphere. Scattering causes and increase in brightness and shorter wavelengths (visible region) are strongly influenced by scattering due to Rayleigh, Mie and nonselective scattering. On the other hand, absorption decreases brightness and longer wavelengths (infrared region) are strongly influenced by water vapor absorption **(Lathrop, 1988).**

There are two types of atmospheric correction techniques namely absolute and relative atmospheric correction. Absolute removal of all atmospheric influences requires a number of assumptions, additional ground and/or meteorological reference data and sophisticated software. ATCOR software developed by Deutsches Zantrum für Luft und Raumfahrt (DLR) is widely used for atmospheric correction. Dark object subtraction (also known as haze removal) Dark object subtraction (DOS) is a

widely used image-based absolute correction approach for classification and change detection applications **(Spanner et al., 1990; Ekstrand, 1994; Song et al, 2001).**

Relative atmospheric correction takes one band and/or image as a baseline and transforms the other bands and/or images to match. Histogram matching, scene-to-scene normalization (Invariant object method) and contrast reduction methods are example for relative atmospheric correction.

Dark Object Subtraction (DOS)/Haze Removal

This approach assumes the existence of dark objects (objects having zero or small surface reflectance) throughout an image and homogeneous atmosphere. In this case, some ground features are so dark that the energy received at the sensor is due almost entireley path radiance (L_d). Thus, L_d is set to the top-of-atmosphere radiance of a dark object less 0.01 radiance. The minimum reflectance value in the histogram from the entire scene is thus attributed to the effect of the atmosphere and is subtracted from all the pixels **(Song et al., 2001; Liang 2001, 2004).**

After applied DOS, haze is removed, and the surface features blocked by haze are recovered. To employ this method, brightness values were examined in an area of shadow or for a very dark object (such as a large clear lake) and the minimum value was determined. The correction is applied by subtracting the minimum observed value, determined for each specific band, from all pixel values in each respective band. Since scattering is wavelength dependent the minimum values will vary from band to band, therefore each band must be evaluated independently. This method is based on the assumption that the reflectance from these features, if the atmosphere is clear, should be very small, if not zero **(Lathrop, 1998; Liang 2001, 2004; Schroeder, 2006).**

Histogram Matching

This method is based on the assumption that the surface reflectance histograms of clear and hazy regions are the same. After identifying clear and hazy regions in an image, the histograms of the hazy regions are shifted to match the histogram of their reflectance of the clear regions **(Liang 2001, 2004).**

The major limitation of this method is its assumption that the reflectance histogram of a hazy region is the same as the histogram of a clear region, which implies that

there are same portions of various land covers in both hazy and clear regions. This assumption is not valid under most conditions, even if both clear and hazy regions are the same landscape types **(Liang 2001, 2004).**

Scene-to-scene normalization/Invariant Object Method

Assuming that there are some pixels in a scene whose reflectances are quite stable through time. A linear relationship based on the reflectance of these "invariant objects" can be used to normalize imagery acquired at different times. This method is example to relative atmospheric corrections. If there are simultaneous ground reflectance measurements available or some assumptions about surfaces can be made, it can be an absolute correction procedure **(Liang 2001, 2004).**

N "invariant" pixels can be identified from all M imagery occurred at different times. If we can select a clear image, for example J, as the reference, all other images can be normalized to image J using a linear regression based on these N pixels **(Liang 2001, 2004).**

$$L_{jk}=a_{ik} + b_{ik}. L_{ik} \quad \textbf{(3.3)}$$

L_j*:* radiance of reference imagery J.

L_i*:* radiance of any other images.

k: band

The linear regression analysis for each band k will produce two coefficients a and b that are used for normalizing all other pixels of band k for each image i. Ideally, we need to identify "invariant" pixels with variable brightness from dark to bright in each band.

3.1.2 Geometric Correction

There are both systematic and non-systematic geometric errors present in satellite imagery. The systematic errors are primarily functions of scan skew, mirror-scan velocity, panoramic distortion, platform velocity nonlinearities, perspective geometry and Earth rotation. These errors can be corrected using data from platform ephemeris and knowledge of internal sensor distortion. Non-systematic errors are mainly caused by variation through time in the position and attitude angles (roll, pitch and yaw) of the satellite platform. Without accurate sensor platform orientation

parameters, these errors can only be corrected with the use of Ground Control Points (GCPs) and a suitable precision photogrammetric or empirical model **(Mather 1999, Jensen 1996).**

The most widely used geometric correction technique uses GCPs located on the image and the corresponding coordinate system in order to empirically determine a mathematical transformation for the correction of image geometry. Empirical geometric correction models are based on the positional relationship between points on a satellite image and points on a reference system. These models include conventional polynomials, affine and the rational function model (RFM). They are usually applied when there are no ephemeris data or other explicit information on the sources of geometric distortions, as they correct the geometric distortions in an image simultaneously. Furthermore, these models are mathematically simple, computationally efficient, and have ability to correct distortions that are not accounted for by sensor orbital models. **(Kardoulas et al. 1996, Toutin 2004, Kaya et al. 2003, Saroglu, 2004)**

In this research, affine transformation was used to geometrically correct the satellite images. We **(Sertel et al., 2007)** investigated affine transformation in detail. The affine transformation can be expressed by the following equations:

$$Y_i^2 = a_0 + k_y \cos\omega_y Y_i^1 + k_x \sin\omega_x X_i^1 \quad \textbf{(3.4)}$$

$$X_i^2 = b_0 - k_y \sin\omega_y Y_i^1 + k_x \cos\omega_x X_i^1 \quad \textbf{(3.5)}$$

where Y_i^1, X_i^1 and Y_i^2, X_i^2 are the coordinates of the point i in the first (image) and second (reference) coordinate systems, respectively. a_0 and b_0 are the translations, ω_x and ω_y are the rotations and k_x and k_y are the scale factors along the x and y axes, respectively.

If we take $k_x \sin\omega_x=a_1$, $k_y \cos\omega_y=a_2$, $k_x \cos\omega_x=b_1=$, $-k_y \sin\omega_y=b_2$, the general form of the affine transformation can be written as follows:

$$Y_i^2 = a_0 + a_1 X_i^1 + a_2 Y_i^1 \quad \textbf{(3.6)}$$

$$X_i^2 = b_0 + b_1 X_i^1 + b_2 Y_i^1 \quad \textbf{(3.7)}$$

The application of the affine transformation includes two steps (1) determining the coefficients a and b using GCPs and (2) applying these coefficients to transform all other image point coordinates into the reference system coordinates.

The observation equations of the adjustment can be expressed in the following form by adding the residuals v_{xi} and v_{yi} to the previous equation in order to estimate geometric correction parameters.

$$Y_i^2 + v_{yi} = a_0 + a_1 X_i^1 + a_2 Y_i^1 \tag{3.8}$$

$$X_i^2 + v_{xi} = b_0 + b_1 X_i^1 + b_2 Y_i^1 \tag{3.9}$$

If the number of GCPs is equal to n, the matrix form of Equation 3.8 and 3.9 can be written as Equation 3.10.

$$\mathbf{v}_{2n\times 1} = \mathbf{A}_{2n\times u}\mathbf{x}_{u\times 1} - \boldsymbol{l}_{2n\times 1} \tag{3.10}$$

where $\mathbf{v} = \begin{bmatrix} v_{y1} & v_{x1} & \cdots & v_{yn} & v_{xn} \end{bmatrix}^T$ is the residual vector, $\mathbf{x} = \begin{bmatrix} a_0 & b_0 & a_1 & b_1 & a_2 & b_2 \end{bmatrix}^T$ is the vector of unknown parameters. The matrix **A** and the vector $\boldsymbol{l}$ are the design matrix and the vector of constant terms, respectively, given by

$$\mathbf{A} = \begin{bmatrix} 1 & 0 & X_1^1 & Y_1^1 & 0 & 0 \\ 0 & 1 & 0 & 0 & X_1^1 & Y_1^1 \\ \vdots & \vdots & \vdots & \vdots & \vdots & \vdots \\ 1 & 0 & X_n^1 & Y_n^1 & 0 & 0 \\ 0 & 1 & 0 & 0 & X_n^1 & Y_1^1 \end{bmatrix} \tag{3.11}$$

and

$$\boldsymbol{l} = \begin{bmatrix} Y_1^2 \\ X_1^2 \\ \vdots \\ Y_n^2 \\ X_n^2 \end{bmatrix} \tag{3.12}$$

The unknowns in this equation are determined by the least squares method; therefore, the sum of the squared residuals is minimized. As Equation 3.12 corresponds to the adjustment model of indirect observations the parameters are estimated by

$$\mathbf{x} = (\mathbf{A}^T \mathbf{P} \mathbf{A})^{-1} \mathbf{A}^T \mathbf{P} \boldsymbol{l} \quad \textbf{(3.13)}$$

where the matrix **P** is composed of the precision estimations of the observations, i.e. the coordinates of GCP's. The matrix **P** is commonly taken as identity matrix in coordinate transformation. Thus, we obtain

$$\mathbf{x} = (\mathbf{A}^T \mathbf{A})^{-1} \mathbf{A}^T \boldsymbol{l} \quad \textbf{(3.14)}$$

According to this kind of least squares adjustment, $(\mathbf{A}^T \mathbf{P} \mathbf{A})^{-1}$ in Equation 3.13 or $(\mathbf{A}^T \mathbf{A})^{-1}$ in Equation 3.14 gives the cofactor matrix of the unknowns $\mathbf{Q}_{xx}$. Using the cofactor matrix $\mathbf{Q}_{xx}$ the variance-covariance matrix $\mathbf{K}_{xx}$ of the transformation parameters is computed in the following equation.

$$\mathbf{K}_{xx} = m_0^2 \mathbf{Q}_{xx} \quad \textbf{(3.15)}$$

where m_0 is the root mean squared error (RMS) of the unit weighted observations and is obtained by:

$$m_0 = \sqrt{\frac{\mathbf{v}^T \mathbf{P} \mathbf{v}}{2n - u}} \quad \textbf{(3.16)}$$

In the above equation, n is the number of GCPs and u is the number of unknowns.

Geometric correction is a prerequisite for the production of images with high levels of locational accuracy, incorporation of satellite sensor images with other data sets and pixel-based change detection analysis from multi-temporal satellite sensor images. Accuracy of geometric correction should be evaluated to perform reliable location, change detection and Geographic Information Systems (GIS) analysis.

3.1.3 Classification

The objective of classification is to assign all pixels in the image to particular classes or themes (e.g., water, coniferous forest, deciduous forest, urban, ice). The resulting classified image is comprised of a mosaic of pixels, each of which belongs to a particular theme, and is essentially a thematic "map" of the original image.

Unsupervised Classification

Spectral classes, which are groups of pixels that are uniform (or near-similar) with respect to their brightness values in the different spectral channels of the data, are

grouped based on the numerical information in the data. Natural groupings or structures in the data are determined using clustering algorithms. Iterative Self-Organizing Data Analysis (ISODATA) is the most commonly used unsupervised technique and also used in this research.

Figure 3.1 illustrates the steps of unsupervised classification. In the first step, pixels are grouped into the number of clusters that user defined previously. These groups are called spectral classes. Classified groups are then labeled with user expertise, if the result classes are satisfactory then result classified image is used for further analysis. If the result classes are not satisfactory then numbers of clusters or some other statistical parameters such as separation distance, covariance values are changed and classification is conducted again until satisfactory result is achieved.

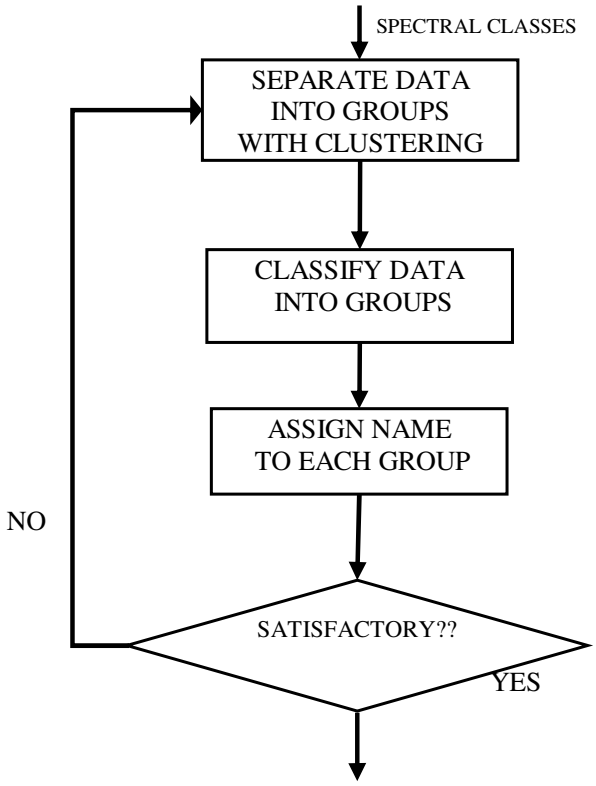

Figure 3.1: Unsupervised Classification

Supervised Classification

In supervised classification, spectrally similar areas on an image are identified by creating "training" sites of known targets and then extrapolating those spectral signatures to other areas of unknown targets. Training sites in the imagery which are homogeneous representative samples of the different surface cover types. It relies on

the *a priori* knowledge of the location and identity of land cover types that are in the image. These are called information classes. Familiarity with the geographical area, topographic maps and some other ancillary data are required to select appropriate training areas. The computer is trained using the numerical information in all spectral bands for the pixels comprising training areas to recognize spectrally similar areas for each class.

Steps of supervised classification are presented in Figure 3.2.

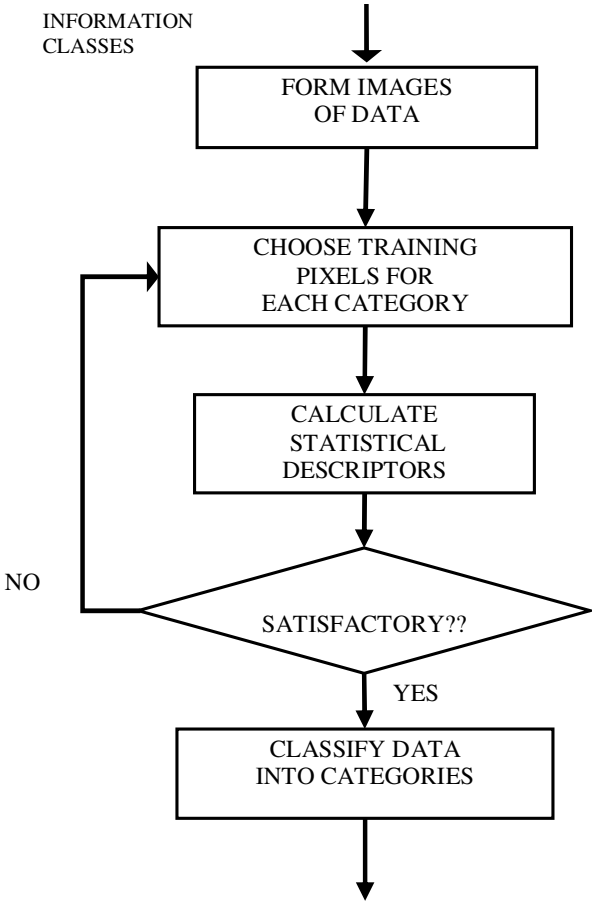

Figure 3.2: Supervised Classification

Classification accuracy

Many methods of accuracy assessment have been discussed in the remote sensing literature by several researchers **(Congalton and Green, 1999; Koukoulas and Blackburn, 2001; Piper, 1983).** The most widely promoted and used, however, may be derived from a confusion or error matrix **(Foody, 2002).** In this research, to assess the accuracy of classification, the confusion matrix and some common measures

derived from this matrix namely, overall accuracy, user's accuracy, producer's accuracy and kappa coefficient are used. The confusion matrix is currently at the core of the accuracy assessment literature in remote sensing. This matrix is a simple cross-tabulation of the mapped class label against that observed in the ground or reference data for a sample of cases at specified locations **(Campbell, 1996; Canters, 1997).** Indeed, the confusion matrix helps to refine the classification or estimates derived from it by providing the basis on which to both describe classification accuracy and characterize errors. For example, the matrix may reveal interclass confusion that could be resolved with the use of additional discriminatory information. Alternatively, the pattern of misclassification evident in the matrix may aid studies that use the map, particularly as a means to estimating the areal extent of classes over a region **(Foody, 2002).**

The design of a confusion matrix is presented in Figure 3.3. The bold elements represent the main diagonal of the matrix that contains the cases where the class labels depicted in the image classification and ground data set agree, whereas the off-diagonal elements contain those cases where there is a disagreement in the labels (Figure 3.3). In the following figure W, F, U and C represent the classes of water, forest, urban and cropland, respectively. The number of classes, q, is 4 in this example.

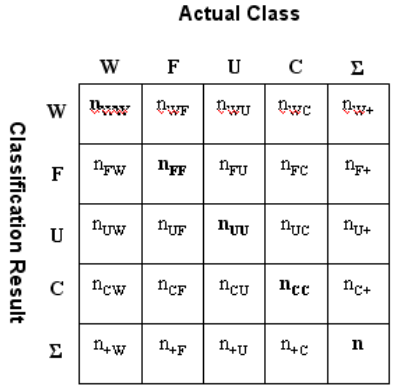

Figure 3.3: Confusion Matrix

$$\text{Overall accuracy} = \frac{\sum_{k=1}^{q} n_{kk}}{n} x100 \qquad \textbf{(3.17)}$$

User's accuracy = $\frac{n_{ii}}{n_{i+}}$ **(3.18)**

Producer's accuracy = $\frac{n_{ii}}{n_{+i}}$ **(3.19)**

Kappa coefficient= $\frac{n\sum_{k=1}^{q} n_{kk} - \sum_{k=1}^{q} n_{k+}n_{+k}}{n^2 - \sum_{k=1}^{q} n_{k+}n_{+k}}$ **(3.20)**

where

q: number of classes error matrix

n: total number of observations in error matrix

n_{ii}: major diagonal element for class i

n_{i+}: total number of observations in row for class i (right margin)

n_{+i}: total number of observations in column for class i (bottom margin)

3.2 Geostatistics

Geostatistics includes the application of probabilistic methods to regionalized variables, which designates any function displayed in a real space. It differs from conventional statistics by searching to exhibit a structure of spatial correlation whatever the complexity and the irregularity of the real phenomenon.

3.2.1 Semivariogram Calculation

Semivariograms, the primary tool of geostatistics, are used in a wide variety of remote sensing applications. A semivariogram provides a concise and unbiased description of the scale and pattern of spatial variability and can be used to investigate and quantify spatial variability and autocorrelation in a region, providing the stationary hypothesis is valid. For example, semivariogram shape has been used to discriminate structurally-damaged forest from healthy forest and semivariogram range has been related to tree size. Semivariograms have been used to select an appropriate spatial resolution for data acquisition and with a fitted mathematical

function; a semivariogram can be used to estimate values at unsampled points **(Sertel et al., 2007; Curran, 1988; Curran and Atkinson, 1998; Woodcock et al., 1988).**

Semivariograms measure the spatial variation of a regionalized variable i.e. a random variable whose position in space or time is known and the theory of regionalized variables underpins the analysis that follows (**Sertel et al., 2007; Woodcock et al., 1988).**

Consider a transect running across a remotely sensed image where the digital number (DN) *z* of pixels x has been extracted at regular intervals (x=1, 2, n). The relation between any pair of pixels, *h* intervals apart (the lag distance), can be given by the average squared difference between all such pairs. As the per-pixel variance is half this value, the semivariance *γ(h)* for pixels at distance *h* apart is defined as **(Sertel et al, 2007; Curran and Atkinson, 1998; Woodcock et al, 1988)**:

$$\gamma(h) = \frac{1}{2} E[Z(x) - Z(x+h)]^2 \qquad \textbf{(3.21)}$$

Z(x) and *Z(x+h)* are the random functions describing the property of interest *Z* at places separated *h* and *E* is the mathematical expectation operator.

The experimental semivariogram, obtained from real data, can be estimated along the transect where P*(h)* pairs of observations separated by the same lag *h.* Their average semivariance at lag *h* is given by

$$\hat{\gamma}_s(h) = \frac{1}{2P(h)} \sum_{i=1}^{P(h)} [Z(x) - Z(x+h)]^2 \qquad \textbf{(3.22)}$$

The quantity $\hat{\gamma}_s(h)$ is an estimate of the semivariance *γ(h)* and is a useful measure of dissimilarity between spatially separate pixels and spatial patterns can be described using experimental semivariograms as the larger the semivariance, the less similar are the pixels. After obtaining experimental semivariograms, it is necessary to fit a continuous and authorized mathematical model such as the linear, spherical, exponential or Gaussian. Lag, sill, range and nugget are terms used to describe these fitted models (Table 3.3, Figure 3.4) **(Sertel et al., 2007; Goaverts, 1999; Curran and Atkinson, 1998, Woodcock et al., 1988).**

Table 3.3: Descriptors of the Semi-variogram

TERM	SYMBOL	DEFINITION
Lag	H	Separation distance between sampling pairs.
Sill	S	The value where the semi-variogram flattens off, maximum level of $\gamma(h)$.
Range	A_0	Point on the h axis where the semi-variogram reaches the sill.
Nugget	C_0	Point where $\gamma(h)$ intercepts the ordinate.

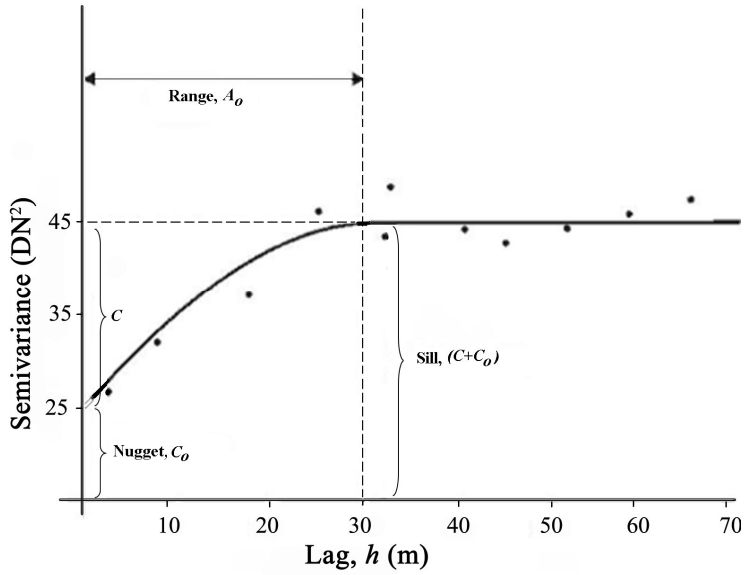

Figure 3.4: A Semi-variogram

The X-axis of a semi-variogram shows the scale of variation; the Y-axis of a semi-variogram shows the amount of variation and the shape of a semi-variogram shows both.

3.2.2 Kriging

Kriging is a widely used method to perform interpolation between sample data, where interpolate means fill in the gaps between sample data. If the property of interest is spatially dependent it is reasonable to assume that sample observations which are close to an unknown value will be more similar to it than observations that are further away. The closer the observations, the more similar they are.

In kriging, weight values are calculated considering the spatial dependency and spatial dependency is determined using semivariograms. In other words, weights are

assigned considering the correlation between sample data and estimated data and this statistical correlation values were obtained from semivariograms explained in the previous section.

Kriging method is a linear predictor because unknown value is determined using linear weighted sum of the neighboring observations to unknown data. Kriging predictor $z(x_0)$ is the linear weighted sum of n observations.

$$\hat{z}(x_0) = \sum_{i=1}^{n} \lambda_i z(x_i) \qquad \text{…...(3.23)}$$

x_i, spatial location of observation i ,

$z(x_i)$, value of i at location x_i,

λ_i, weight value for $z(x_i)$ datum,

$\sum_{i=1}^{n}$ sum operation,

$\hat{z}(x_0)$, estimatad value at location x_0.

Sum of weights are taken as 1 to prevent biases.

$$\sum_{i=1}^{n} \lambda_i = 1 \qquad \textbf{(3.24)}$$

Variance value must be arranged as minimum during the selection of weights.

$$\sigma_e^2(x_0) = \text{var}\left\{\hat{z}(x_0) - z(x_0)\right\} \qquad \textbf{(3.25)}$$

3.3 Geographic Information Systems

Geographic Information System (GIS) is a system dealing with information related to the geographical data. The system is designed to efficiently capture, store, update, manipulate, retrieve, analyze and display all forms of geographically referenced information. Spatial features are stored in a coordinate system referring to a particular place on Earth. Descriptive attributes in tabular form are associated with spatial features. Spatial data and associated attributes in the same coordinate system

can then be layered together for mapping and analysis There are two kinds of data in a GIS namely raster and vector. Raster and vector data can be obtained from satellite remote sensing, aerial photography, digitized and scanned maps, field survey and Global Positioning System (GPS) **(Seker et al., 2004).**

Geographical Information Systems provide a flexible environment and a powerful tool for the manipulation and analysis of spatial information. Landscape characteristics and the maps of all variables related to phenomenon were combined to extract information to present better solutions for environmental problems and improve understanding of nature of the problems **(Weng, 2001).** GIS technology provides the integration of information, methods and policies, where the same or similar integration is not possible or costly via conventional methods. Research and operational applications have demonstrated the advantages of GIS and remote sensing integration on environmental monitoring and management **(Kaya and Curran, 2006; Demirel et al., 2007; Musaoglu et al., 2005; Seker et al., 2003).**

The integration of Remote Sensing (RS) and Geographic Information Systems (GIS) is a powerful and effective tool which has been widely utilized to many multidisciplinary applications to realize rapid, economic, reliable and accurate solutions **(Weng, 2001; Seker et al., 2005; Sertel et al, 2008).** Although wetlands have important role in regulation of water flow and nutrient, erosion reduction, flood control, and diversity of vegetation and wildlife habitats, some of them are dried and converted to agricultural areas because of the lack of understanding their ecological importance.

3.3.1 Database Design

Database is an organized and structured collection of records or data stored in a computer where a computer program can select and query desired pieces of data. In simple words, a database is an electronic means of storing data in an organized manner. Databases are organized by fields, records and files, where field represents a single piece of information, record includes one complete set of field and file is a collection of records.

Once stored, data in the database can be retrieved, processed and displayed by programs as information to the reader. As a result of queries, one can obtain information from data which can be used in decision making. In a database system,

the data is managed, accessed and queried by a database management system (DBMS).

Database approach ensures the following advantages:

- Data redundancy is reduced
- Data consistency can be maintained and data sharing is aesier
- A logical conceptualization of data is enforced, leading to a reasonable organization
- Complex relations among data may be identified

4. STUDY AREA AND DATASETS

4.1 Study Area

The Marmara Region occupies the northwest corner of Turkey with a surface area of 67.000 km² and represents approximately 8.6% of the Turkish national territory. It is the smallest but most densely populated of the seven geographical regions of Turkey. This region includes eleven cities, namely İstanbul, Bursa, Edirne, Kocaeli, Balıkesir, Kırklareli, Tekirdağ, Çanakkale, Bilecik, Sakarya and Yalova.

The Marmara Region forms a passage between the Balkan Peninsula and Anatolia, and connects Europe and Asia. As a result of being very close location to Europe, the existence of the Bosphorus and Dardanelles Straits as a passage from Black Sea to Aegean Sea, ports on the Black Sea and Aegean Seas make this region highly developed in industry, commerce, tourism and transportation. İstanbul, Bursa and Kocaeli cities are the center of main industrial establishments and produce processed food, textile, cement, paper, petrochemical products, automotive, house furniture, leather and ship construction. This region is the most industrialized region in Turkey and one third of the country's industry has been situated in this region.

The population of Turkey was 13 648 270 in 1927 and it increases approximately five fold in seventy three years and reached 67 803 927 in 2000. According to the U.S. Census Bureau, the population of Turkey will reach 82 205 000 by 2025. The Marmara region has the highest population rate and is the densest population among the other seven regions of Turkey **(DIE, 2007; U.S. Census Bureau, 2007).** Based on 2000 census data, population of the Marmara Region was 17 300 000 with a population increase rate of 27%, whereas this rate is 18.34% for Turkey between 1990 and 2000.

Rapid demographic and economic development, industrialization and urbanization occurred in the Marmara Region after the 1980s and the population of the Marmara Region has increased dramatically as a result of intense migration from other regions.

Rapid industrialization and population increase have caused to changes in landscape characteristics of the Marmara region. Urbanization had increased and several agricultural and forest areas had been transformed into urban and built-up areas. İstanbul has been affected because of huge immigration, the city population was 3 million in 1970s, it became 7.4 million in 1990s and current population is around 12 million **(Kaya et al., 2002).** Bursa, another important city of the Marmara region had a population of 275 953 in 1970 but it reached to 1 194 687 in 2000.

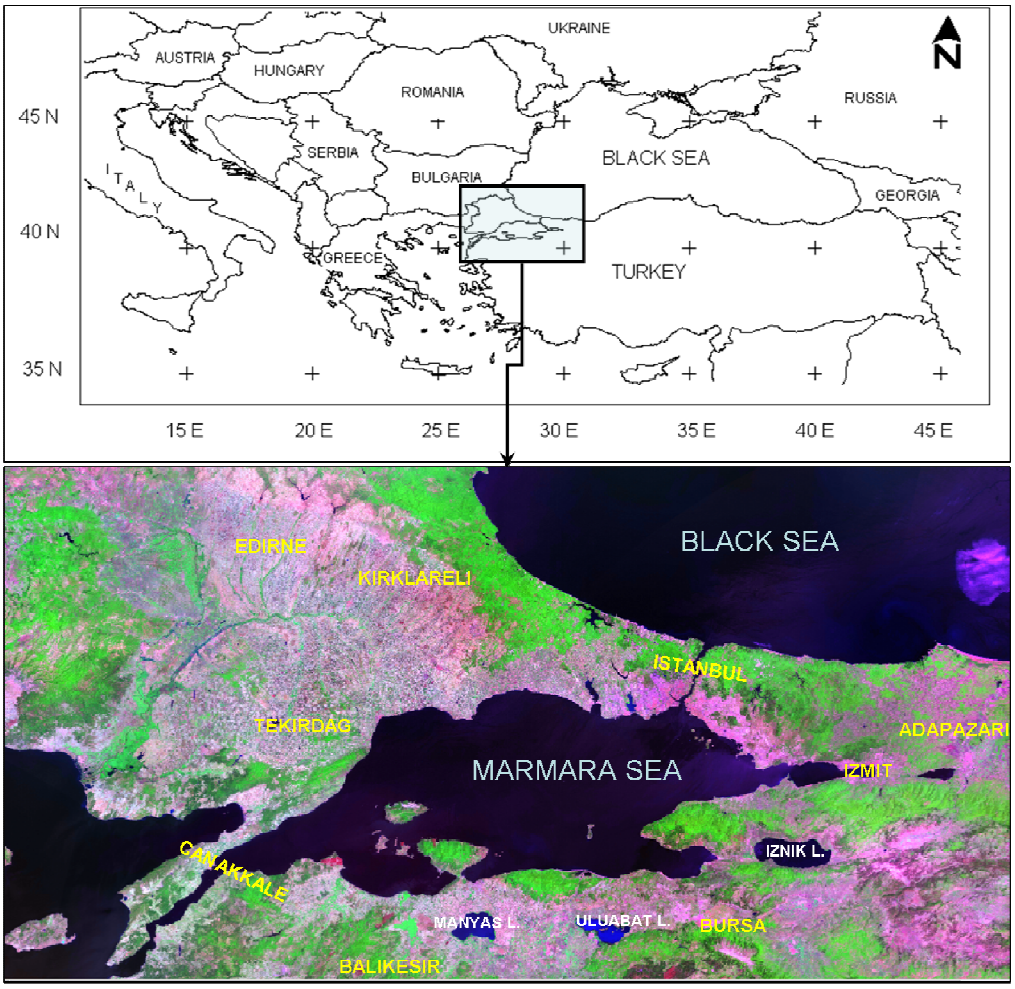

Figure 4.1: Location of the Study Area

The location of the study area is shown in Figure 4.1.

4.1.1 Climate and vegetation of Turkey and Study Area

Turkey is in a region which is often described as having a warm and moderate climate **(Erinc, 1984).** Its diverse regions have different climates, with the weather system on the coasts contrasting with that prevailing in the interior. The Aegean and

Mediterranean coasts have cool, rainy winters and hot, moderately dry summers. The Black Sea coast receives the greatest amount of rainfall. The highest maximum temperature is observed in the southeast of the country, particularly in summer months. The temperature decreases gradually towards the northwest and northeast, yet this decrease is less strong during summer due to the continental effects of the inner regions. At low altitudes, the coastal regions are warmer than the inner regions, which are separated from the former by high mountains. On average, the Mediterranean coast has the highest temperature, followed by the Aegean, the eastern part of the Black Sea region and the Marmara coasts. In eastern Anatolia, owing to continental effects and high altitudes, there is a widespread temperature decrease **(Tayanc et al., 1998).**

The distribution of temperature variability is determined by the extension of the continental and the topographic effects. The highest temperatures during winter are observed along the Mediterranean coast, which is influenced by subtropical air masses. The lowest temperature values are observed in the northeastern Anatolian Plateau. During summer, the differences between the monthly mean temperature series and those of the extremes are greatest in the coastal areas. The extreme temperatures have maxima in the southeastern region of Anatolia during summer. The average maxima are smallest in the Black Sea region. In central Anatolia it is common for the monthly mean temperature to fall below zero in January. In winter, these values are usually well below zero towards eastern Anatolia, while moderate values are observed in the coastal areas **(Tatlı et al., 2005).**

Karaca et al. (2000) revealed four main cyclone tracks that have affected Turkey by analyzing the 15-year period daily surface and 500-hPa weather maps. There are also other cyclones originating at various places and affecting Turkey, however in general their number are small and cyclone strength is weaker compared to these main tracks.

The tracks are as follows (Figure 4.2):

1. The path which originates from north of Turkey over the southwestern parts of Russia and passes from the Black Sea region (Path 1).

2. The path which originates from the Balkans and affects Marmara and the Black Sea region, and also partly affects inner parts of Anatolia (Path 2) .

3. The path which is generated in the Genoa Gulf and affects Turkey. It is possible to investigate this path in two sections: both of the sections extend to the western Aegean Sea on the same track but later they split up into:

(a) The path which moves to the northeast direction and affects the northern Aegean region, all the Marmara region and western and middle Black Sea region (Path 3a).

(b) The path which moves towards the east and affects western Turkey and passes over middle Anatolia. Later it obtains a northeasterly direction and middle-eastern Black Sea region (Path 3b).

4. The path which originates from the western or middle Mediterranean with some cases originating from south of the Genoa Gulf and some cases from north of the Sahara Desert which move towards the eastern Mediterranean. It affects the southern parts of Turkey, Crete, Cyprus and Middle East (Path 4).

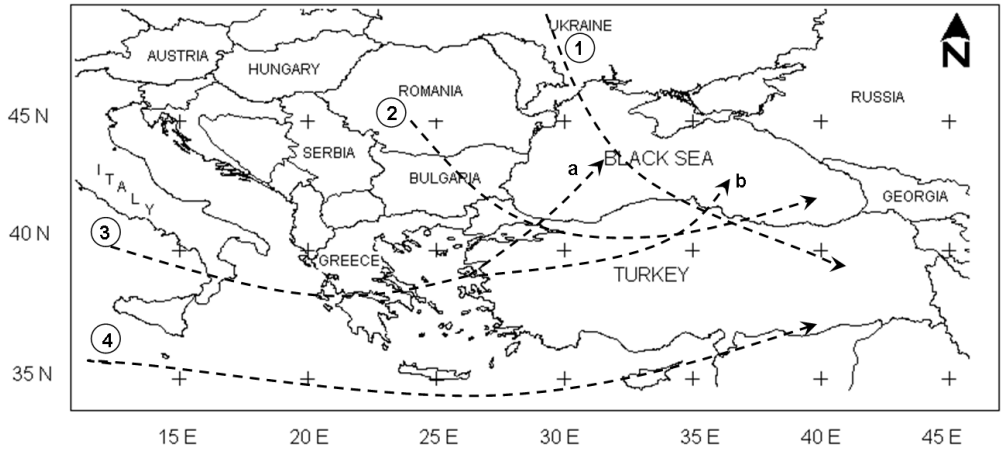

Figure 4.2: The Paths of Atmospheric Cyclones over Turkey (adopted from **Karaca et al., 2000**)

Paths 1 and 2 are typical summer-time trajectories that bring summer storms over the other parts of Turkey. They bring abundant rain with them, and in some cases, causing the floods. In winter, cold air masses from the Balkan Region and northern Europe are associated with these trajectories. They are characterized by substantial amplification of the planetary-scale flow waves during the development phase of the cyclone that can bring cold air to very low latitudes.

Paths 3 and 4 are more frequent in winter months. These types of cyclones are generally associated with above normal temperatures in their warm sector and normal or a little below-normal temperatures at the back of the cold front. Thus, it is

not common to have snow blizzards when the cyclones are of these types. Air–sea interaction during the cyclogenesis process has a contribution to the moisture content of the cyclones, generally causing them to become unstable leading to thunderstorms.

Cyclones generated in Path 2 and Path 3a affect the Marmara Region. Path 2 is important for this research since it affects the Marmara Region in summer time.

Turkey is surrounded by Black Sea in the north, Aegean Sea in the west and Mediterranean Sea in the south. Cyclones originating from the North Atlantic region bring over moisture-laden air to Turkey and cause a lot of rainfall, especially in the coastal areas of Turkey due to orographic effects, in the cold half of the year. Cyclones affecting Turkey were illustrated in previous paragraphs and variation in the intensity and frequency of these cyclones will cause variation in the precipitation in Turkey. Since cyclones are passing through the surrounding seas before reaching to Turkey, SSTs might have an important a role in the amount of rainfall in Turkey as the overpassing air masses are modified by SSTs in some degree **(Bozkurt and Sen, 2007).**

Climate of Marmara displays a transition between Black Sea Climate and Mediterranean Climate. It is divided into four sub regions namely, Yıldız, Ergene, Catalca-Kocaeli and South Marmara. *Yıldız Section* is located on the northwestern part of the Marmara region and includes Yıldız Mountains and there are not many plains in the area. The sections of Yıldız Mountains towards to the Black Sea have Black Sea climate and sections towards to the inner pats have dry climate namely Mediterranean type. Black sea climate has cooler temperatures in both winter and summer, and usually experiences more rains compared to the climate of the Mediterranean coasts of Turkey. Vegetation cover is forest along the Black Sea coast whereas sparsely vegetation occurs towards to the inner part. Ergene plains constitute the huge part of *Ergene Section*. Common vegetation type here is sparsely vegetated areas as a result of dry climate. There are great agricultural lands in this section including potatoes, rice, grapes, wheat, sunflower and tobacco. Çatalca-Kocaeli Section includes two peninsulas located at the eastern and western parts of Bosphorus. Low plateus are available in this section. Forests cover the Black Sea coast of this section, where Black Sea climate occurred. Whereas, forests become sparser in southern parts and climate is dryer. Adapazarı plain is the main agricultural land of this section where beet, sunflower, corn, potatoes and linen are

grown. The fourth section of Marmara region is Southern Marmara which includes southern pert of the region and Galippolu Peninsula. This section has medium-height mountains and productive plains among these mountains. Uludag is the highest mountain of the section, where also a meteorological station is located.

4.2 Satellite Images

Landsat MSS obtained between 1972 and 1975 and Landsat ETM images obtained between 2001 and 2005 were used to create land cover maps of the study region. 2005 Landsat ETM image was belonged to İstanbul and neighborhood region where most land cover changes has occurred. The study region covers six Landsat frames and each frame evaluated individually to derive accurate information. Landsat MSS images have four spectral bands and 80 m spatial resolution, whereas Landsat ETM images have seven spectral bands and 30 m spatial resolution.

The Landsat Program is a series of Earth-observing satellite missions jointly managed by NASA and the U.S. Geological Survey. Since 1972, Landsat satellites have collected information about Earth from space. The purpose of the Landsat program is to provide the world's scientists and application engineers with a continuing stream of remote sensing data for monitoring and managing the Earth's resources. Landsat 7 is the latest NASA satellite in a series that has produced an uninterrupted multispectral record of the Earth's land surface since 1972 **(Landsat Program, 2007)**.

In addition to Landsat MSS and ETM images, available Landsat TM, SPOT and IKONOS images in ITU Remote Sensing Laboratory were used to assist classification and geometric correction procedure.

4.3 Meteorological Data

4.3.1 Station Data

Station data including daily temperature (min, max and average), daily average wind, and daily total precipitation were obtained from the State Meteorological Office of Turkey. There are approximately 270 stations over Turkey collecting data since 1970s and the spatial distributions of these stations are shown in Figure 4.3.

Time series obtained from station datasets were compared with the model simulated results to investigate the accuracy of the model results.

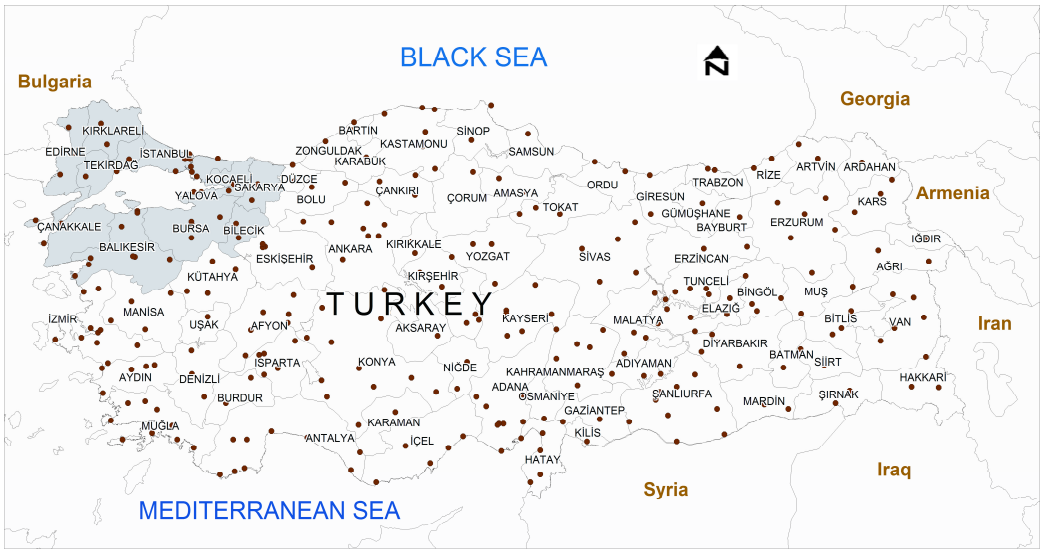

Figure 4.3: Locations of Meteorological Stations in Turkey with Emphasis on the Marmara Region

4.3.2 NCEP/DOE AMIP II Reanalysis Data

National Centers for Environmental Predictions (NCEP)/Department of Energy (DOE) Atmospheric Model Intercomparison Project (AMIP)-II Reanalysis (NCEP/DOE AMIP-II Reanalysis) is an updated and improved version of the NCEP/National Center for Atmospheric Research (NCEP/NCAR Reanalysis) Project, since in Reanalysis-2, global analyses are made using an updated forecast model, updated data assimilation system, improved diagnostic outputs and fixes for the known processing problems of N/N Reanalysis **(Kanamitsu et al, 2002).**

The resolution of the global Reanalysis II is T62 (209 km) with 28 vertical sigma levels. Results are available at 6 hour intervals starting from 1979. NCEP/DOE Reanalysis II data were used as initial and boundary condition for the research.

4.3.3 GPCP Data

The Global Precipitation Climatology Project (GPCP) was established by the World Climate Research Program (WCRP) to address the problem of quantifying the distribution of precipitation around the globe over many years. The general approach is to combine the precipitation information available from each of several sources

into a final merged product, taking advantage of the strengths of each data type **(Adler et al., 2003; Huffman et al., 2001).**

The dataset includes the following data sources:

- Special Sensor/Microwave Imager (SSM/I; 0.5°x0.5° by orbit, GPROF algorithm) provides fractional occurrence of precipitation, and
- GPCP Version 2 Satellite-Gauge (SG) combination (2.5°x2.5° monthly) provides monthly accumulation of precipitation to algorithms applied to
- geosynchronous-orbit IR (geo-IR) T_b histograms (1°x1° grid in the band 40°N-40°S, 3-hourly),
- low-orbit IR (leo-IR) GOES Precipitation Index (GPI; same time/space grid as geo-IR),
- TIROS Operational Vertical Sounder (TOVS; 1°x1° on daily nodes, Susskind algorithm), and
- Atmospheric Infrared Sounder (AIRS; 1°x1° on daily nodes, Susskind algorithm).

The current data set extends from October 1996--June 2007 with 1°x1° latitude—longitude resolution.

4.3.4 Soil Moisture

The Global Soil Moisture Data Bank contains data from over 400 stations for many years for different countries such as Ukraine, Illinois and Russia. The global distribution of soil moisture dataset is shown in the following figure. Volumetric soil moisture values obtained from Ukraine dataset were used in this study to analyze the accuracy of model derived soil moisture values. Volumetric (*W*) or as total volumetric soil moisture (*WT*), expressed as the depth of a column of water contained in a given depth of soil, or as the volumetric percent of water in a given soil depth **(Robock et. al, 2000).**

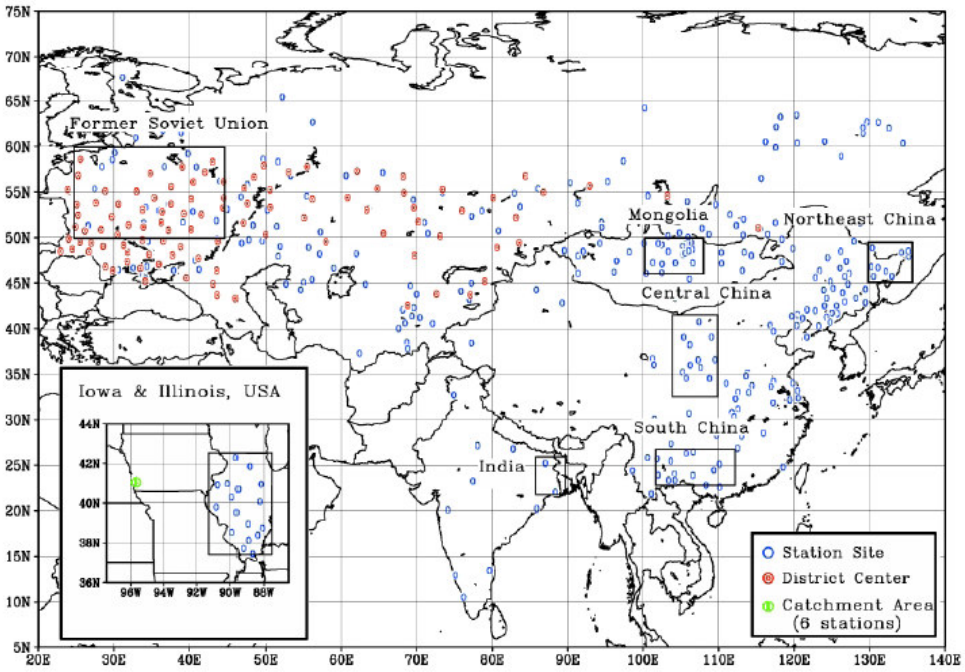

Figure 4.4: Locations of soil moisture observation sites (source: **Robock et al., 2000**)

4.4 Land Cover Datasets

Land cover is a fundamental variable impacting and linking many parts of the human and physical environments. Since remote sensing provides a map-like representation of the Earth's surface that is spatially continuous and highly consistent, as well as available at a range of spatial and temporal scales, it is an attractive source of thematic maps such as those depicting land cover. Mostly image classification is applied to satellite images to create thematic maps of concerned region **(Foody, 2002).** There are several global land cover data sets based on satellite images created by different organizations. Most commonly used three land cover datasets were examined in this study to determine the utility of these datasets for the study area.

4.4.1 Global Land Cover Characterization

Global Land Cover Characterization (GLCC) data was generated by the U.S. Geological Survey (USGS) National Center for Earth Resources Observation and Science (EROS), the University of Nebraska-Lincoln (UNL), and the European Commission's Joint Research Centre (JRC). The global land cover characteristics database was developed on a continent-by-continent basis. All continental databases

have map projections Interrupted Goode Homolosine and Lambert Azimuthal Equal Area map projections, 1-km nominal spatial resolution. The data set is derived from 1-km Advanced Very High Resolution Radiometer (AVHRR) data spanning April 1992 through March 1993 **(Loveland and others, 2000).**

The following derived data sets are included in the global land cover data base:

- Global Ecosystems **(Olson, 1994a, 1994b)**
- IGBP Land Cover Classification **(Belward, 1996)**
- U.S. Geological Survey Land Use/Land Cover System **(Anderson et al, 1976)**
- Simple Biosphere Model **(Sellers et al 1986)**
- Simple Biosphere 2 Model **(Sellers et al, 1996)**
- Biosphere Atmosphere Transfer Scheme **(Dickinson et al, 1986)**
- Vegetation Lifeform **(Running et al, 1995)**

Land cover data based on U.S.G.S Land Use/Land Cover System Legend have been being used by many climate models such as MM5 and WRF climate models. Legend of U.S.G.S Land Use/Land Cover System is illustrated in Table 4.1.

Figure 4.5 illustrates GLCC based on USGS land use/cover legend which is also used in WRF modeling system.

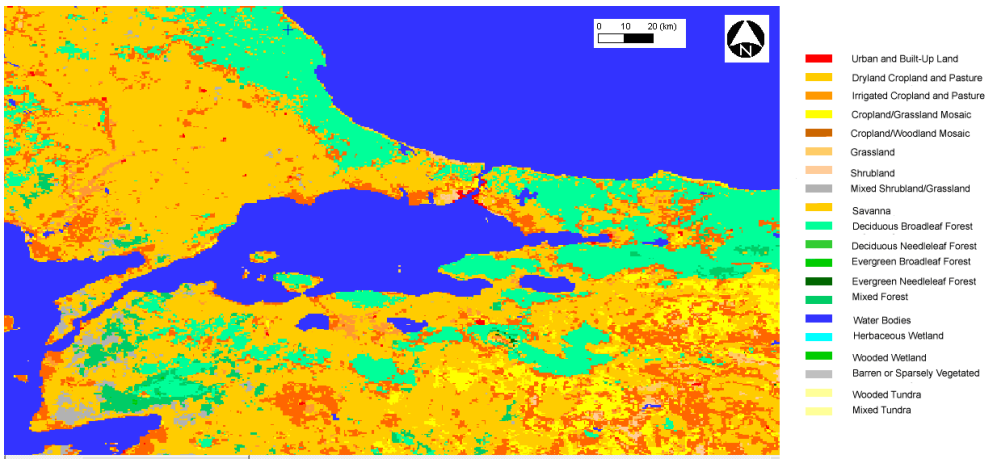

Figure 4.5: GLCC Based on USGS Land Use/Cover Legend

Table 4.1: USGS Land Use/Land Cover System Legend (Modified Level 2)

Value	Code	Description
1	100	Urban and Built-Up Land
2	211	Dryland Cropland and Pasture
3	212	Irrigated Cropland and Pasture
4	213	Mixed Dryland/Irrigated Cropland and Pasture
5	280	Cropland/Grassland Mosaic
6	290	Cropland/Woodland Mosaic
7	311	Grassland
8	321	Shrubland
9	330	Mixed Shrubland/Grassland
10	332	Savanna
11	411	Deciduous Broadleaf Forest
12	412	Deciduous Needleleaf Forest
13	421	Evergreen Broadleaf Forest
14	422	Evergreen Needleleaf Forest
15	430	Mixed Forest
16	500	Water Bodies
17	620	Herbaceous Wetland
18	610	Wooded Wetland
19	770	Barren or Sparsely Vegetated
20	820	Herbaceous Tundra
21	810	Wooded Tundra
22	850	Mixed Tundra
23	830	Bare Ground Tundra
24	900	Snow or Ice
99		Interrupted Areas (Goodes Homolosine Projection)
100		Missing Data

4.4.2 Global Land Cover 2000

Joint Research Center has produced a new global landcover classification for the year 2000 (GLC2000), in collaboration with over 30 research teams from around the world. The project was carried out to provide accurate baseline landcover information to the International Conventions on Climate Change, the Convention to Combat Desertification, the Ramsar Convention and the Kyoto Protocol.

Furthermore, the GLC2000 land cover database has been chosen as a core dataset for the Millennium Ecosystems Assessment. This means in particular that the GLC2000

dataset is a main input dataset to define the boundaries between ecosystems such as forest, grassland, and cultivated systems.

In contrast to former global mapping initiatives the GLC2000 project is a bottom up approach to global mapping. In this project more than 30 research teams have been involved, contributing to 19 regional windows. Each defined region was mapped by local experts, which guaranteed an accurate classification, based on local knowledge.

Each regional partner used the VEGA2000 dataset, providing a daily global image from the Vegetation sensor onboard the SPOT4 satellite. Figure 4.6 illustrates the result of GLC2000 for the study region with GLC legend illustrated in Table 4.2.

Table 4.2: GLC2000 Global Legend

Class Name	**Code**
Tree cover, broadleaved evergreen, closed to open (>15%)	1
Tree Cover, broadleaved deciduous, closed (>40%)	2
Tree cover, broadleaved deciduous, open (15-40%)	3
Tree cover, needleleaved evergreen, closed to open (>15%)	4
Tree cover, needleleaved decidous, closed to open (>15%)	5
Tree cover, mixed leaftype, closed to open (>15%)	6
Tree cover, closed to open (>15%), regularly flooded, fresh or brackish water:	7
Tree cover, closed to open (>15%), regularly flooded, saline water: Mangroves	8
Mosaic of tree cover and other natural vegetation (crop component possible)	9
Shrubcover, closed to open (>15%) , evergreen(broadleaved or needleleaved)	11
Shrubcover, closed to open (>15%), deciduous (broadleaved)	12
Herbaceous cover, closed to open (>15%)	13
Regularly flooded (> 2 month) Shrub or Herbaceous cover, closed to open	15
Cropland (upland crops or inundated/ flooded crops as e.g. rice)	16
Mosaic of Cropland / Tree cover/ Other Natural Vegetation	17
Bare Areas	19
Water Bodies (natural or artificial)	20
Snow or Ice (natural or artificial)	21
Urban Areas	22
Tree Cover, burnt (mainly boreal forests)	10
Sparse Herbaceous or sparse Shrub cover	14
Mosaic of Cropland / Shrub or Herbaceous cover	18

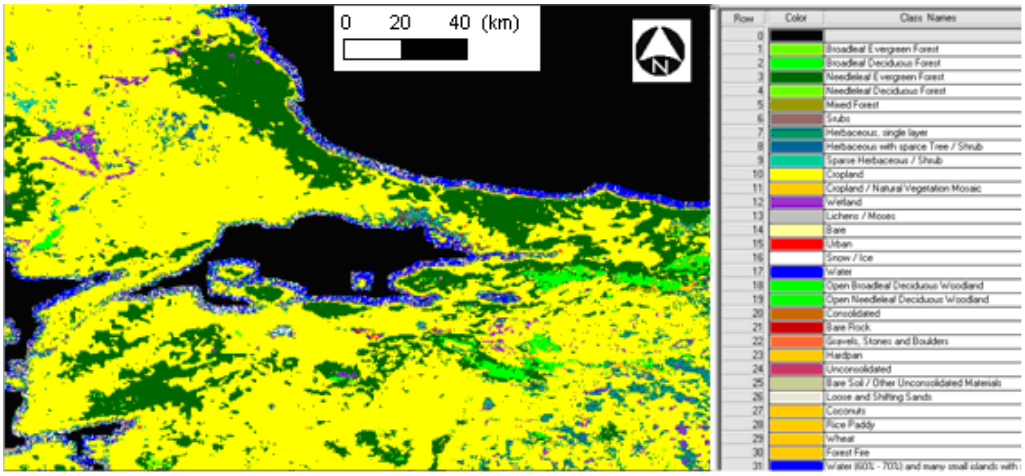

Figure 4.6: GLC2000 Classification

4.4.3 UMD Land Cover Classification

The University of Maryland Department of Geography generated this global land cover classification collection in 1998. Imagery from the AVHRR satellites acquired between 1981 and 1994 were analyzed to distinguish fourteen land cover classes. This product is available at three spatial scales: 1 degree, 8 kilometer and 1 kilometer pixel resolutions **(Hansen et al, 2000).** Figure 4.7 illustrates the classification result of UMD for the Marmara Region and Table 4.3 is the legend for UMD classification.

Table 4.3: UMD Classification Legend

Value	Label
0	Water
1	Evergreen Needleleaf Forest
2	Evergreen Broadleaf Forest
3	Deciduous Needleleaf Forest
4	Deciduous Broadleaf Forest
5	Mixed Forest
6	Woodland
7	Wooded Grassland
8	Closed Shrubland
9	Open Shrubland
10	Grassland
11	Cropland
12	Bare Ground
13	Urban and Built

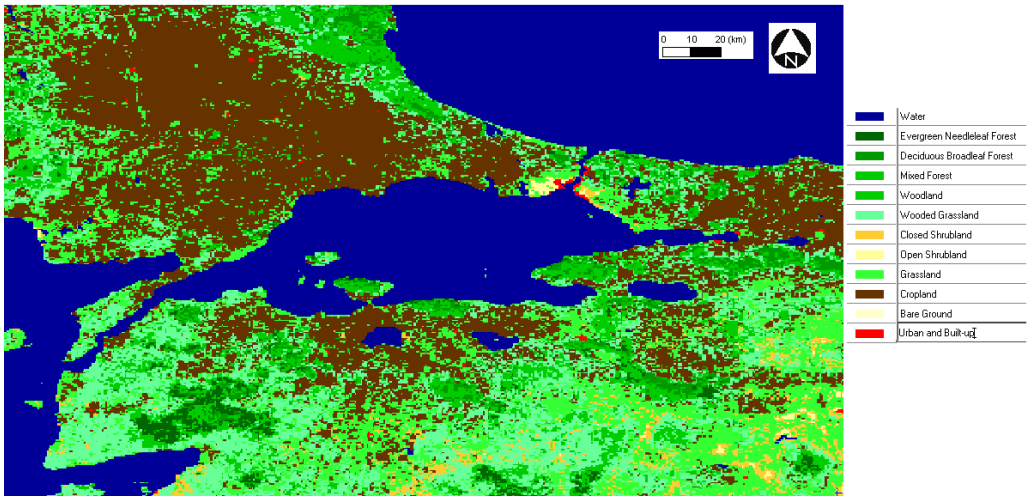

Figure 4.7: UMD Classification Result for the Study Area

4.5 Ancillary Data

Ground photographs, Digital Elevation Model, field samples, 1/25 000 scaled topographic maps, forest maps, socioeconomic data were used in this study. Most of the maps, photographs and field samples were used to select training sites and perform accuracy assessment for the classification.

Digital elevation model was used to classify vegetation types based on their elevations and in regional climate modeling.

Figure 4.8 is a ground truth photograph for evergreen forest.

Figure 4.8: Ground photograph for evergreen forests

5. CASE STUDY

5.1 Digital Image Processing of Satellite Images

Several digital image processing techniques were conducted to remove atmospheric, radiometric and geometric distortions available within satellite images and make images more understandable. At the last stage of digital image processing procedure, images were classified to obtain land cover maps of the study area.

5.1.1 Radiometric and Atmospheric Correction

Digital numbers of all images were first converted into radiance then to at satellite reflectance values. Equations, gain and offset parameters presented in title 3.1.1 were used for the procedure. Following example illustrates the calculation of radiance value of DN=125 for the first band of Landsat ETM image.

Gain = 0.7756863 mW cm^{-2} sr^{-1} μm^{-1}

Bias = -6.1999969 mW cm^{-2} sr^{-1} μm^{-1}

L = -6.1999969 + (0.7756863)xDN

L= -6.1999969 + (0.7756863)x125

L= 90.76079 W m^{-2} sr^{-1} μm^{-1}

Using gain and offset values of each band, radiance values of all images were calculated.

One of the Landsat MSS has line drop error and this error was corrected by replacing the pixels of this line with the average of the above and below pixels.

Atmospheric correction of the satellite images were performed using dark object subtraction method since this approach is a widely used by many scientists and it is simple as explained in title 3.1.1.

Dark objects having very small surface reflectance namely lakes, seas or other water bodies were selected for each Landsat frame. It is assumed that these minimum reflectance values in the histograms from the entire scenes are attributed to the effect of the atmosphere. The correction is applied by subtracting the minimum observed value, determined for each specific band, from all pixel values in each respective band. After employment of DOS, haze was removed, and the surface features blocked by haze were recovered.

5.1.2 Geometric Correction

Six Landsat MSS images and six Landsat ETM images were geometrically corrected using affine transformation model presented in title 3.1.2. Landsat MSS images were obtained from 192, 193 and 194th paths and 31st and 32nd rows. Landsat ETM images were obtained from 179, 180 and 181th paths and 31st and 32nd rows. All images were transformed into latitude and longitude coordinate system with WGS 84 Datum. Locations which can be easily and accurately identified such as highway and road intersections, ports and bridges and approximately homogeneously distributed on the images were selected as GCPs. Ground coordinates of these points were provided from 1:25,000 topographical map and other satellite sensor images.

Table 5.1: Geometric Model Parameters

Parameter	Value
a_0	41357.078
a_1	0.196
a_2	-0.035
b_0	-914883.741
b_1	0.0348
b_2	0.1967

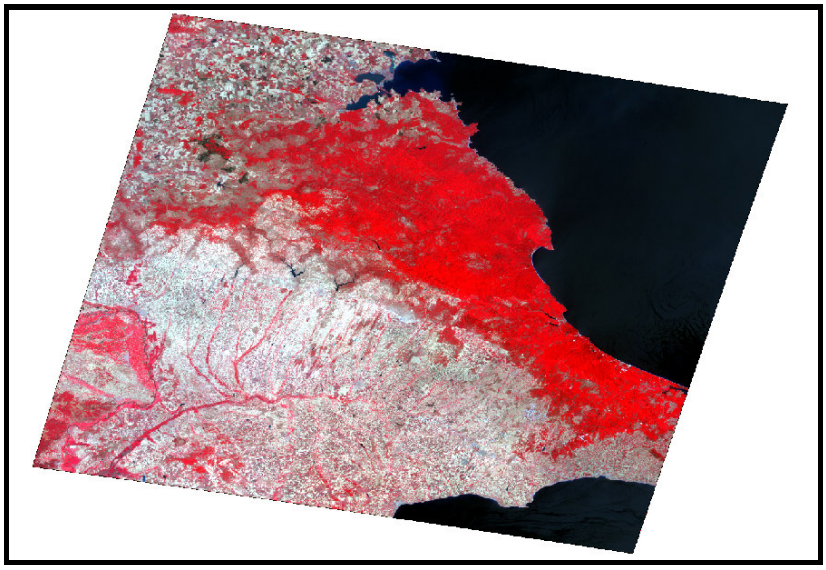

Figure 5.1: Original Landsat ETM Image (Bands:4,3,2)

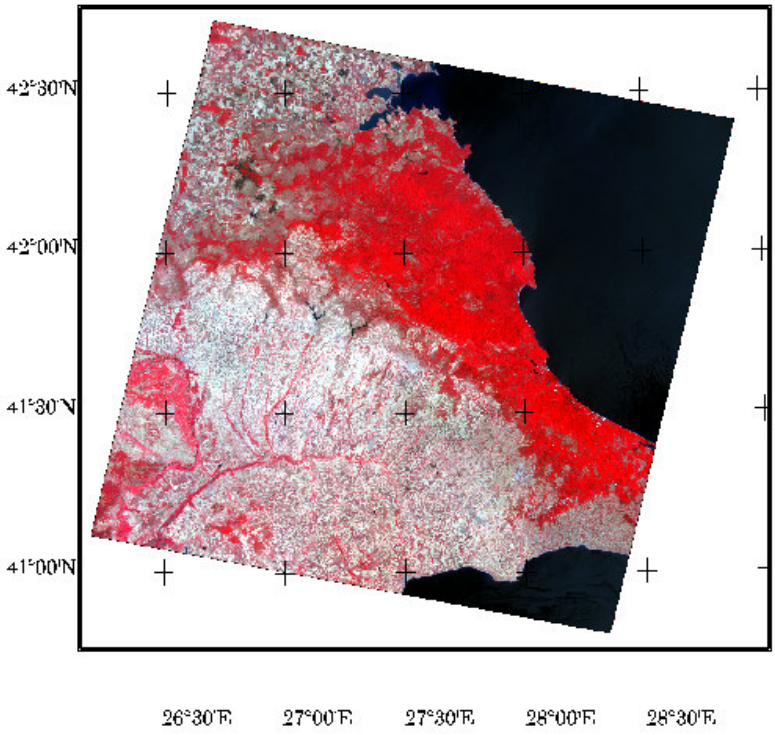

Figure 5.2: Geometrically Corrected Landsat ETM Image (Bands:4,3,2)

For the geometric corrections of Landsat images the affine model parameters required were estimated by the least square adjustment. Each geometric correction has Root Mean Square Error (RMSE) lower than 0.5 pixel. Transformation parameters derived for 181/31 Landsat ETM image is shown in Table 5.1.

The original Landsat ETM image for the frame of 181/31 is shown in Figure 5.1 whereas the geometrically corrected image is shown in Figure 5.2.

5.1.3 Use of semivariograms for the selection of appropriate band combinations and determination of abrupt land cover changes

In remote sensing, accurate usage of multi-spectral satellite sensor data introduces important information to many studies. Incorrect usage of different band combinations or panchromatic band directly affects the results obtained from satellite image data. In this part of the research, we **(Kaya and Sertel, 2006)** analyzed Ikitelli region in İstanbul European side, having the highest spatial growth. The semivariogram model approach was applied to 1992 and 2001 Landsat TM and ETM images to find out the best band combinations for the study. In general, correlation matrix of satellite bands is used to decide selection of appropriate band combinations. Using this matrix, one can have general idea about band combinations but it is hard to find out appropriate bands for different land cover data types using this approach. On the other hand, we could find out the best band combinations for different land cover data types using semivariograms of different land categories. To perform this, twelve transects having 10 km length and parallel to each other which represents the pilot area were selected and their semivariograms were plotted after the geometric correction of each image. Lag distance was taken as 90 m and active lag distance was taken as the half of the transect**.**

Investigation of semivariograms of the same transect for different bands (Figure 5.4 left side and right side) revealed that semivariograms of first three bands representing the visible region are very similar to each other. On the other hand, semivariograms of the same transect for infrared band show differences. These differences illustrated that land cover changes occurred in urban areas were determined clearly using infrared bands. Since Marmara Region has different land cover types, all of the bands except the thermal band were used in the study. However, selected bands from the semivariogram analysis were considered and used in visual interpretation of different land cover types. For example infrared bands were used for the visual interpretation of urban surfaces, visible bands were used for the interpretation of water bodies (Figure 5.3, 5.4).

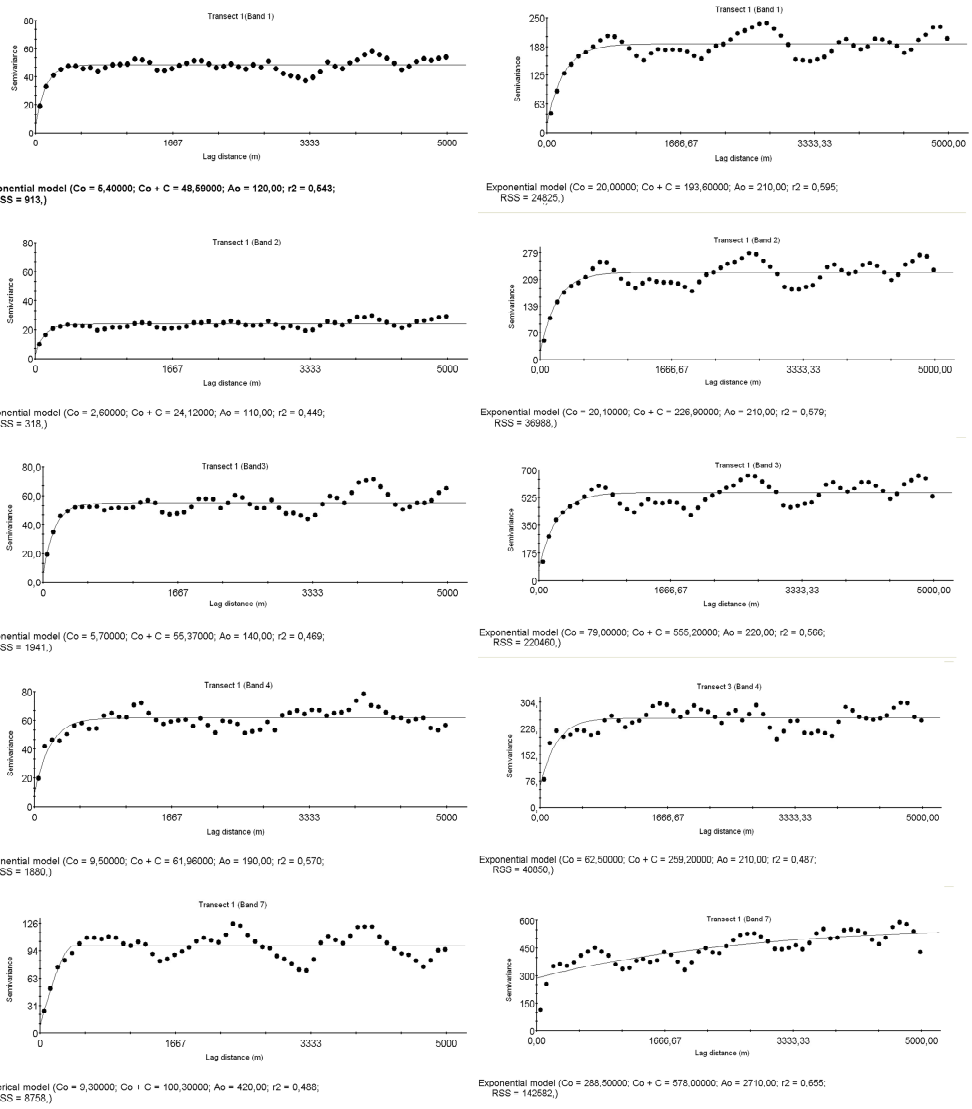

Figure 5.3: Semivariograms of Transect 1, Left side: 1992 Landsat TM Image, Right Side: 2001 Landsat ETM Image

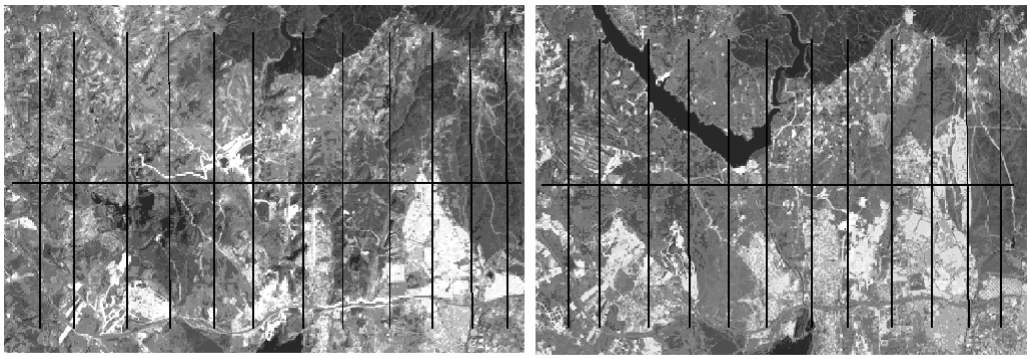

Figure 5.4: Locations of Transects. 1992 Image (left), 2001 Image (right)

5.1.4 Classification

Both supervised classification using Maximum Likelihood technique and unsupervised classification using ISODATA clustering were conducted to classify imageries. Each frame was analyzed independently, in some regions especially for urban and sandy areas, pilot regions were created and they were classified separately to minimize the mixed pixel problem.

There were spectral mixing problem for crop and urban areas. To eliminate this effect, pilot areas determined by semivariogram and spatial profile approach were subsetted from images and evaluated separately. Therefore, urban areas were acquired more accurately.

It is easier to find ground truth data like maps, ground surveys and photographs for current condition which can be used during classification. However, ground truth data for the past was limited and only topographic maps were used to assist the classification of past images. There were some problems for Landsat MSS data because of sensor characteristics. Quality, spectral and spatial resolution of Landsat ETM data was better then Landsat MSS, therefore classification results for Landsat ETM was better. However, both Landsat ETM and MSS data are more accurate and higher in quality compared to NOAA AVHRR images which were used to derive some global land cover data sets and the land cover data set within the model.

Besides the topographic maps, sample points collected by **Okyar (1999)** were used for training site selection and classification accuracy assessment (Figure 5.5).

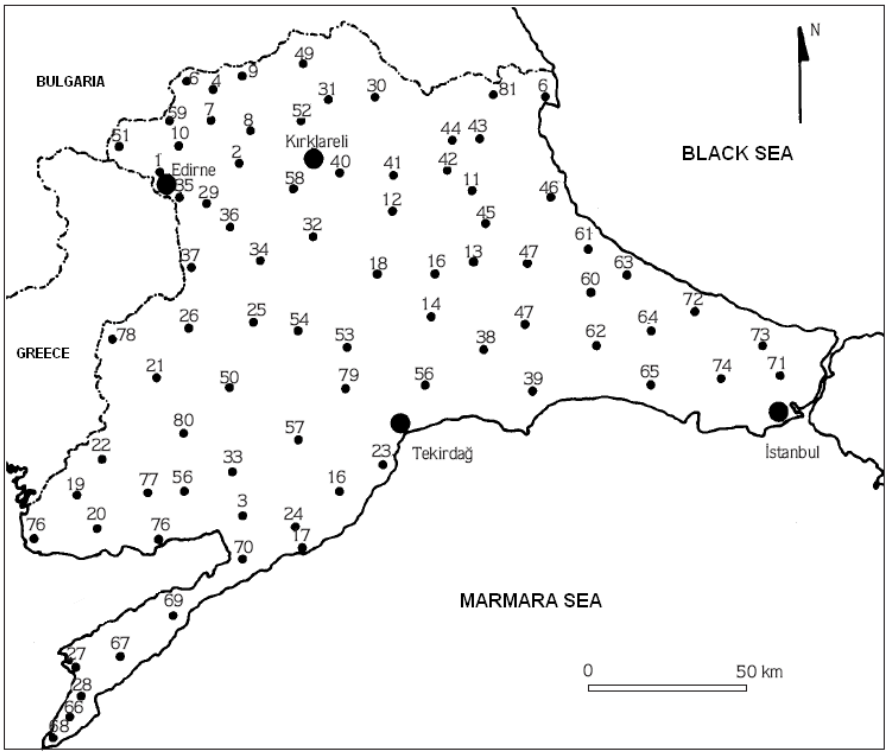

Figure 5.5: Location of Sample Points (Source: **Okyar, 1999**)

Classified images were aggregated to 1 km and change detection analyses were performed from these 1 km classified images which were then implemented into WRF modeling system.

Accuracy assessments of classified images were performed from aggregated images since these data were used for land cover change determination, land cover comparison with global datasets and climate modeling. 250 ground points for each classification were selected and the comparison made between classification result and real land cover. Confusion matrix and kappa statistics explained in title 3.1.4.3 were used to determine the accuracy of classified images. 1975 classified image has overall accuracy of 80% and kappa value of 79%, 2005 classified image has overall accuracy of 83% and kappa value of 82%.

5.2 Land Cover Data and Land Cover Change

The use of satellite imagery has made the mapping of land cover much easier and faster. Currently, it is possible to look at land cover from global to local scales using satellite imageries. Classification technique was applied to satellite images to obtain

land cover data and land cover data of different years were compared to obtain land cover change.

5.2.1 Preliminary Studies to Determine Land Cover Change in İstanbul

The semivariograms in the previous section were used to find out land cover change in Ikitelli region. Quantity and direction of the spatial variations were related with the semivariogram parameters. The shape, range, nugget, and sill of the twelve semi-variograms were interpreted to determine the location of abrupt change areas within the pilot region. Figure 5.4 illustrates band semivariograms of transect 1 for 1992 and 2001, a location where urbanism occurred between these years. Semivariograms of band 1,2, 3 and 4 are different for both years emphasizing a change in this region. Many other examples showed that semivariograms for different years were very similar to each other, if there were not any land cover change in related region. As a result of land cover change pixel values changed causing differences in semivariances therefore in semivariograms.

We **(Kaya and Sertel, 2006)** found that the semivariogram shape was different for 1992 and 2001 transects if the area faced with significant land cover change, but similar if the area did not change. Semivariogram range was used to quantify coarse spatial variability. The transects covering areas of significant land cover change had even larger increases in range whereas transects covering unchanged areas had similar ranges for 1992 and 2001.

In some cases, the semivariograms obtained does not pass through the origin and have nugget effects which may be the result of short-range spatial variation that had not been measured (that is, variation within, rather than between, pixels) **(Sertel et. al, 2007).** The nugget therefore provides information about fine scale spatial variation. The transects covering areas of changed areas had a much larger increase in nugget than the transects of unchanged areas.

Figure 5.6 is the result of our study **(Sertel et. al, 2007)** which illustrates a transect covering an unchanged region (a,b) and transect covering a region changed significantly (c,d).

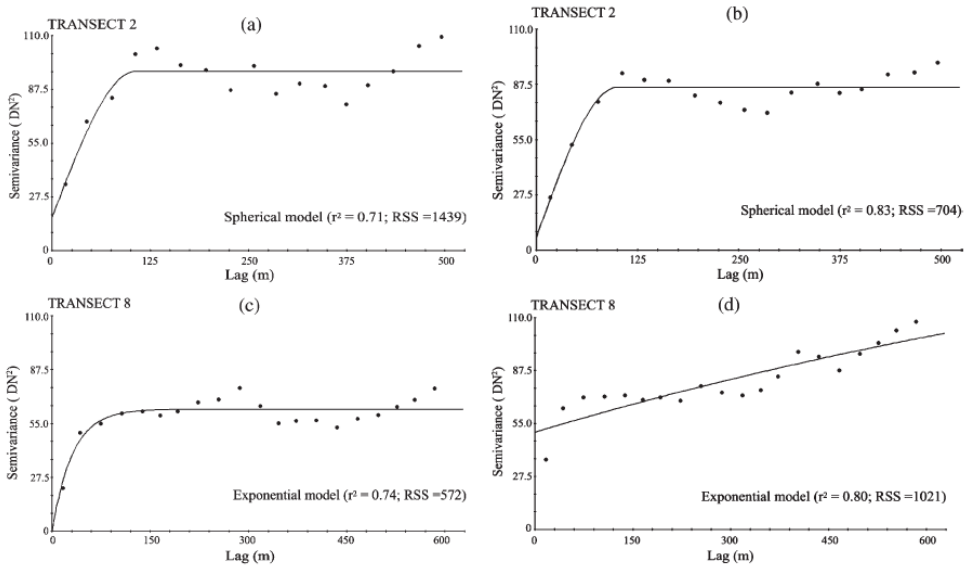

Figure 5.6: Semivariograms of Unchanged Region (a-b), and Changed Region (c-d).

We conducted another study **(Kaya et. al, 2007)** to analyze the changes in Kilyos-Karaburun coastline between 1984 and 2001 using spatial profiles. The spatial profiles obtained from Kilyos-Karaburun site clearly revealed the negative land cover change in the area. Figure 5.7 illustrates the spatial profile of a transect having 9800 m length and located on the northwest through northeast direction of Kilyos Karaburun coastal line. This transect was located on the sea in 1984 therefore the spatial profile of this transect follows a straight line with lower brightness values. Spatial profiles of this transect for 1992 and 2001 years show significant changes due to the filling of the coast with mining activities. Considering the northwestern part of the transect as a starting point, 900-2100 m, 4500-6800 m and 7200-9000 m distance of this transect has higher brightness values in 1992 delineating the filled areas in the sea. The spatial profile of the transect in 2001 has higher brightness values in 700-900 m, 4500-6800 m, and 7200-9000 m distances, pointing out the changed areas in coastal line. Comparison of 1992 and 2001 profiles figured out the erosion impact on coast through the northwest direction in the transect (Figure 5.7). There was considerable reduction in filled areas between 1992 and 2001 as a result of coastal erosion **(Kaya et. al, 2007).**

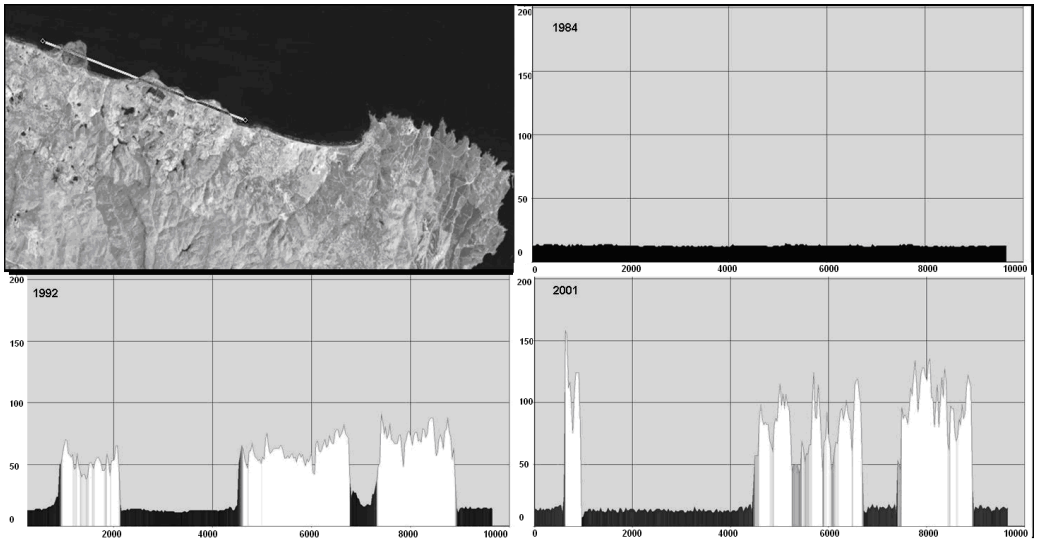

Figure 5.7: Spatial Profiles and Location of the Transect

We **(Saroglu et al, 2003)** examined the region between Sile and Agva, located in northern part of İstanbul along the Black Sea coastline using satellite images and a digital elevation model. We used 1987 Landsat TM and 2001 Landsat ETM data. Coastline changed during this period and the area of agricultural lands decreased from 2387.52 ha (in 1987) to 600.93 ha (in 2001) in this region.

5.2.2 Land Cover Change in Marmara

Land cover changes occurred in Marmara Region both in coastal areas and inner parts as a result of human activities. Metropolitan cities in the region like İstanbul, Adapazarı and Bursa raced with industrialization and immigration which resulted in increase of urban and built-up areas. Besides, in İstanbul forest areas and sand dunes were destroyed by open mining activities performed in Black Sea coast of European part. As a result of filling of materials extracted from open mining areas into the sea, ecosystem and topographic structure were damaged **(Kaya et. al, 2007).** In this region, natural land cover changes also occurred as a result of coastal erosion.

Classification results of 1975 and 2005 are shown in figure 5.8 and 5.9.

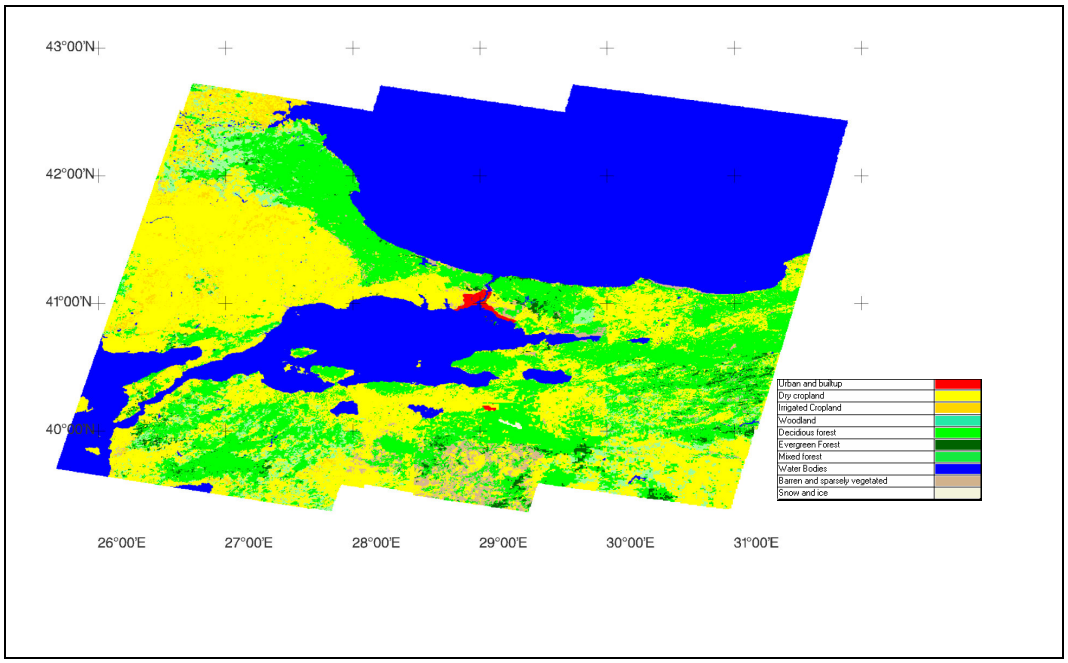

Figure 5.8: Classification result of 1975

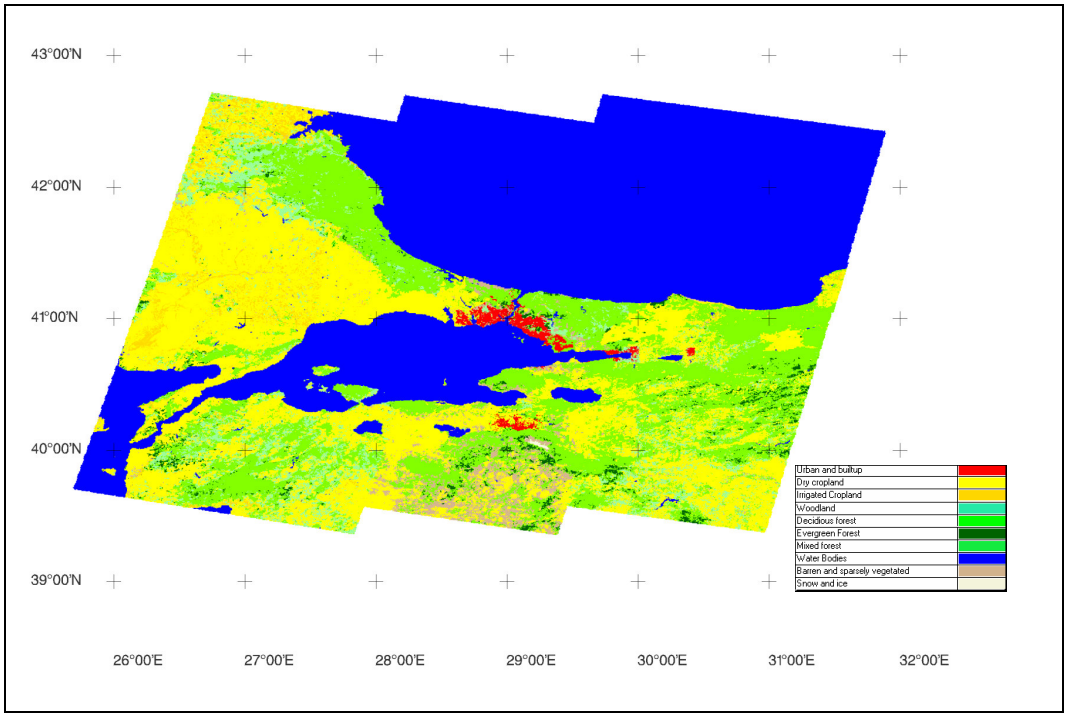

Figure 5.9: Classification result of 2005

There were three significant land cover changes in Marmara between 1975 and 2005. Firstly, urban areas increased dramatically between this period. Figure 5.10 a,c and e show the urban areas in 1975 whereas 5.10 b,d and f shows urban areas in 2005 in original images. Figure 5.10 a and b show urban sprawl in İstanbul, figure 5.10 c,d in

Bursa and figure 5.10 e,f in Izmit. These cities are the highly industrialized zones of the Marmara region. Also, as explained in section 4.2 population of İstanbul increased 4 times and population of Bursa increased 4.5 times between 1970 and 2000, which are relatively close years to land cover data. Increase in urban areas can be seen from classified images with red color (Figure 5.8 and 5.9). Both original images and classified images illustrate the increase in urban areas. According to classification results, total urban areas were 25659.3 ha in 1975 but 104966.1ha in 2005. In thirty years period, urban areas increased four times in the Marmara Region.

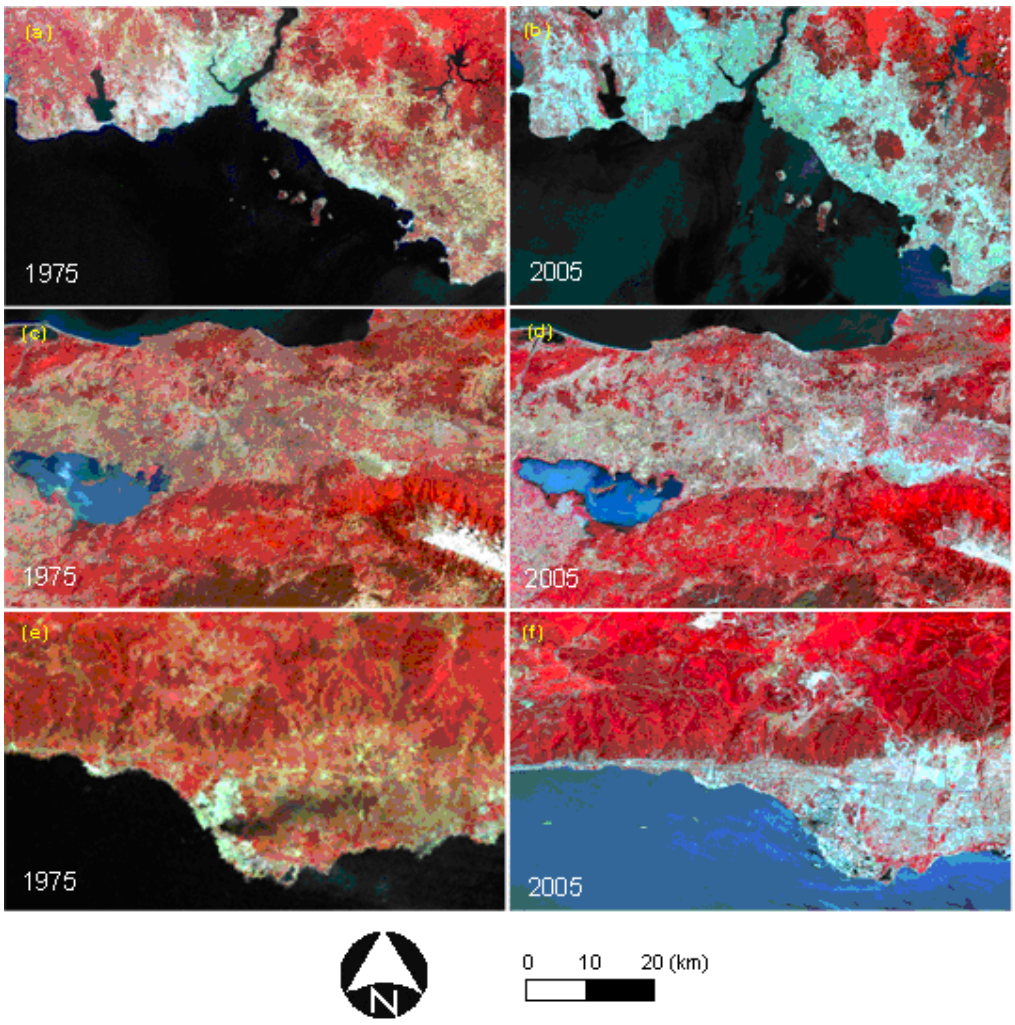

Figure 5.10: Urban Sprawl in İstanbul (a), Bursa (b) and Izmit (c). Band Combinations 3,2,1 for 1975; 4,3,2 for 2005

Secondly, there was a decrease in crop areas between 1975 and 2005. The total crop area was 4480105 ha in 1975 whereas 4364569 ha in 2005. 45906.1 ha crop area was converted into urban area and 23843.44 ha crop area was converted to water area

between this period. İstanbul Metropolitan Municipality conducted some regulations in water basins to increase the amount of fresh water. Alibeykoy and Sazlidere dams were constructed to increase water holding capacity (Figure 5.11). Some regions in Anatolian and European side of İstanbul was crop in 1975 but became urban in 2005 (Figure 5.10 a, b).

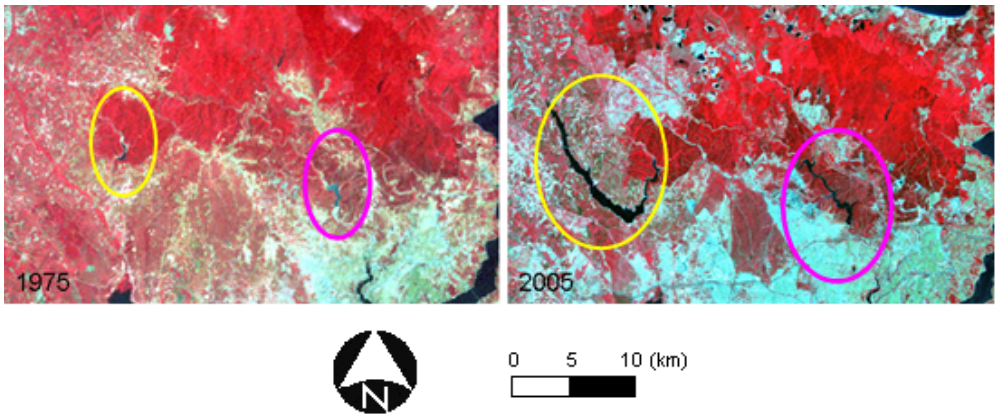

Figure 5.11: Changes in Alibeykoy and Sazlidere

There were 4123348 ha and 4090827 ha forest area in 1975 and 2005, respectively. 14133.31 ha barren and sparsely vegetated land transformed into urban but 41760 ha forest land transformed into barren and sparsely vegetated area between 1975 and 2005. Figure 5.12 illustrates the conversion of forest areas into barren and sparsely vegetated areas as a result of open mining activities discussed in previous section. Also coastline in this region changed with the filling of mining residuals into the black Sea.

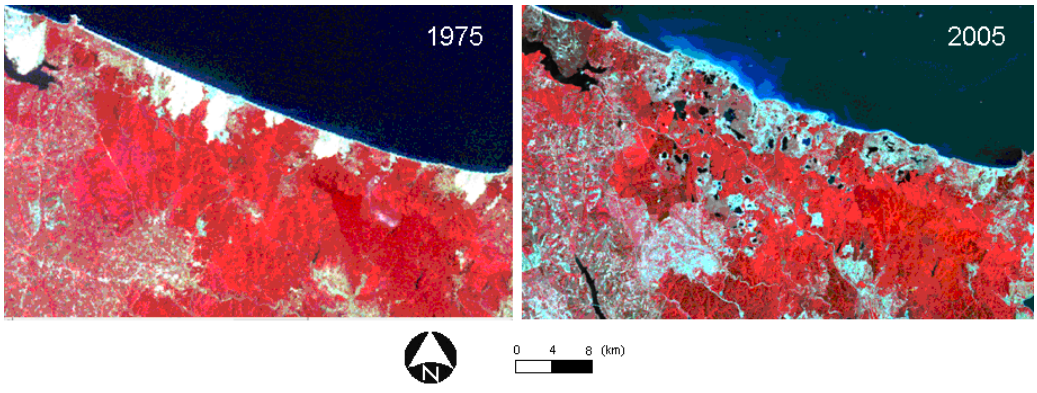

Figure 5.12: Land Cover Change in European Side Coastline

5.2.3 Comparison of Land Cover Data with other Global Land Cover Data Sets

In this section, land cover data created from 2001-2005 Landsat images was aggregated to 1 km resolution and comparisons were made between this data and global land cover datasets namely GLC2000, GLCC and UMD explained in Section 4.4. Each global dataset has problems for some land cover classes and for some locations.

First of all, there are significant problems for land-sea boundaries in GLC2000 data. The boundaries between land and sea can be easily discriminated in GLCC, UMD and Landsat derived data, whereas this is not the case in GLC2000. In addition to boundaries, Bosphorus and Dardanelles straights can not be identified in this data set (Figure 5.13). There are considerable noises along the land sea boundaries in GLC2000. Also, some irrigated and dry croplands in Thrace Region were classified as wetlands in GLC2000.

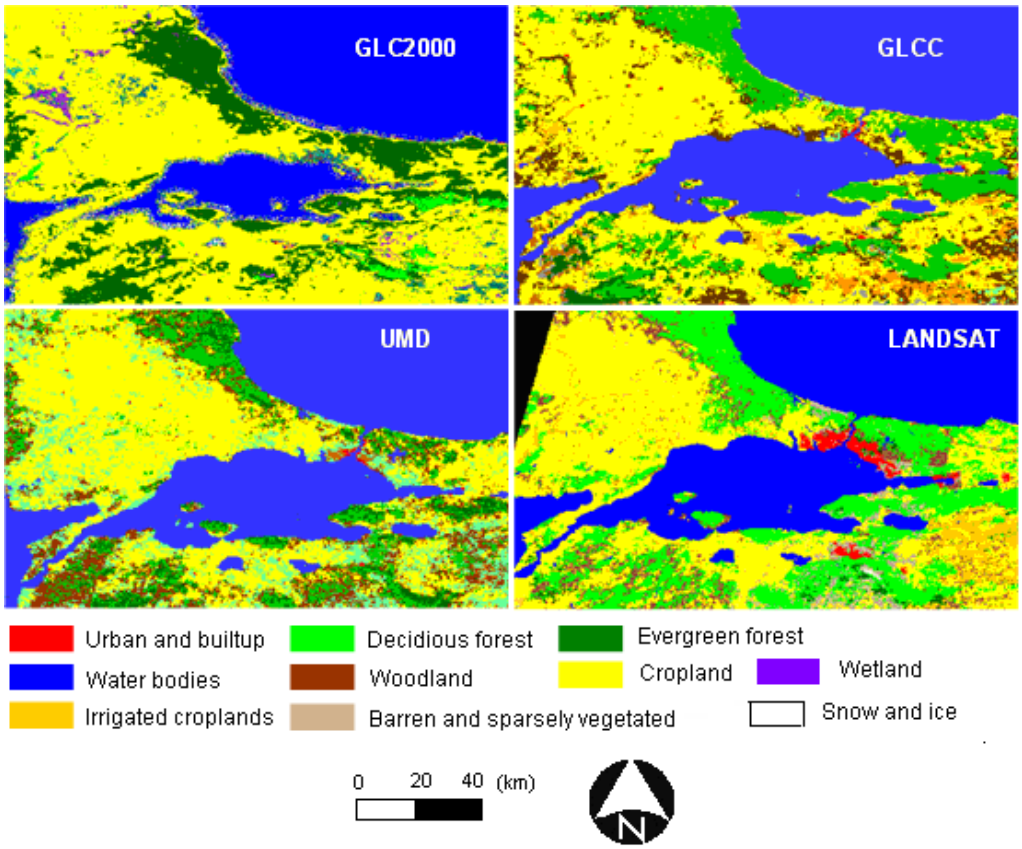

Figure 5.13: Different Land Cover Data Sets

None of the datasets can represent urban areas correctly in the cities of İstanbul, Izmit, and Bursa (Figure 5.14). Only a small area along the Bosphorus was

represented as urban in GLCC and UMD. Most of the urban areas were represented as grassland in UMD data. Moreover, sparsely vegetated areas along Kilyos-Karaburun coastline were classified as grassland in this data set.

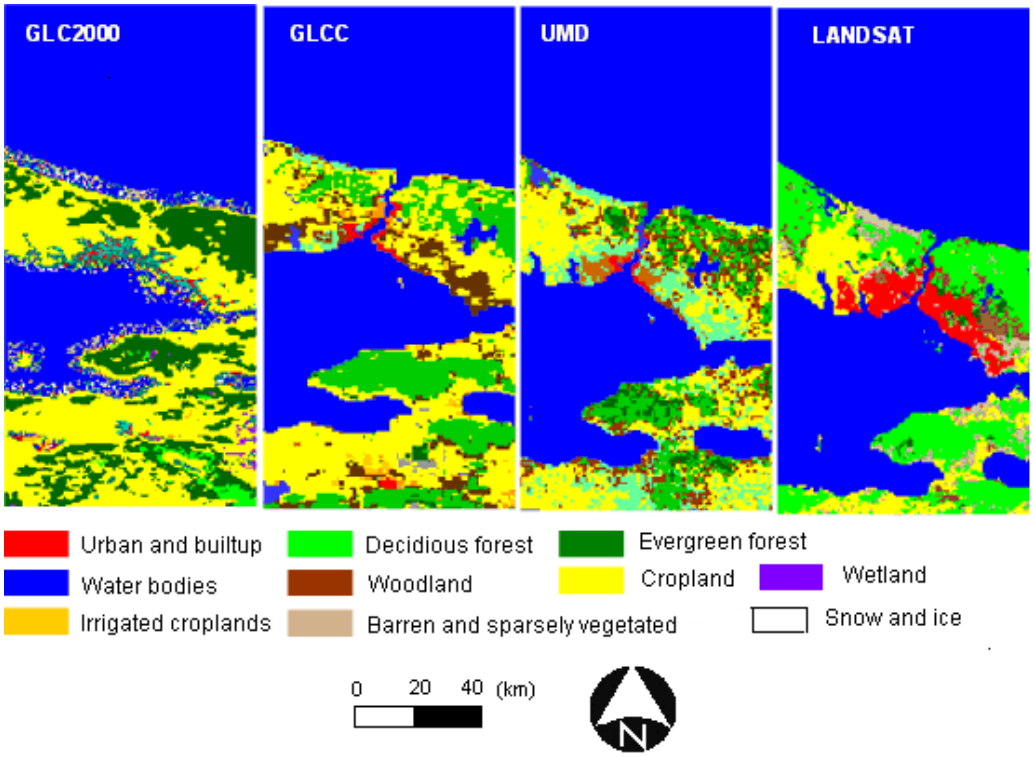

Figure 5.14: Comparison of Different Land Cover Data Sets

In GLC2000, most of the Marmara Region was represented as croplands and there were problems in some forest areas. Basic forest type is deciduous forest in the Marmara Region which can be seen in GLCC, UMD and Landsat data. However in GLC2000, most of the deciduous forests were classified as evergreen forest. UMD land cover data seems the simplified version of USGS data. USGS data has 24 four classes, whereas UMD has 13 classes.

5.2.4 Comparison of Produced Current Land Cover Data with Model Land Cover Data

Detail analyses were conducted for USGS data, since it is the data set used in WRF climate model. USGS land cover data is not up-do-date and accurate for some parts of the Marmara Region, especially for İstanbul where significant land cover changes occurred.

As an example, both original satellite images and produced land cover data showed the expansion of urban areas into the İstanbul metropolitan area, but in the WRF land cover data only a limited area along the Bosporus is shown as urban. Most of the urban areas were classified as woodlands in this data set (Figure 5.15).

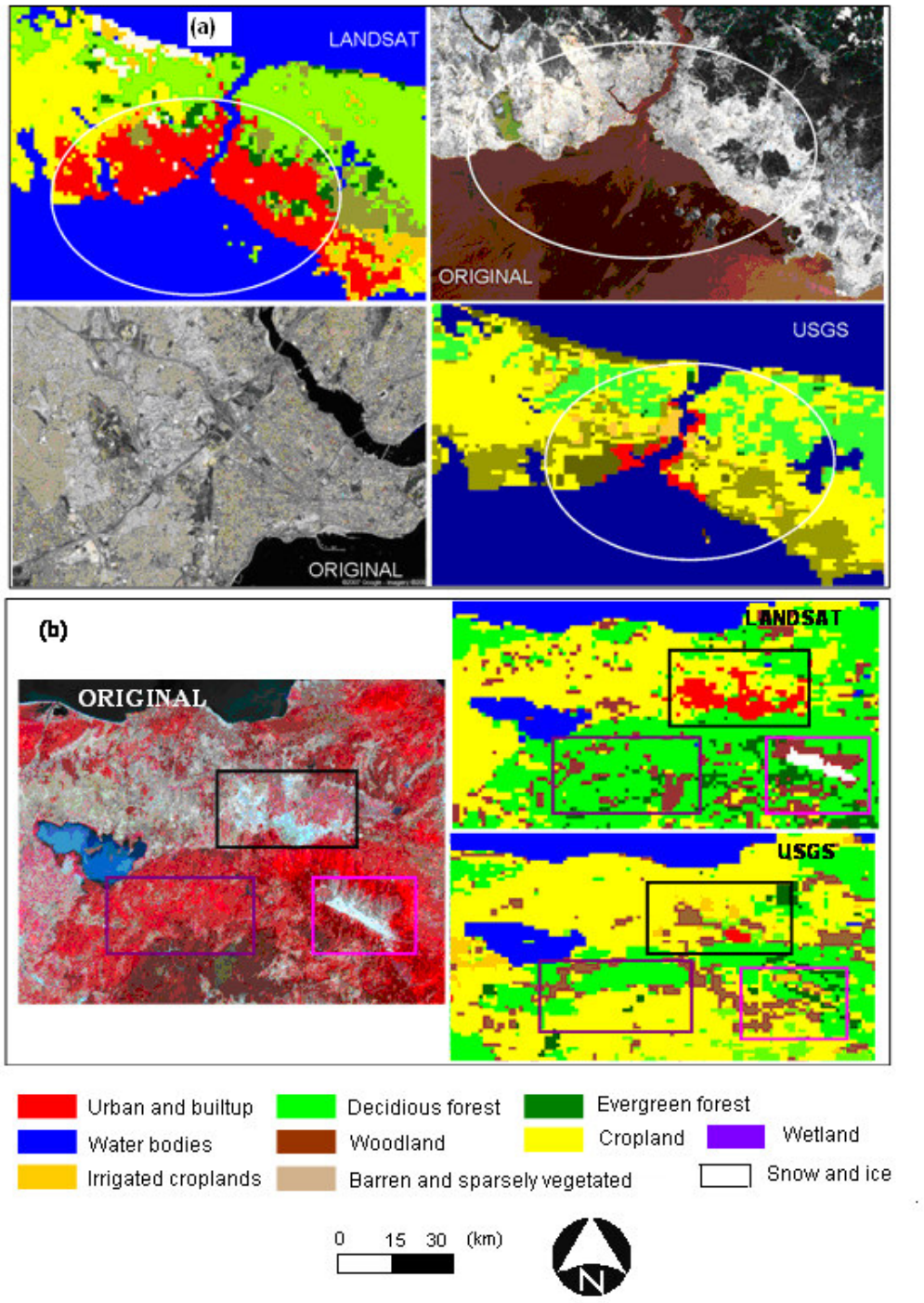

Figure 5.15: Comparison of New Land Cover Data with Model Land Cover Data With Emphasize on Urban Areas (in red)

Urban Heat Island in İstanbul was studied by **Karaca et al, (1995a, b)** and **Ezber et al (2007)**. They pointed out the temperature increase in İstanbul as a result of urbanization. **Ezber et al (2007)** fixed some parts of land cover data based on topographic maps and determined the inaccuracy in model land cover data. My results over İstanbul emphasized the inaccuracy of USGS data for urban areas.

There are problems in USGS data for other land cover classes in the Marmara Region. Landsat derived new land cover data indicated that the northern part of İstanbul is covered by evergreen and deciduous forest (verified by ground truth data), but the USGS data indicated that most of this region is covered with croplands (Figure 5.16)

In the northern part of the Marmara Region towards to Black Sea cost, there are bare grounds as a result of open mining activities. Details of region and changes occurred were explained in the previous section using spatial profiles. This barren land class can be identified in new Landsat derived land cover data, whereas the USGS data indicated this region as woodland.

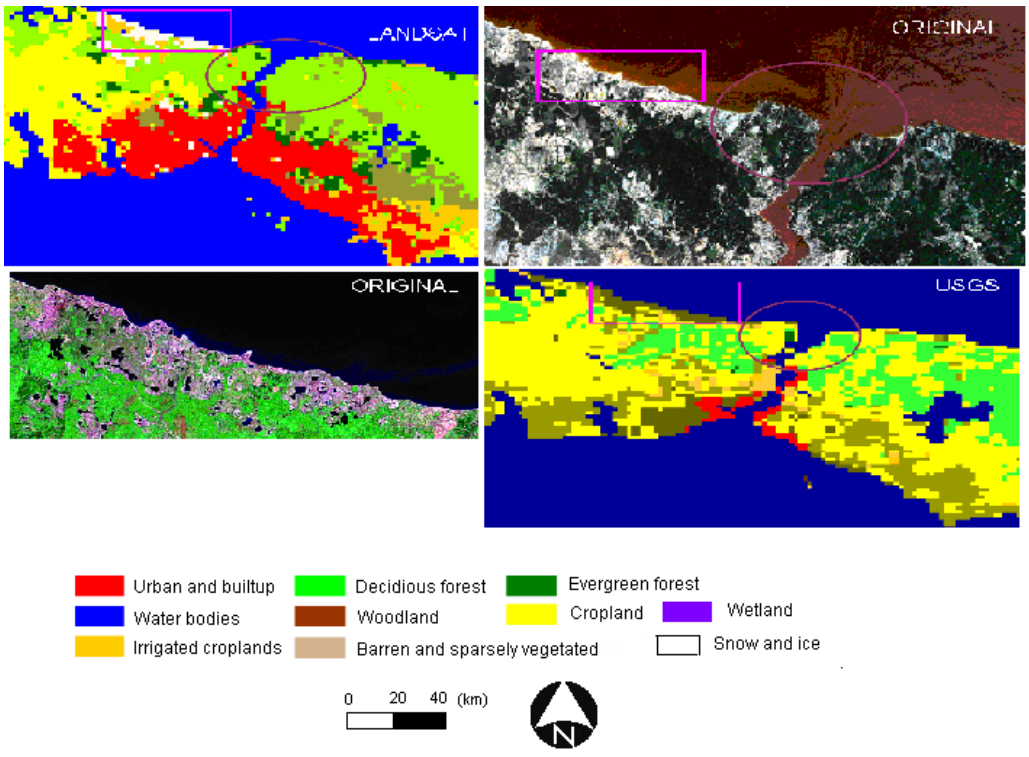

Figure 5.16: Comparison of New Land Cover Data with Model Land Cover Data with Emphasize on Forest, Crops, Barren and Woodland

USGS land cover data is generally successful for water bodies and land/water boundaries but one important problem was discovered for Ömerli Water Basin. USGS data illustrated Ömerli Basin extremely larger then its original size, which might cause problem for the calculation of latent and sensible heat fluxes. Figure 5.17 emphasizes Ömerli Water Basin with original Landsat TM, new land cover and USGS land cover data. Water bodies have great importance on the amount of evaporation.

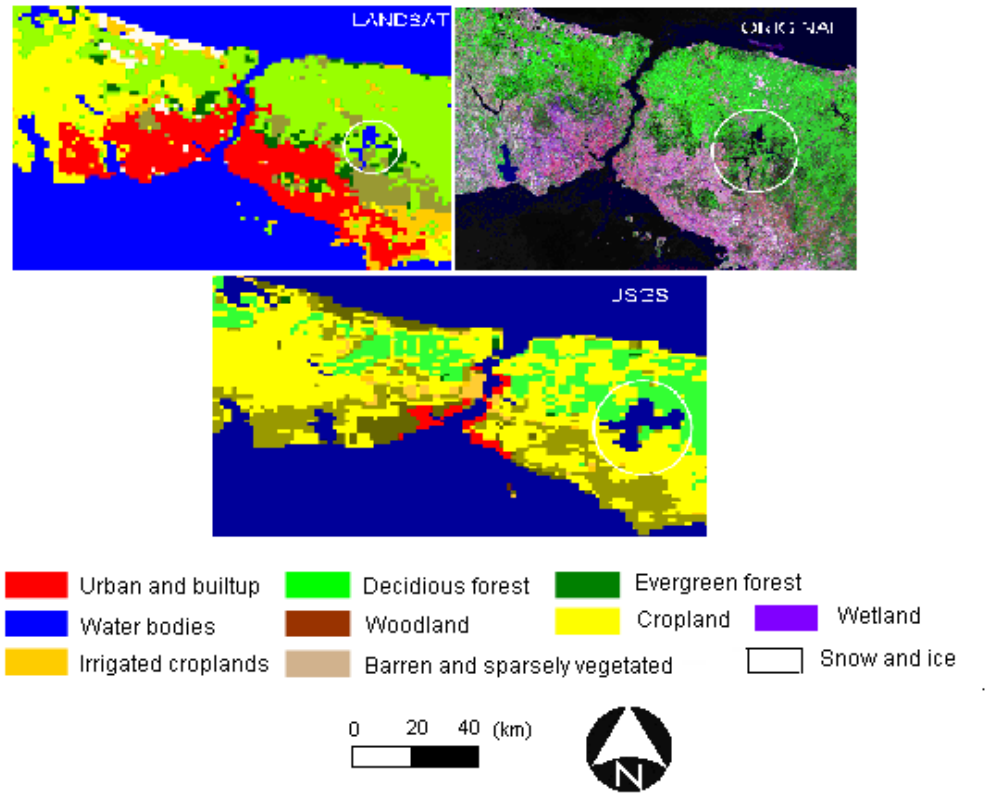

Figure 5.17: Comparison of New Land Cover Data with Model Land Cover Data with Emphasize on Water Areas (blue: water bodies)

5.3 Database Design

There are approximately 270 meteorological stations over Turkey, where the Marmara Region includes 35 of these stations. Available meteorological data was in ASCII format for daily maximum temperature, daily minimum temperature, daily mean temperature, daily average wind and daily total precipitation spanning from 1950s to 2006. Total number of records for each variable is given in the following table.

Since it is not an easy task to handle, retrieve and query these sizes of data, a meteorological database was created and data were structurally organized. Usage of the created database facilitated data retrieval, query analysis and incorporation of data into GIS.

Table 5.2: Total Number of Record for Each Meteorological Variable.

Variable Name	Total number of records
Maximum temperature	4715451
Minimum temperature	4727014
Mean temperature	4699147
Average wind	3458637

Totally six tables were created, five of them were for the variables collected in meteorological stations and the last table was for the description of station data and their geographical locations. Station data for the last table and ID for the other tables were selected as primary key which uniquely identifies each record in the table. Database was created as a relational database and relations were formed using Station ID fields which are common for each table. Tables and their fields were illustrated in the following figure.

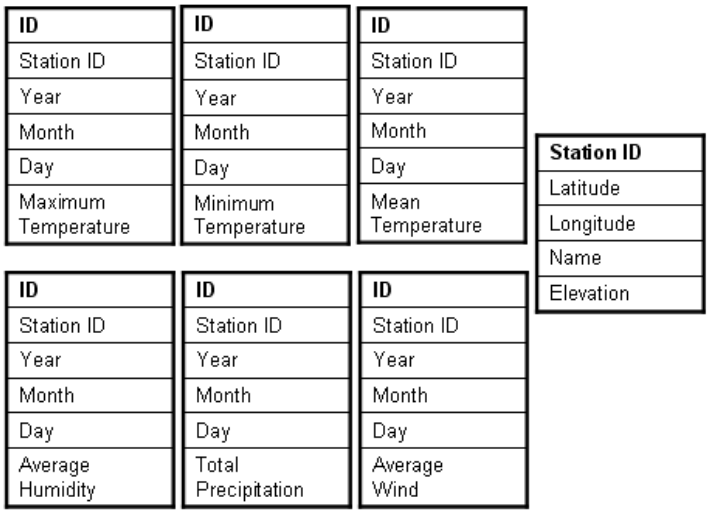

Figure 5.18: Database Design for Meteorological Data.

Once creating the meteorological database, it became easier to select and retrieve data for the determined period, region and parameter. In this study meteorological data of the Marmara Region (26°-32°E, 38°-43°N) for 2004 June, July and August

period was selected using appropriate queries. A sample query written in Structured Query Language (SQL) is as follow:

Selection of all variables for June-August 2004 period:

SELECT Max_temp_total.ID, Max_temp_total.Year, Max_temp_total.Month, Max_temp_total.Day, Max_temp_total.Maxtemp, Min_temp_total.Mintemp, Humd_total.Humd, Mean_temp_total.Meantemp, Wind_total.Wind **FROM** (((Max_temp_total **INNER JOIN** Min_temp_total **ON** Max_temp_total.ID=Min_temp_total.ID) **INNER JOIN** Humd_total **ON** (Max_temp_total.ID=Humd_total.ID) **AND** (Min_temp_total.ID=Humd_total.ID)) **INNER JOIN** Mean_temp_total **ON** (Max_temp_total.ID=Mean_temp_total.ID) **AND** (Humd_total.ID=Mean_temp_total.ID)) **INNER JOIN** Wind_total **ON** (Max_temp_total.ID=Wind_total.ID) **AND** (Mean_temp_total.ID=Wind_total.ID) **WHERE** (((Max_temp_total.Year)=2004) **AND** ((Max_temp_total.Month) Between 6 And 8));

The following figure illustrates the query result of maximum temperature for 2004 June-August period with latitude and longitude values of stations. It has 23976 records.

Latitude	Longitude	Year	Month	Day	MaxTemp
41.45	31.8	2004	8	16	24.5
41.45	31.8	2004	8	17	23.2
41.45	31.8	2004	8	18	22.3
41.45	31.8	2004	8	19	24.2
41.45	31.8	2004	8	20	25.5
41.45	31.8	2004	8	21	28.8
41.45	31.8	2004	8	22	27
41.45	31.8	2004	8	23	25
41.45	31.8	2004	8	24	20
41.98	33.77	2004	6	11	19.8
41.98	33.77	2004	6	12	21.6
41.98	33.77	2004	6	13	25.3
41.98	33.77	2004	6	14	24.6
41.98	33.77	2004	6	15	23.5
41.98	33.77	2004	6	16	24.7
41.98	33.77	2004	6	17	27.4
41.98	33.77	2004	6	18	25.3
41.98	33.77	2004	6	19	28

Record: 1 of 23975

Figure 5.19: Maximum Temperature for 2004 June-August in the Marmara Region.

5.4 Geographic Information Systems

Land cover data obtained for 1975, 2005 and USGS were transferred to GIS as different layers. Meteorological station data and model results were gathered in a database and this database was connected to GIS using spatial information of meteorological stations. Digital elevation model, census data and all other ancillary data were collected in GIS. All data were represented in common geographic latitude longitude system with WGS 84 datum.

Global land cover data sets and created Landsat land cover data were compared within the system to determine the differences between these data and problems in global data sets. Overlay analyses were also used to identify difference between data sets. Buffer zones were created around the meteorological stations to find out land cover changes around these stations and impact of these changes on climate simulations.

5.5 Climate Experiments

Climate experiments of the research were designated considering the literature on land cover change impact on climate, studies conducted for mid latitudes and model parameterization. Experiments were employed in NCAR super computers.

5.5.1 Study Domain

There are four air masses affecting Turkey which are also considered while selecting the main domain for the study region. These air masses are cP, mP, mT and cT, where m denotes for maritime, c for continental, T for tropical (15ºN -35ºN or S) and P for polar (40º -60ºN or S) (Table 5.3, Figure 5.20).

Table 5.3: Description of Air Masses **(Robinson and Henderson-Sellers, 1999)**

Type	Source region	Properties at source
Continental polar (cP)	Siberia	Cold and dry, very stable
Maritime polar (mP)	Atlantic Ocean	Cool, rather damp, unstable
Maritime tropical (mT)	Trade-wind belt and subtropical oceans	Moist and warm, stability variable
Continental tropical (cT)	Sahara and North Africa	Hot and very dry, unstable

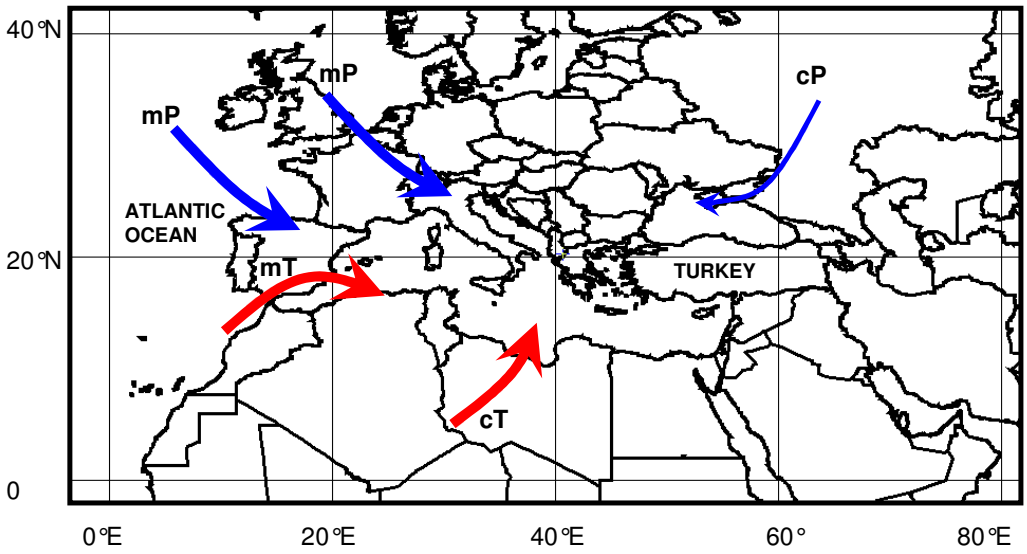

Figure 5.20: Air Masses Affecting Turkey

One main and two nested domains were formed to conduct numerical simulations presented in this work. To analyze the general circulation of the atmosphere, main domain was created to cover 25ºN -60ºN latitudes and -15ºW-55ºE longitudes and constitutes 180x142 grid points. Figure 5.21 shows the main and nested domains created within the study area. First nested domain includes Turkey and its near surrounding and the second nested domain includes the Marmara Region, which will be main focus of this research from land cover change perspective. Main domain has 27 km spatial resolution where nested domains have 9 km and 3 km, respectively. The vertical domains of both main and nested domains extend over thirty two vertical levels.

Climate simulations were conducted for summer 2004 because:

- Observations data were obtained from 1950 to 2005. 2005 observations had many lack days for the summer period however 2004 observations were complete for this period.
- Precipitation amount in summer is minimum during the summer in the Marmara Region. However, in June and August 2004, some extreme precipitation events occurred and it was investigated if WRF modeling system could capture these events.

Table 5.4: Experimental designs of different cases.

Case No	Climate Model	Domains	Simulation Period	IC/BC	LSM	PBL	Cumulus Parameterization	Microphysics	LW/SW Radiation
Case 1	WRF-ARW	1 Main	June-July-August 2005	NCEP Reanalysis II	Noah	Yonsei University Scheme	Kain-Fritsch Scheme II	WRF Single Moment 3-Class Scheme	RRTM/ Dudhia scheme
Case 2	WRF-ARW	1 Main	June-July-August 2004	NCEP Reanalysis II	Noah	Yonsei University Scheme	Kain-Fritsch Scheme II	Lin et al. Scheme	RRTM/ Dudhia scheme
Case 3	WRF-ARW	1 Main	June-July-August 2004	NCEP Reanalysis II	Noah	Yonsei University Scheme	Kain-Fritsch Scheme II	WRF Single Moment 3-Class Scheme	RRTM/ Dudhia scheme
Case 4	WRF-ARW	1 Main	June-July-August 2004	NCEP Reanalysis II	Noah	Yonsei University Scheme	Kain-Fritsch Scheme II	Lin et al. Scheme	RRTM/ Dudhia scheme
Case 5	WRF-NMM	1 Main	1-20 August 2004	NCEP Reanalysis II	Noah	Mellor-Yamada-Janjic	Kain-Fritsch Scheme II	Ferrier Scheme	GFDL/GFDL
Case 6	WRF-NMM	1 Main	1-20 August 2004	NCEP Reanalysis II	Noah	Mellor-Yamada-Janjic	Kain-Fritsch Scheme II	Ferrier Scheme	GFDL/GFDL
Case 7	WRF-ARW	1 Main and two nested	June-July-August 2004	NCEP Reanalysis II	Noah	Yonsei University Scheme	Kain-Fritsch Scheme II	Lin et al. Scheme	RRTM/ Dudhia scheme
Case 8	WRF-ARW	1 Main and two nested	June-July-August 2004	NCEP Reanalysis II	Noah	Yonsei University Scheme	Kain-Fritsch Scheme II	Lin et al. Scheme	RRTM/ Dudhia scheme

- Land cover data was created from Landsat images collected between 2001 and 2005. Therefore, it can represent the year of 2004 correctly.

Several preliminary experiments were conducted to find out the best model configuration for the study region (Table 5.4). These experiments were performed for the main domain and the results of these experiments were compared with NCEP R2 temperature and mean sea level pressure, GPCP precipitation, meteorological station and Global soil moisture data bank data.

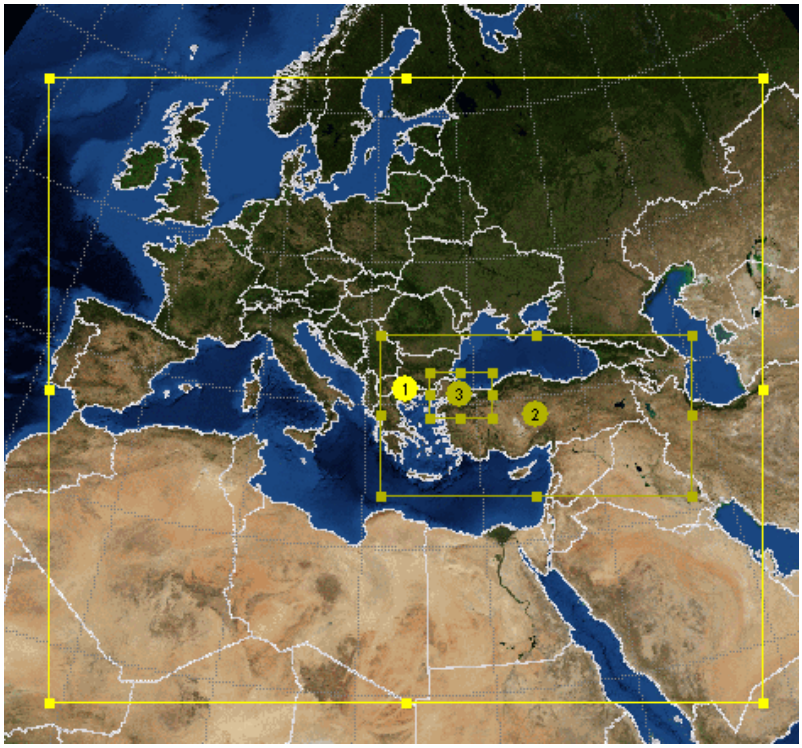

Figure 5.21: Boundaries of Research Domains

Initial experiments were conducted for the main domain and a 120 seconds time step was employed for this domain. Initial and boundary conditions were obtained from National Centers for Environmental Prediction-Department of Defense NCEP-DOE Reanalysis II (2.5x2.5 degree) dataset **(Kamamitsu et al, 2002)**. The Reanalysis II data is available at 6 hour interval. Over sea surfaces of the model domain, the sea surface temperature (SST) was specified using the one degree, weekly climatological dataset from NCEP **(Reynolds and Smith, 1994).**

First experiments were conducted for June, July and August 2004 period and 6 hourly outputs were obtained. 2 m air temperature, precipitation and mean sea level

pressure obtained from the model were plotted and the results of these parameters were compared with Reanalysis II 2 m air temperature data, GPCP precipitation data and Reanalysis II mean sea level pressure data, respectively.

Case1 includes the default parameters used for WRF-ARW simulations. However, results over Turkey with this configuration were not good. Precipitation was not captured over Turkey and average monthly model temperatures were 6°C colder then Reanalysis II data. Average monthly mean sea level pressure values were 2 or 3 mb higher then those of Renalysis II. Case 3 gave very similar results to case 1.

Case 4 has the same configurations with case 2 except the starting and ending times of model simulations to test the sensitivity of results to initial conditions. Precipitation patterns could be captured with case 4 configuration as in case 2, however it was found out that initial data has an impact on model simulations. Changing starting date of simulation affected the results and the model results became more drier towards to the end of the simulation time. Since the aim of the research was studying the summer climate and considering the computer time following experiments were conducted for June, July, August as in case 1, case 2 and case3.

WRF-NMM core which is widely used for weather prediction also used in this study and case 5 and 6 were conducted with this core. In case 5, default parameters for WRF-NMM core were used. With this core, general pattern and amount of precipitation was captured but there was a problem with the amount. In addition, this core did not work fine for longer simulations for the study area. It is better to use this core for numerical weather prediction of shorter periods. Therefore, WRF-ARW core was used for further experiments of the research.

For nesting, both one way and two way nesting were tested. Case 7 was conducted with two way nesting and case 8 was conducted with one two way nesting. It was found that both temperature and precipitation values were better with two-way nesting when the results of third domain were compared with observations from meteorological stations.

Among several tested model configurations and physics options, the following configuration gave the best results using WRF ARW model.

Cumulus Parameterization: Kain-Fritsch Scheme

LSM: Noah land-surface model

Microphysics: Lin et al. Scheme

PBL: Yonsei University Scheme

Longwave/Shortwave Radiation: RRTM/ Dudhia scheme

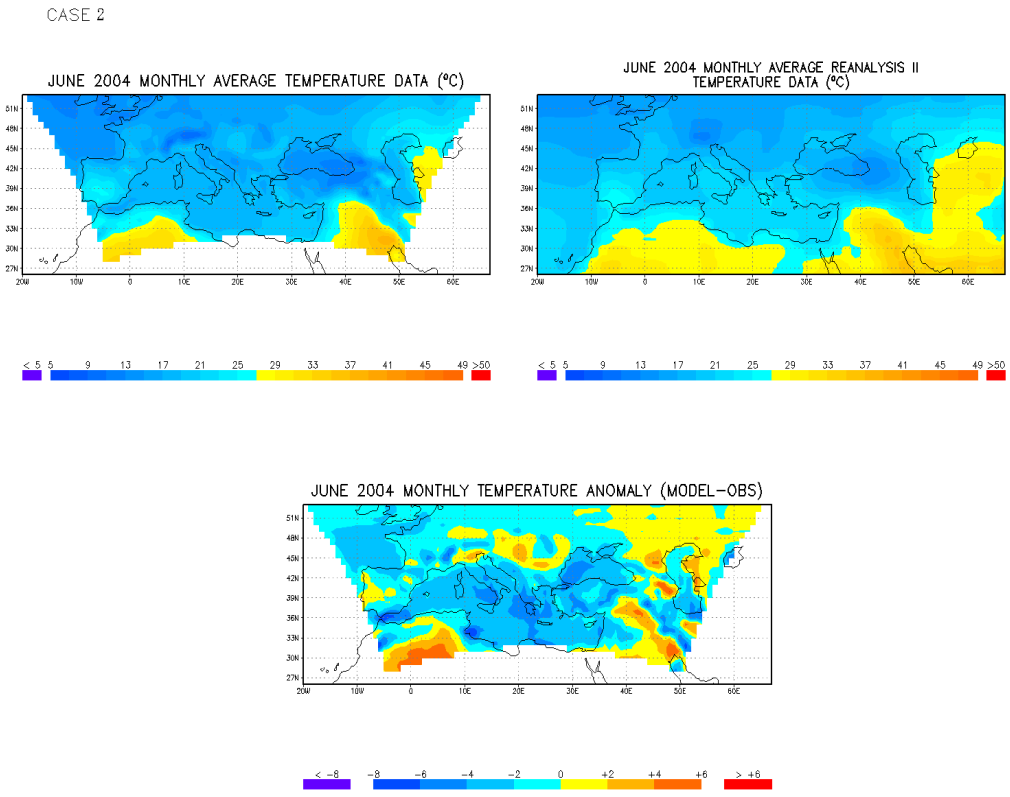

Figure 5.22: Monthly Average Temperature Obtained in June 2004.

Figure 5.22 illustrates the monthly average temperature obtained from the model, Reanalysis II and the difference between model and Reanalysis II data for June 2004.

Figure 5.23 shows the monthly accumulated total precipitation (mm) obtained from the model result, GPCP data and the difference between model and observation for July 2004. Since the horizontal resolution of the model is comparatively higher, it can simulate the precipitation in mountainous regions like Alps. Total precipitation term used in the study reflects the sum of large scale and convective precipitation.

CASE 2

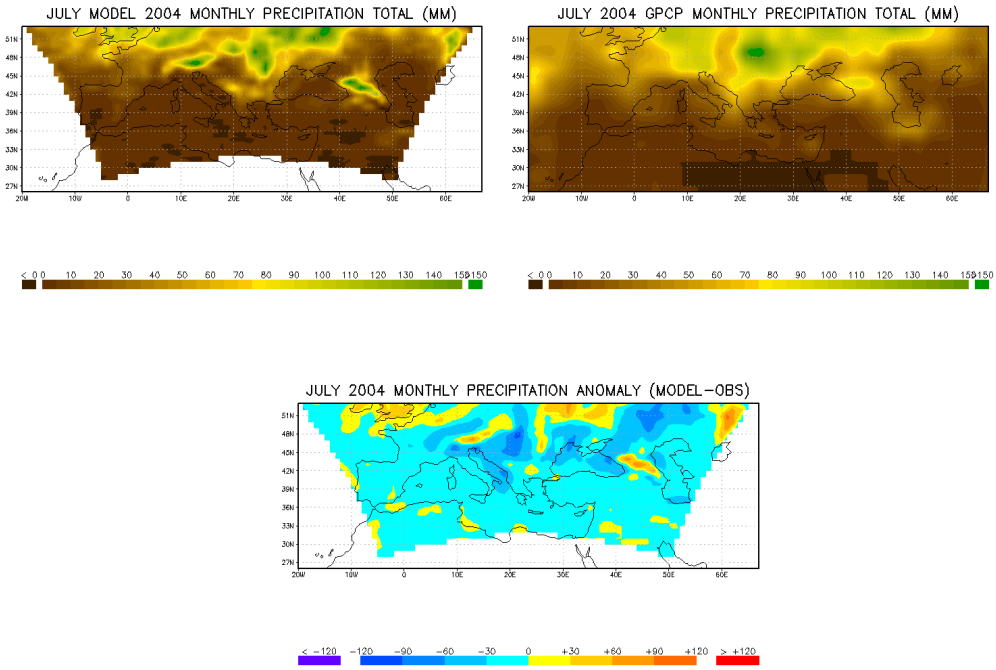

Figure 5.23: Monthly Accumulated Total Precipitation (mm) for July 2004.

Figure 5.24 shows the monthly average mean sea level pressure results obtained from the model, Reanalysis II and the difference between model and Reanalysis II data for June 2004. The results obtained from the model and Reanalysis II data are quite similar, maximum difference between model derived mean sea level pressure and those obtained from Reanalysis II is around -2 and 2 mb.

To analyze the accuracy of soil moisture, a box formed over the Black Sea region including the soil moisture observation for Ukraine from the Global Soil Moisture data set and a time series plot was formed for June-August 2004 period. Figure 5.25 shows the time series plot of total soil moisture (cm) for model, observations and Reanalysis II data. The model-derived soil moisture and observations have quite similar values.

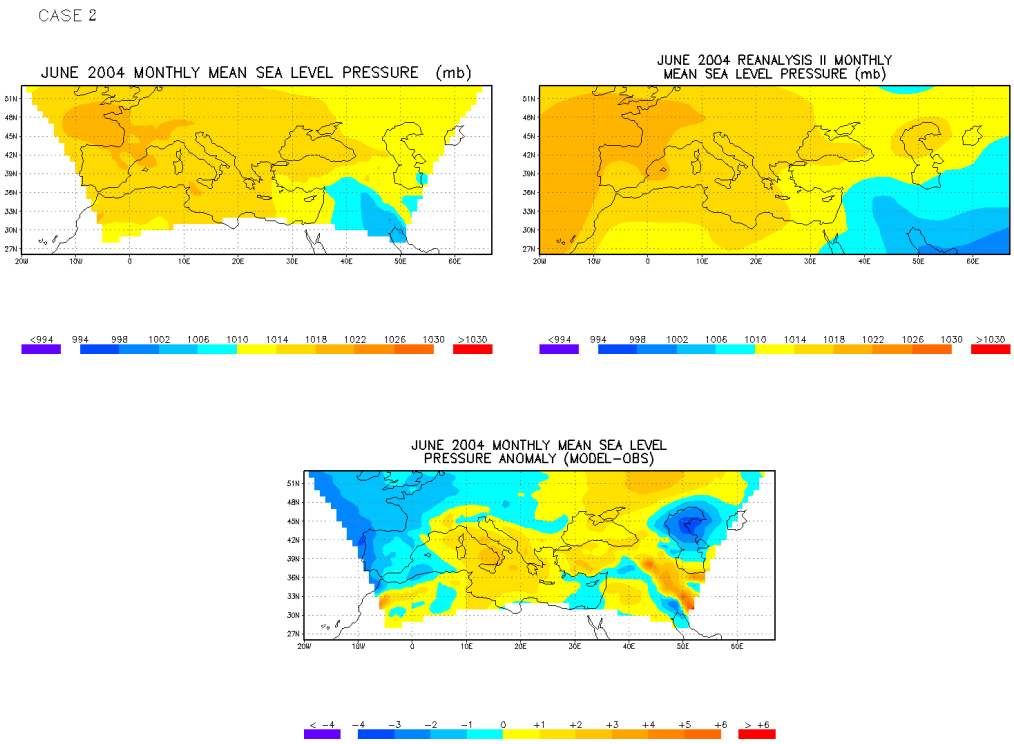

Figure 5.24: Monthly Average Mean Sea Level Pressure Results for June 2004.

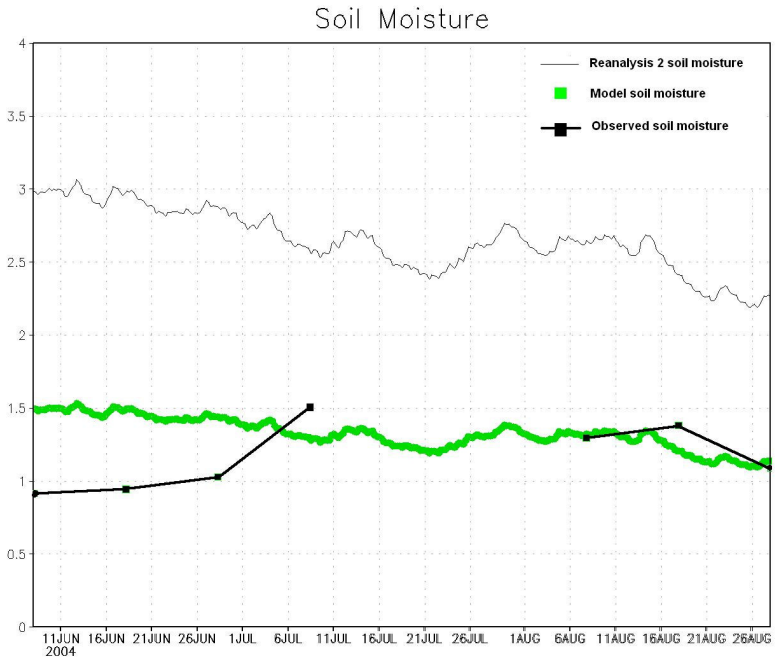

Figure 5.25: Total Soil Moisture (cm) for Model, observations and Reanalysis II Data.

5.5.2 Simulation Results

Control run was conducted with the best model configuration obtained in case 2, using model land cover data and two-way nesting option for June-August 2004 period. Size and location of first nested domain was changed to save computer time and have the second domain (Marmara region) approximately center of first nested domain since location of domains also affected the results. Borders of main and first nested domain were taken over oceans to eliminate the topography effects in boundaries. Since the main study area is Marmara Region and the land cover data was produced for this area, it is not this research's primary goal to look all Turkey. This nesting of fine grids within coarse ones is a compromise, forced by existing limitations on computing technology, between simulating the region of interest with a high enough resolution to capture the important scales and processes and simulating a large enough domain to correctly represent all the relevant meteorological forcing. Main domain was kept same to represent general circulations affecting the study area.

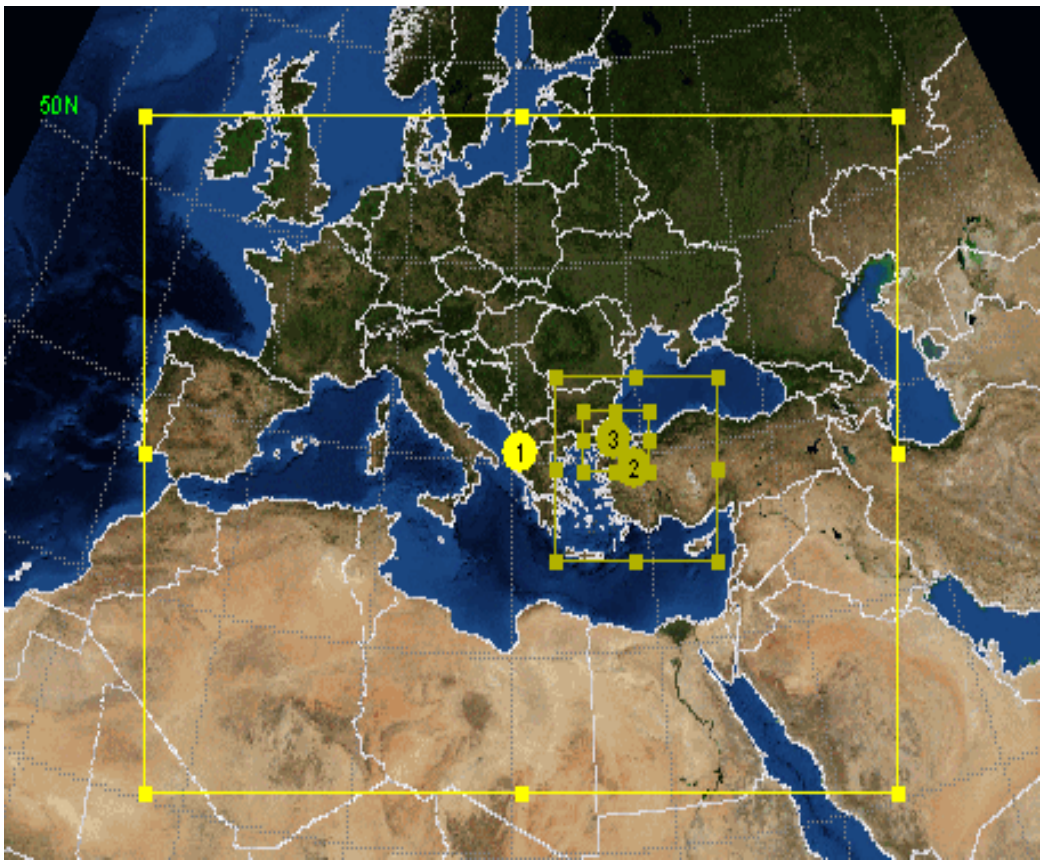

Figure 5.26: Domain Design for Control Run.

Main domain has 180x142 grid points, first nested domain has 130x115 grid points and the most inner domain has 166x130 grid points. Locations of the domains are shown in Figure 5.26.

While I use the convective parameterization on Domain 1 and 2, I left it turned off on domain 3: particularly for 3-km grid spacing, use of the convective scheme would be inappropriate, and any convection occurring on the fine grids must therefore be explicitly resolved.

After completing the control experiment, land cover classes based on USGS classification scheme were implemented to WRF modeling system. These classes were created using Landsat ETM and MSS data and then aggregated to 1 km horizontal resolution. Datasets were designed to represent 1975 and 2005 conditions.

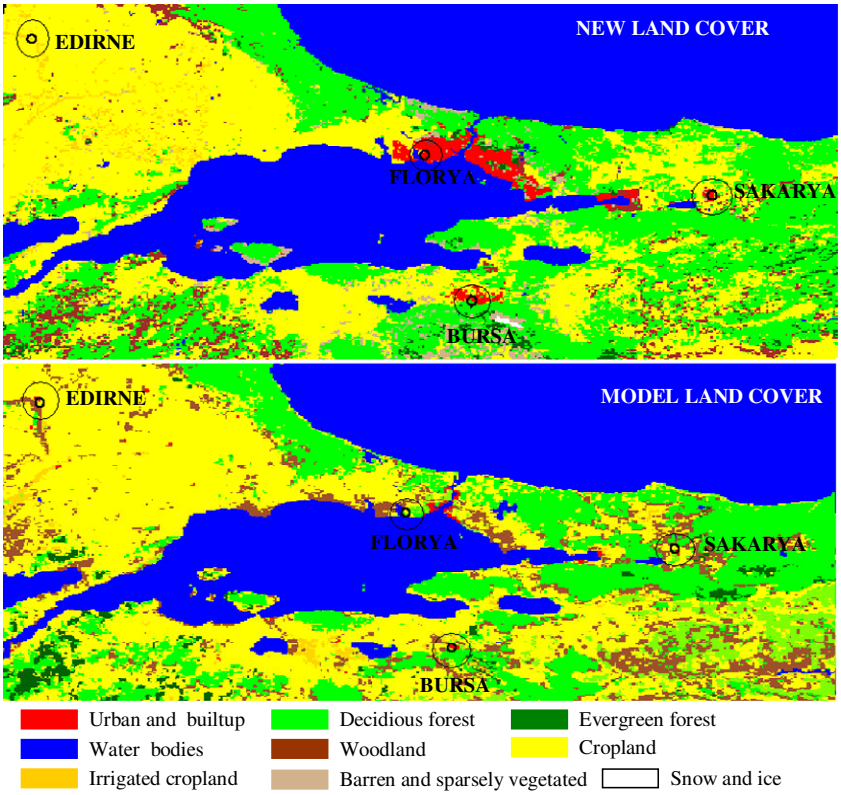

Figure 5.27: Locations of Selected Meteorological Stations, (Black Circles).

A comparison was made between the results obtained with 2005 land cover data and control run to find out if the new land cover data can improve the results of the study. Four stations were selected and comparisons were made for minimum, maximum and average temperature values. 3 km buffer zone was formed around the location of

these meteorological stations and land cover type percentages in model and in Landsat derived data were calculated in GIS environment. The locations of the meteorological stations with 3 km buffer zone are illustrated in Figure 5.27. The selected stations were Edirne in Ergene Section, Florya in İstanbul, Sakarya in Catalca-Kocaeli Section and Bursa in Southern Marmara Section.

Figure 5.28 shows the minimum, maximum and average temperatures of Florya station obtained from observations, control run and the run with new land cover data. GIS analyses illustrated that Florya has 60% crop and 40% woodland in model land cover, whereas 90% urban and 10% in new land cover. Minimum, maximum and average temperatures obtained from new land cover have closer values to observations. Both maximum and average temperatures obtained from control run are lower than observations. Since the dominant land cover around Florya is urban, introducing new land cover data improved the results and gave higher temperature values compared to control run. Conversions of land cover type from crop to urban and from woodland to urban cause warming.

Bowen ratio, ratio of sensible heat to latent heat, changed as a result of land cover change near the meteorological station. Conversion from woodland to urban increased the amount of sensible heat flux emitted from the surface which leads an increase of maximum temperature. The changes in the surface properties affect the surface radiation, energy and water balance. An increase of impervious surfaces results in a decrease in evapotranspiration and loss of latent heat from the ground, thus causing a warming of the urban area.

Figure 5.29 shows minimum, maximum and average temperatures of Bursa obtained from model simulations and observations. Minimum temperature values obtained from control and new land cover data run are similar to each other, however better maximum and average temperatures were obtained with improved land cover data. Buffer analyses in Bursa showed that this region has 50% urban and 50% forest in model land cover data but 70% urban and 30% forest in new land cover data which leads better maximum and average model temperatures. Conversion from forest to urban increased the amount of sensible heat similar to Florya station.

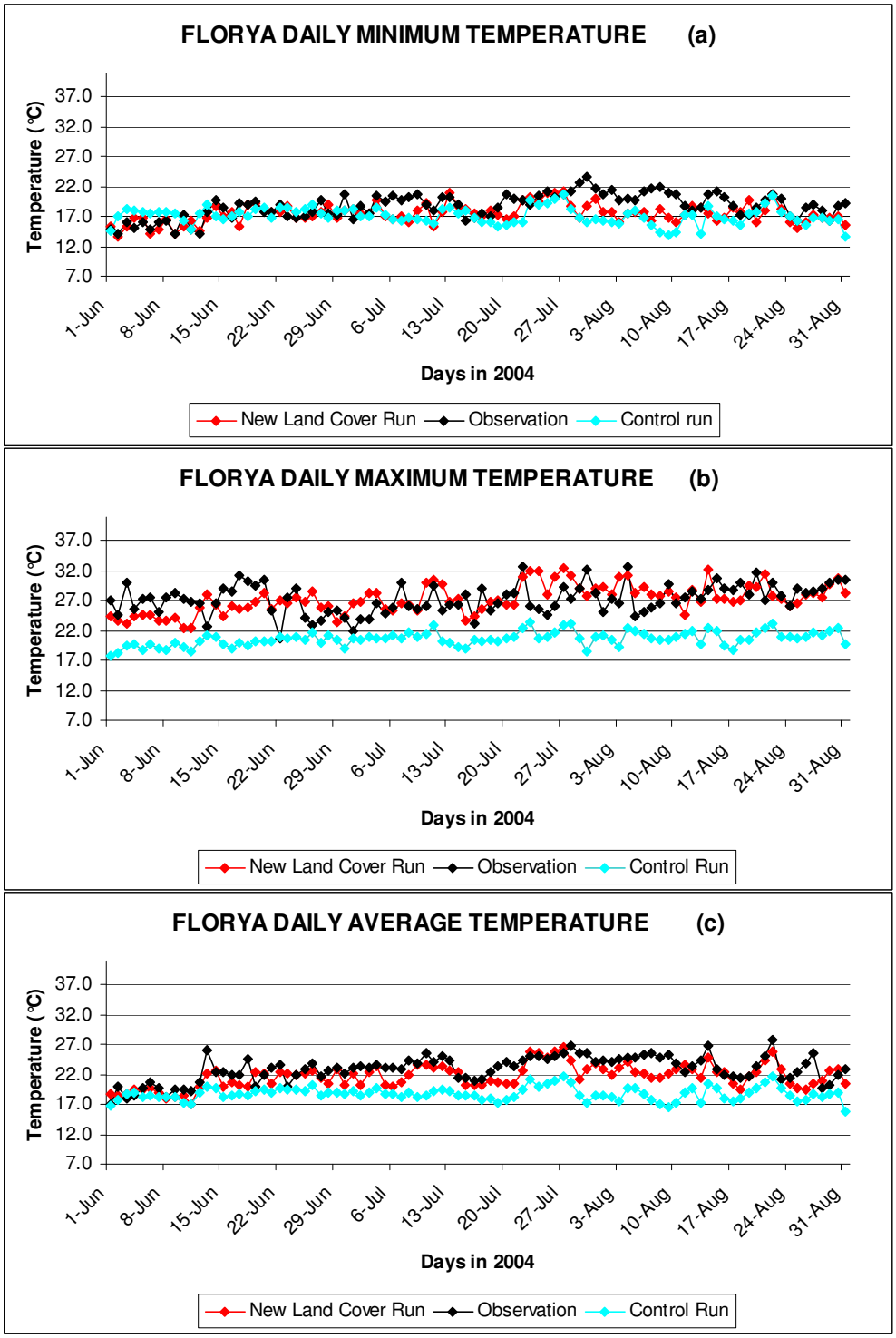

Figure 5.28: Minimum, Maximum and Average Temperatures of Florya.

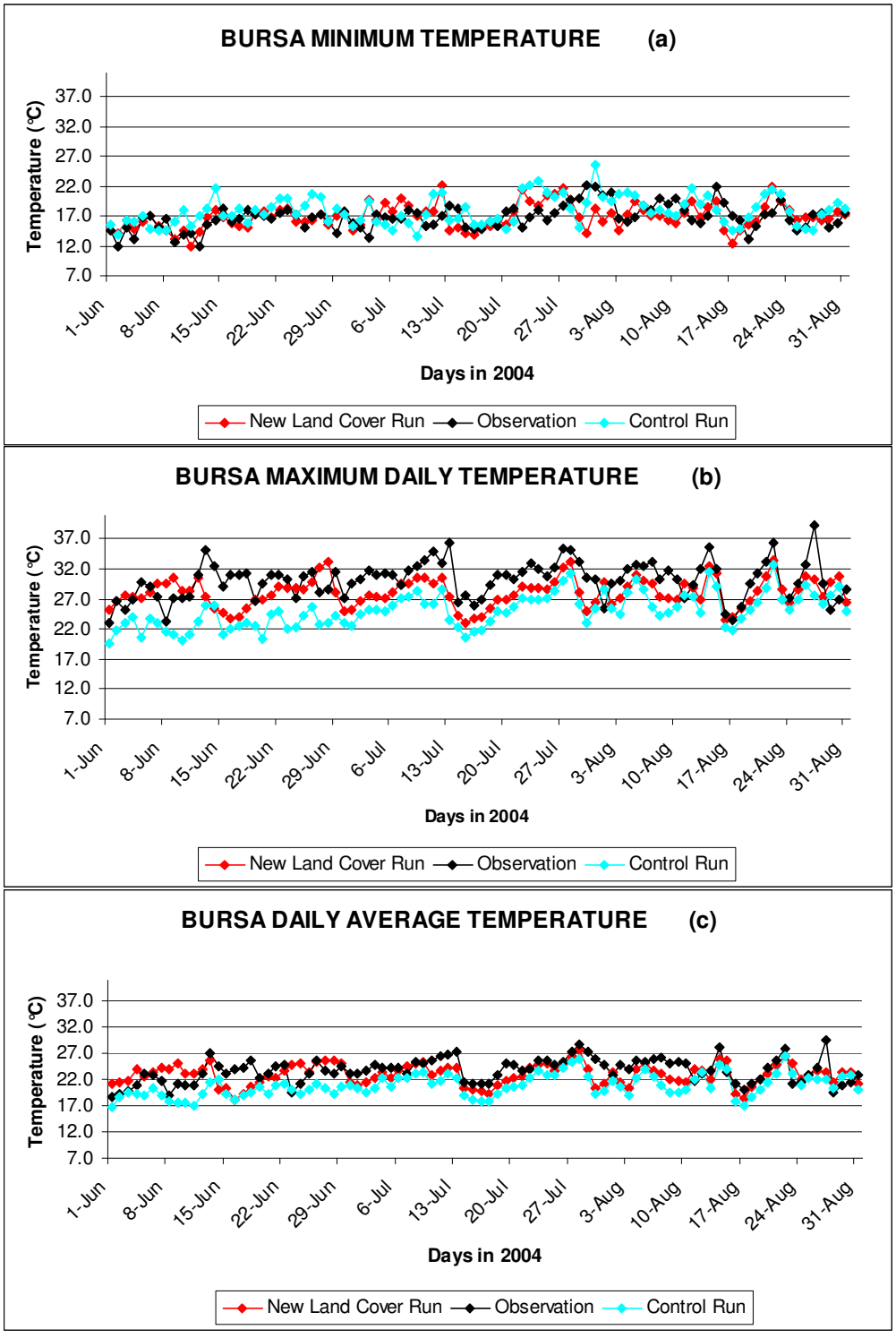

Figure 5.29: Minimum, Maximum and Average Temperatures of Bursa.

Figure 5.30 is the same as figure 5.29 except it is for Sakarya station. Model land cover data within 3 km buffer of Sakarya is 40% urban and 60% crop whereas it is 60% urban and 40% crop in new land cover. Since the land cover types are very

similar and change is very small for model and new land cover data, results are very similar to each other except for the minimum temperature which is better and comparatively higher with new land cover.

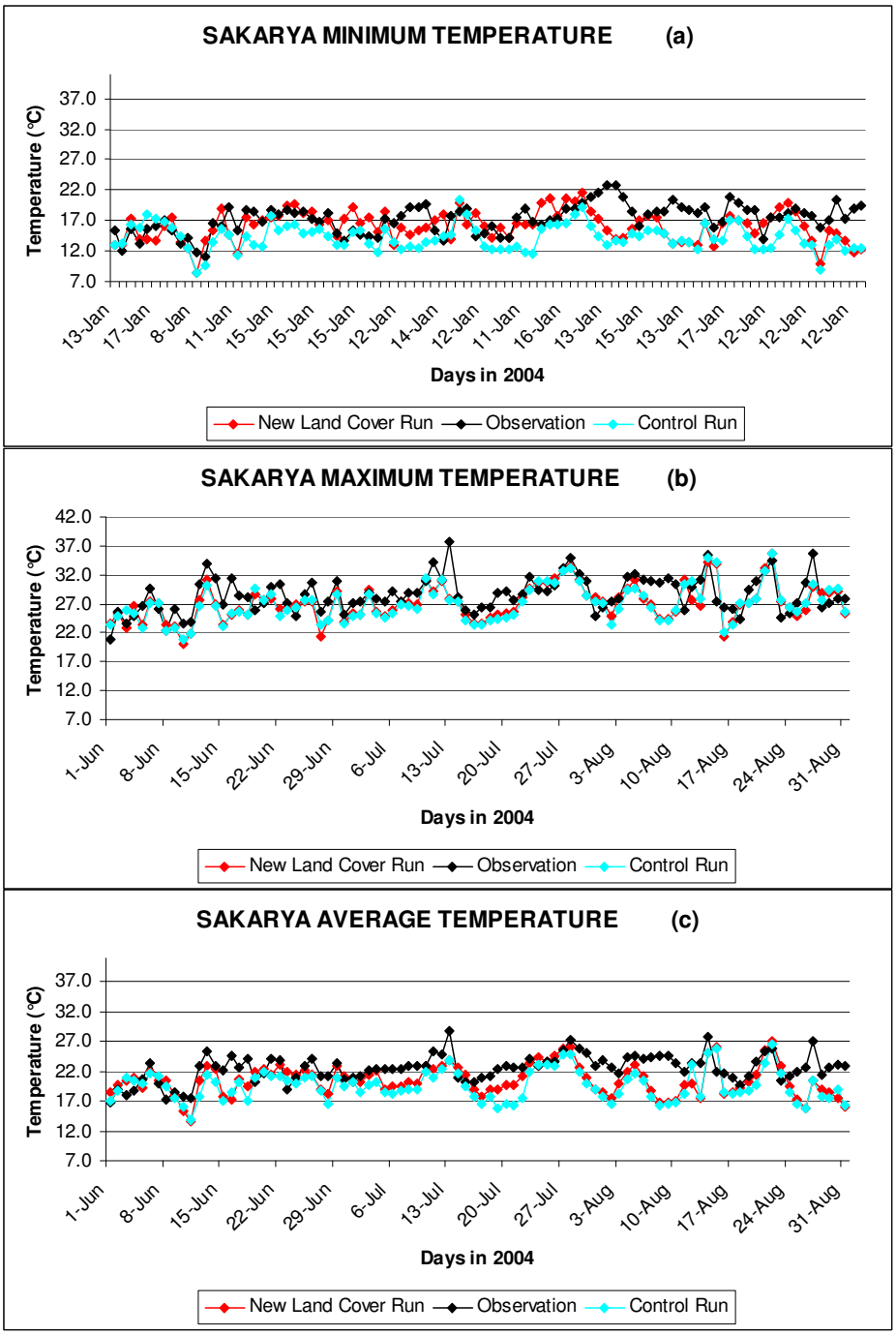

Figure 5.30: Minimum, Maximum and Average Temperatures of Sakarya.

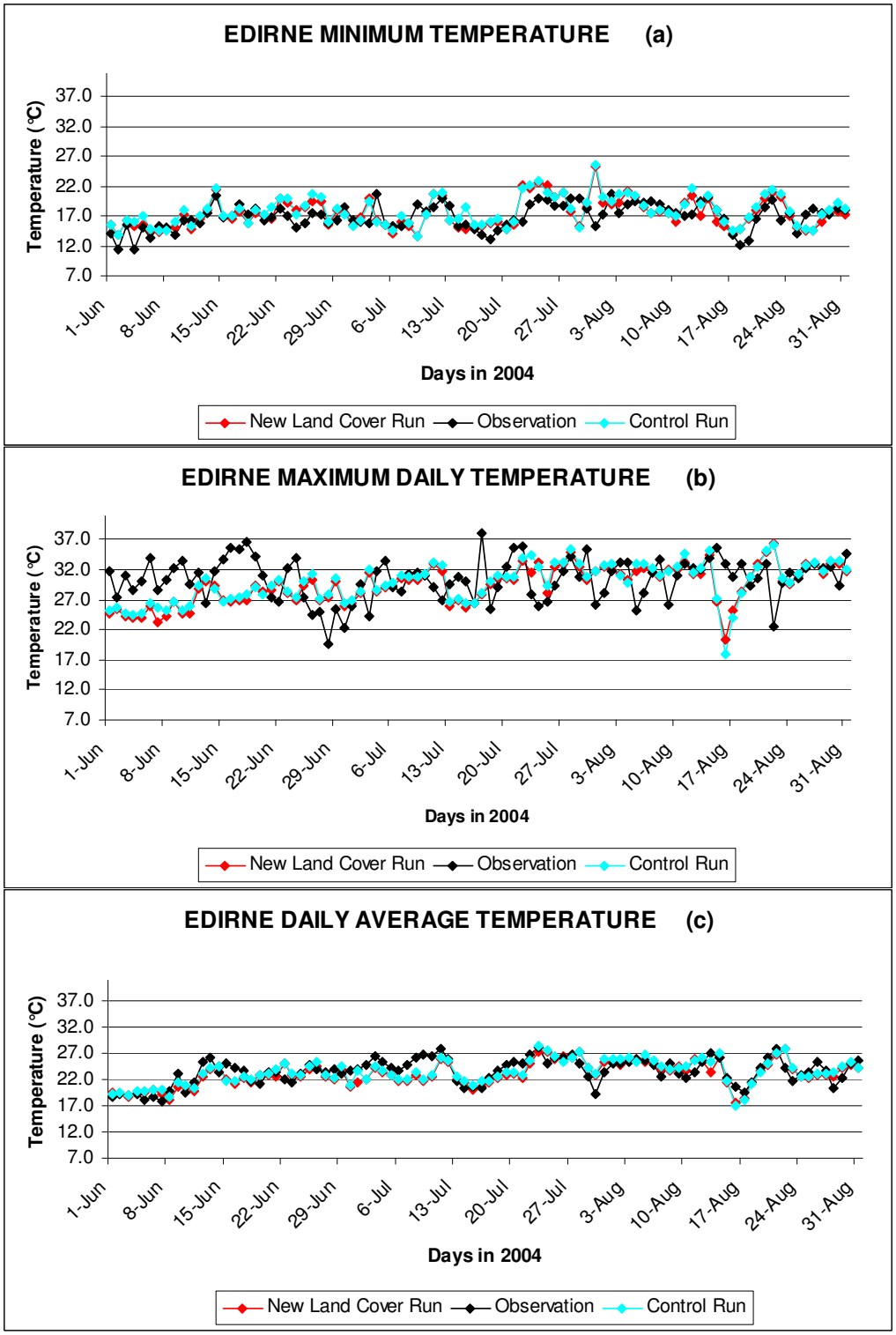

Figure 5.31: Minimum, Maximum and Average Temperatures of Edirne.

Last comparison was conducted for Edirne station and its results are shown in Figure 5.31. Both model and new land cover data have 100% crop in Edirne. As a result of

this, both simulations gave similar results for minimum, maximum and average temperature values.

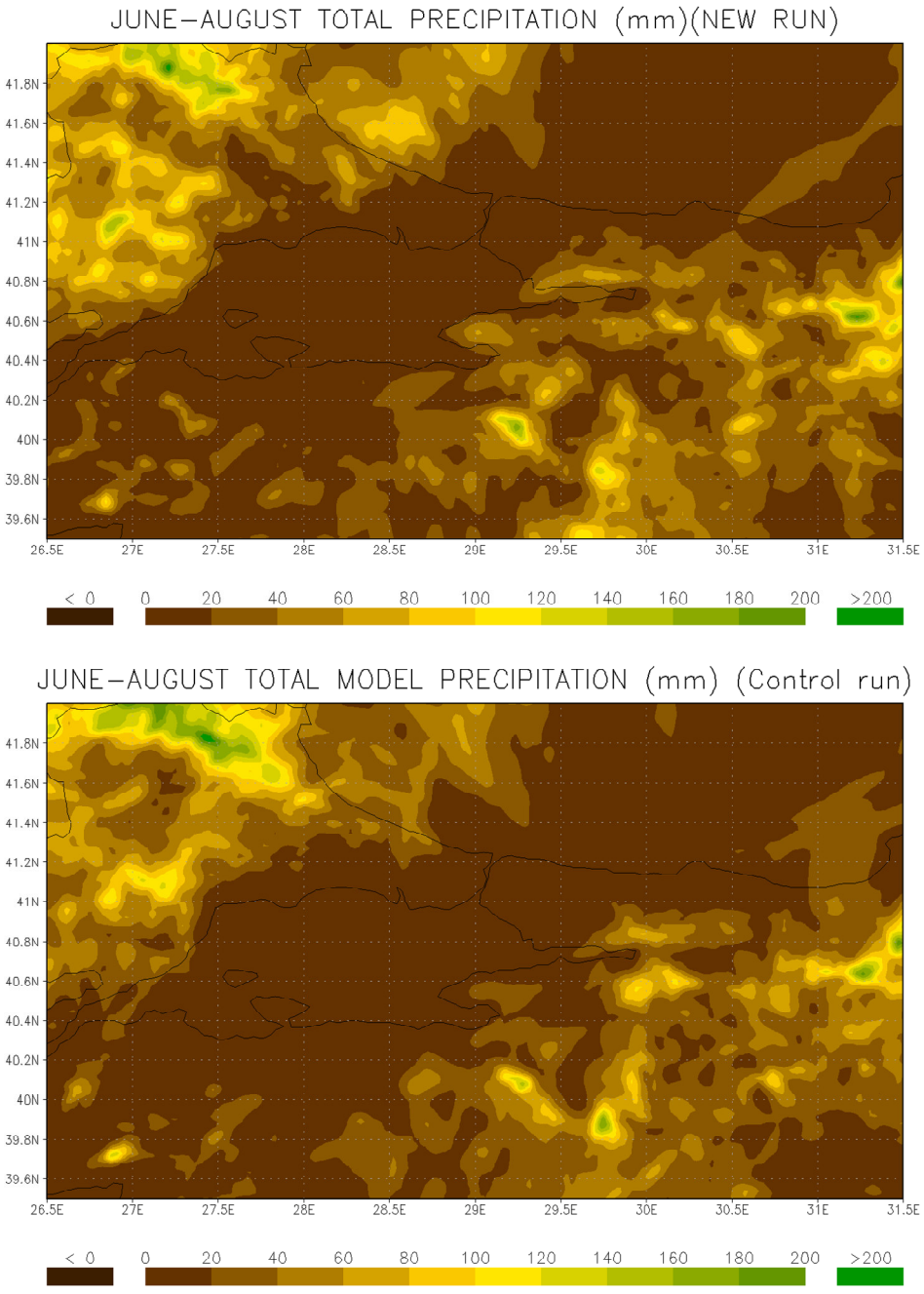

Figure 5.32: Precipitation Obtained from Control Run and New Land Cover Data Run.

Precipitation results obtained with model land cover and new land cover data were very similar to each other (Figure 5.22). The simulated precipitation showed that the

model was able to capture the main features of the observed precipitation except around the Bosphorus.

Modifying the model land cover by correcting the land cover classification to reflect current conditions improve the simulation of minimum, maximum and average 2m air temperature results significantly. The results showed that temperature is more sensitive to local land cover change than precipitation.

Last experiment was conducted with 1975 land cover data. Comparison was made between the simulation results obtained from 1975 and 2005 land cover, which illustrate the heat islands over İstanbul Anatolian and European side, Adapazarı and Bursa.

Heat islands develop when a large fraction of the natural land cover in an area is replaced by built surfaces that trap incoming solar radiation during the day and then re-radiate it at night **(Quattrochi et al. 2000; Oke 1982).** This slows the cooling process thereby keeping nighttime air temperatures high relative to temperatures in less urbanized areas **(Oke 1982).** This increase in urban air temperatures as compared to surrounding suburban and rural temperatures is referred to as the heat island effect. Marmara Region faced with conversion of crop and barren areas into urban areas in İstanbul, Bursa, İzmit and Adapazarı which lead increase of minimum and average temperatures in these areas.

Temperature increase as a result of urbanization can be easily determined by using average temperatures difference obtained from 1975 and 2005 land cover data runs (Figure 5.33). UHI intensity tends to increase with increasing city size and/or population. The most intense UHI effect occurs in İstanbul where the population and city size is the biggest. Second most densely populated and big city is Bursa and UHI effect is also strong here.

Unwin (1980), Tapper (1990) and **Steinecke (1999)** reported that UHI may disappear by day and the city may be cooler than the rural environments. Since daily temperatures over the cities were cooler, average temperature differences became smaller but still there were significant average temperature differences over İstanbul, Bursa, Izmit and Adapazarı. Urbanization in Anatolian part of İstanbul was bigger then in European part which resulted in average temperature increase between 0.5 and 1°C in European part, between 0.5 and 1.5°C in Anatolian part.

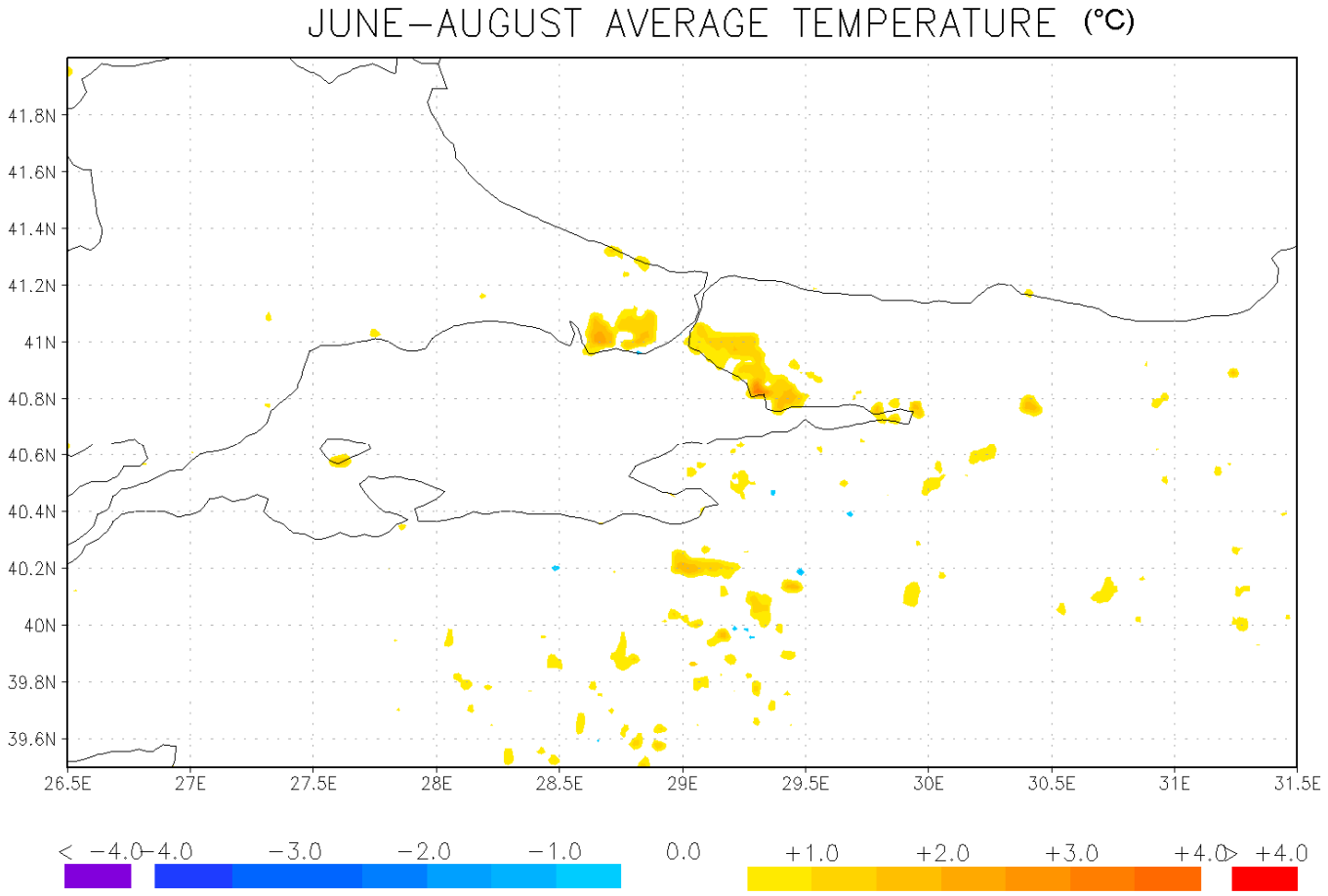

Figure 5.33: June-August Average Temperature Difference between 2005 and 1975 Land Cover Run

Average temperature differences over Bursa, Adapazarı and Izmit were found between 0.5 and 1°C.

Conversion from forest to barren areas increased average temperatures 0.5°C in coastline of İstanbul European side (Figure 5.24).

0.5°C cooling of average temperatures occurred in a small region around Bursa with the conversion of the sparsely vegetated areas into forest areas (Figure 5.24).

Overall temperature results comparisons showed that there is a warming trend in maximum and average temperatures of Marmara Region. This trend was also found by Tayanc et. al. 2007. They used meteorological station data obtained between 1950 and 2004 and illustrated the warming and cooling trends over Turkey for different seasons. Their results showed the warming trend of minimum, maximum and average temperature over the Marmara Region for the summer season.

Precipitation amounts obtained from 1975 and 2005 land cover runs were also compared (Figure 5.34). There is an increase in precipitation over urban areas of Izmit, Adapazarı and Bursa. Increase in rainfall over urban areas attributed largely to the Urban Heat Island (UHI) initiated convergence zone and to a lesser extent, to the increased surface roughness (Pielke et. al, 2007). Although WRF modeling system can simulate increase temperature over urban areas, no precipitation difference can be simulated over İstanbul urban area.

In general precipitation increase was detected over urban areas and over the areas where land cover changed from sparsely vegetated to deciduous forest. Precipitation decrease was detected over Thrace Region with the increase of crop areas (Figure 5.35). Precipitation changes were heterogonous.

Studies in the USA conducted for St Louis, Atlanta and Houston generally demonstrated increases over and downwind of urban areas attributed largely to the UHI initiated convergence zone. The role of urban aerosols on urban-induced precipitation is still a big unknown **(Pielke et al, 2007)**

There are some problems to simulate the precipitation with WRF modeling system but this is a state-of-the art modeling system that has been used by several scientists and it is harder to simulate precipitation in summer season. Many researchers have been developing new coupled models which incorporate water table dynamics and

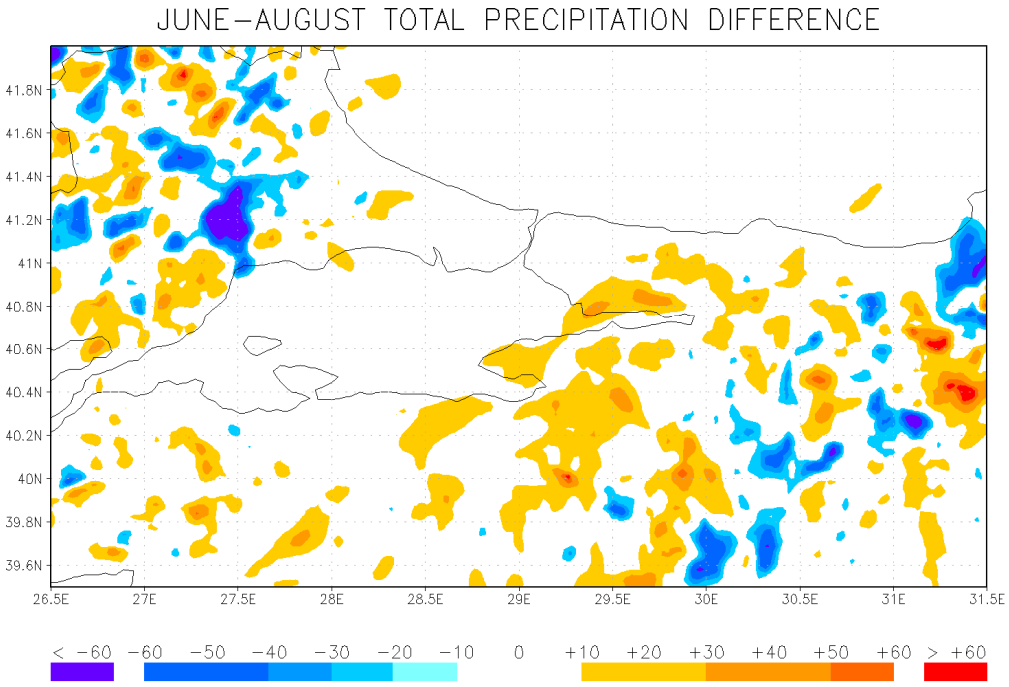

Figure 5.34: June-August Total Precipitation difference between 2005 and 1975 Land Cover Run

ground water processes into climate modeling to improve the precipitation simulations **(Miguez-Macho et al, 2007; Fan et al, 2007).**

Figure 5.35 illustrates the differences of average 10 m wind for June-August period. Bigger differences occurred where land cover changed from crop to urban and sparsely vegetated to deciduous forest. It seems that the urbanization decreases the wind magnitude over the city and surrounding areas. The wind vectors show a southwesterly anomaly over İstanbul. The changes in wind magnitude and wind vectors together imply that the velocity of the northeasterly winds (prevailing winds in July) was reduced over İstanbul. This should primarily be a response to the increased roughness length when the landscape changed from crop to urban, which usually has larger roughness length. Changes in direction and magnitude of winds are important when air pollution and its transport were considered.

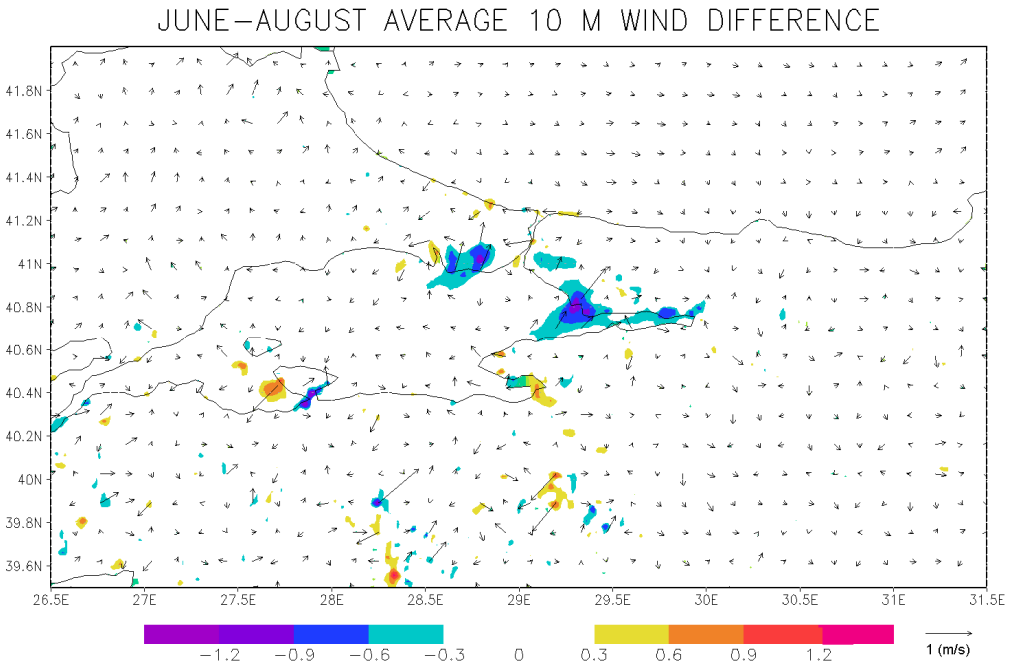

Figure 5.35: June-August Average 10 m Wind difference between 2005 and 1975 Land Cover Run

5.5.3 Significance Test of Simulations

Simulation results obtained with 1975 and 2005 data were analyzed using t-test to find out whether the variations in temperature, precipitation and wind due to the land cover change are significant or not.

Wang et. al (2006) used t-test to determine the statistical significance of regional climate change caused by land use and land cover variation in West China. **Min et al. (2006)** tested the statistical significance of their experiments conducted for future climate changes over East Asia for each grid point using univariate two-sided t-test with 0.01 confidence level. **Roy et al. (2007)** used student's t-test to determine the significance of differences in means between pre-and post-Green Revolution period for climatic variables with 0.05 confidence level.

In this research, t-test was used with 95% significance and the null hypothesis assumed that the results of 1975 and 2005 simulations are equal. Using the mean, standard deviation and number of data points for each simulation, t test was conducted to determine whether the changes between 1975 and 2005 are significant or not.

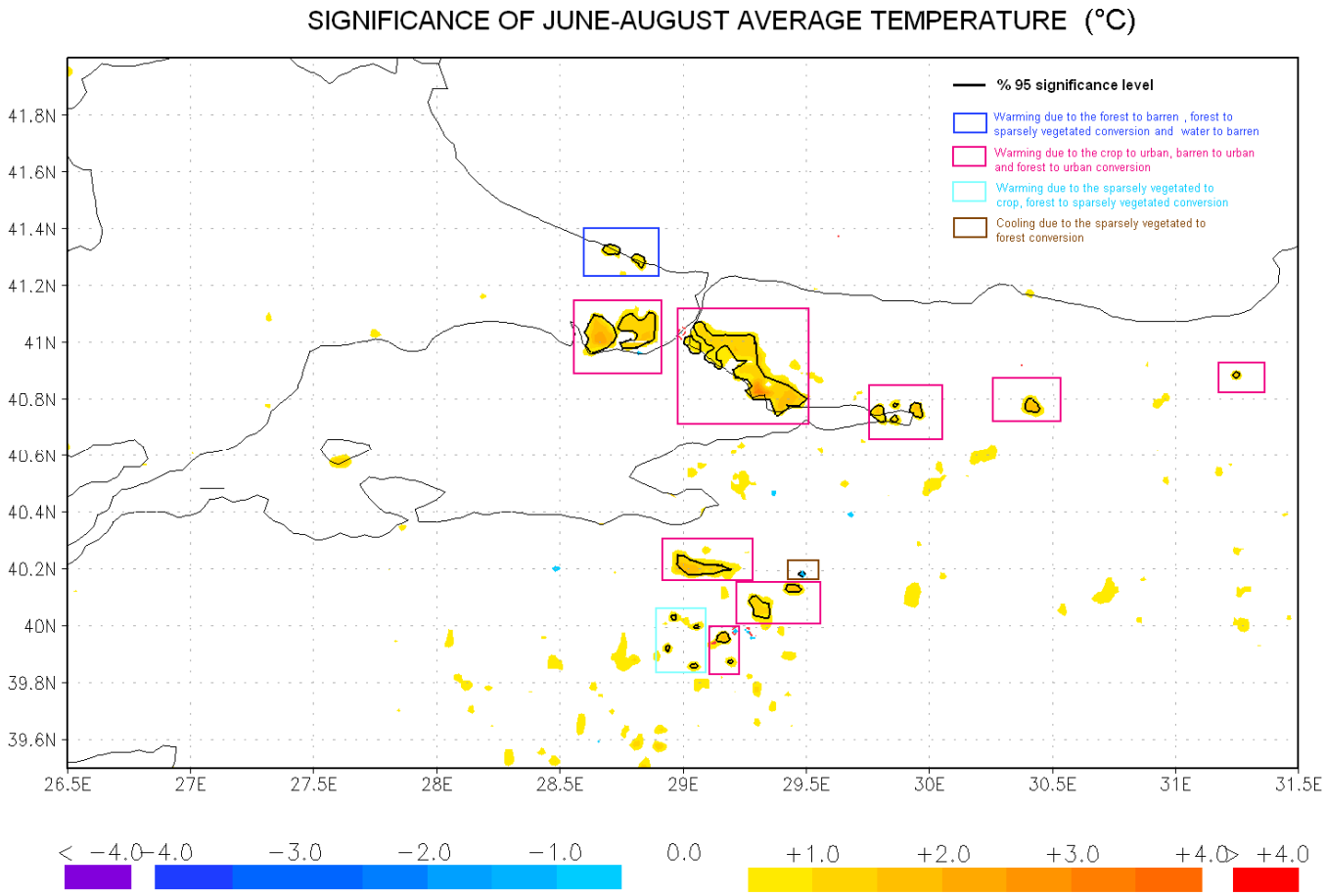

Figure 5. 36: Significance Test Results for June-August Average Temperature

Figure 5.36 shows the significance of June-August average temperature differences. Areas having thick black line around the temperature differences passed the significance test with 0.05 confidence level. Each box in the figure pointed out the significantly warmed or cooled regions due to the land cover change and the type of land cover conversion in those regions. Significant warming over the urban areas of İstanbul, Bursa, Adapazarı and Izmit can be observed in the Marmara Region (pink boxes in figure 5.36). Also some significant warming trends were found on the coastline of İstanbul because of forest to barren, water to barren and forest to sparsely vegetated conversion (blue boxes in figure 5.36). These regions were where the open mining activities were conducted and sea was filled with the residuals of these activities. Significant cooling of average minimum temperature was found for limited areas because of the conversion of sparsely vegetated to forest and grass to forest (brown and green boxes in figure 5.36). Conversion from forest to sparsely vegetated and sparsely vegetated to crop caused significant warming for some small regions (cyan boxes in figure 5.36).

Although some small precipitation increase and decreases (figure 5.34) were found over the different parts of the Marmara Region, none of these trends was statistically significant.

Introducing multitemproral land cover data in WRF modeling system produced different results emphasizing the impact of land cover change impact on climate. There are warming affects because of urbanization, open mining activities and deforestration and there are cooling affects because of reforrestration and increase in water areas. There are also increases and decreases in precipitation patterns and changes in distribution and magnitudes of winds. However, not all these changes in climatic variables are significant and application of t test helped us to find out significantly changed climatic variables and their locations.

The results of this study pointed out that the Marmara Region is under the impact of human induced climate change. Changes in land cover with further human activities will also impact the future climate of the region. This conclusion has important implications for land-use planning and water and natural resource protection in the Marmara Region.

6. CONCLUSIONS

Land cover is a fundamental variable impacting and linking many parts of the human and physical environments. Since remote sensing provides a map-like representation of the Earth's surface that is spatially continuous and highly consistent, as well as available at a range of spatial and temporal scales, it is an attractive source of creating land cover data. Several digital image processing techniques should be conducted to create accurate and reliable land cover data using remotely sensed images.

The first step of any image processing procedure is to select appropriate band combinations for the study. Incorrect usage of different band combinations or panchromatic band directly affects the results obtained from satellite image data. The results of this study illustrated that besides the widely used correlation matrix, semivariograms can also be used to select appropriate band combinations to study different land cover types. Semivariogram analysis showed that infrared bands can be used for the interpretation of urban surfaces; visible bands can be used for the interpretation of water bodies and near infrared band for forest areas.

Atmospheric, radiometric and geometric corrections of satellite images must be employed to eliminate atmospheric distortions, sensor problems and geometric distortions. Classification is the last step to create land cover data and determine land cover changes using multitemporal satellite images.

Besides the classification methods to determine land cover change, semivariograms and spatial profiles were also used in this study. Using semivariograms and spatial profiles, regions faced with significant land cover changed determined easily and accurately. Semivariogram parameters were used to identify abrupt land cover changes within the pilot regions. Based on the information obtained from semivariograms and spatial profiles, training areas were selected and some regions were subsetted to classify separately. This procedure improved the classification accuracy.

Classification results pointed out that land cover changes occurred in Marmara Region both in coastal areas and inner parts as a result of human activities between 1975 and 2005. Because of intense immigration to this region, industrialized and urban areas expanded therefore areas of urban and built up increased dramatically. Mostly, croplands, barren and sparsely vegetated areas were transformed into urban areas. İstanbul, Bursa and Izmit are examples of this situation. As a result of filling of materials extracted from open mining areas into the sea, ecosystem and topographic structure were damaged and there had been land cover changes towards to Black Sea coast. Forest areas were transformed into barren and sparsely vegetated areas in this region. According to classification results, total urban areas were 25659.3 ha in 1975 but 104966.1 ha in 2005 which means urban areas increased by a factor of 4 in the Marmara Region in a 30 yr period. 45906.1 ha crop area was converted into urban area in İstanbul, Bursa and Adapazarı. 23843.44 ha crop area was converted to water area with the regulations of water basins to increase the amount of fresh water in İstanbul. 14133.31 ha barren and sparsely vegetated land transformed into urban but 41760 ha forest land transformed into barren and sparsely vegetated area between 1975 and 2005. Also coastline in this region changed with the filling of mining residues into the Black Sea.

There are some advantages and disadvantages to use Landsat ETM and MSS data. It is easier to classify current Landsat ETM images since they have better spectral and spatial resolution. In addition, it is easier to find ground truth data belonging to present. While classifying past images obtained from Landsat images, there were some limitations. First of all, spectral and spatial resolution was a drawback compared to Landsat ETM images. Since Landsat MSS images were belonged to first Landsat series, they also have some sensor problems like line drop effects. Also, it is hard to find ground truth data for the past. Quality of Landsat ETM data was better then Landsat MSS data however when compared to NOAA AVHRR used in global land cover data sets both types of Landsat images were superior.

Available global land cover data sets like GLC2000, UMD and GLCC data have some deficiencies and inaccuracies. Comparisons of Landsat derived land cover data with these global data sets emphasized problems about them. These data sets have problems in representing land sea boundaries and urban areas and have classification errors for some land cover types. GLCC data used in many regional climate models

was obtained from 1-km Advanced Very High Resolution Radiometer satellite images spanning April 1992 through March 1993 with an unsupervised classification technique; therefore it is not up-to-date and is not accurate for all regions and some land cover types such as urban areas. Detailed comparison employed between GLCC and Landsat derived land cover data discovered misrepresentation of land cover types for the Marmara Region. Results of these comparisons suggested that any researcher that will use this global dataset should check its accuracy and consistency for the concerned region.

Comparison of observations with experiments conducted with model land cover data (control run) and Landsat derived land cover data (new land cover run) showed that better simulation results can be obtained with new land cover data since it reflects actual land surface accurately. Minimum, maximum and average temperatures obtained with new land cover data run were very close to actual observations. Results of control run and new land cover run were very similar if both model and new land cover data have same land cover types. Changing the model land cover by Landsat derived land cover data to reflect current conditions improve the simulation of minimum, maximum and average 2 m air temperature results significantly.

Horizontal resolution used in regional climate models are increasing and accurate representation of land surface is becoming more important to capture local effects on climate like effects of urban on wind, temperature and precipitation. Land surface controls the partitioning of available energy at the surface between sensible and latent heat, and controls partitioning of available water between evaporation and runoff, therefore it is important to have accurate land cover data within climate models. In this research, Landsat images were used to derive land cover data of the Marmara Region and succesfully implemented into WRF modeling system. New land cover data improved the simulation results significantly.

Land cover change impact on local climate of the Marmara Region was quantified by comparing results of the experiments conducted with 2005 and 1975 land cover data. Differences in maximum summer temperatures pointed out the urban heat island effects over İstanbul, Sakarya and Bursa. Urbanized areas occurred with conversion of cropland and barren areas. Since daily temperatures over the cities were cooler, average temperature differences became smaller but still there were significant average temperature differences over İstanbul, Bursa, Izmit and Adapazarı. Average

temperature differences over Bursa, Adapazarı and Izmit were found between 0.5 and 1°C. Urbanization in Anatolian part of İstanbul was bigger then in European part which resulted in average temperature increase between 0.5 and 1°C in European part, between 0.5 and 1.5°C in Anatolian part. Conversion from forest to barren areas increased average temperatures 0.5°C in coastline of İstanbul European side. 0.5°C cooling of average temperatures occurred in a small region around Bursa with the conversion of the sparsely vegetated areas into forest areas.

In general, precipitation increase was detected over urban areas and over the areas where land cover changed from sparsely vegetated to deciduous forest. Precipitation decrease was detected over Thrace Region with the increase of crop areas. Average 10 m wind difference for 1975 and 2005 land cover data runs in June-August period displayed bigger differences where land cover changed from crop to urban and sparsely vegetated to deciduous forest. Urbanization decreased the wind magnitude over the city and surrounding areas.

Time series of minimum, maximum and average temperatures and average temperature differences indicated that there is a significant warming trend in the Marmara Region. Relationship between climate parameters and land cover change denoted that temperatures are more sensitive to local climate changes. Wind patterns also changed as a result of land cover changes especially with urbanization. Precipitation changes were heterogeneous.

The results of this research suggested that Landsat derived land cover data can be used as an alternative land cover source in regional climate modeling. Digital image processing and geostatistical techniques that should be conducted to derive land cover map from Landsat images were presented. Also, archieve Landsat images can be used to reconstruct past land cover. It is possible to create land cover data for 1970s and determine land cover change for 30-35 year period and its impact on climate using Landsat images.

Creation of a meteorological database from meteorological station data reduced data redundancy, maintained data consistency, lead reasonable organization of data and ensured the identification of complex relation among the data. Since it is not an easy task to handle, retrieve and query these sizes of data, a meteorological database was created and data were structurally organized. Usage of the created database facilitated data retrieval, query analysis and incorporation of data to GIS.

A Geographic Information System (GIS), including the data from several sources, such as climate simulation results, land cover maps derived from remotely sensed data, meteorological data and other ancillary data (digital elevation models, soil maps, demographic data etc.) was used to evaluate the relationships between these different data sets, analyze the different sources of data simultaneously and determine the impacts of land cover change on climate. Buffer zone analysis within the system introduced the land cover change impact on climate in detail. This integrated framework might be a base for multidisciplinary applications and support the decision-making mechanisms.

Urbanization and industrialization have resulted in modification of local city climates. I concluded that the results presented in this work are evidence that land cover change has impacted the local climate of the Marmara Region. Summer time 2m air temperatures, direction and magnitude of winds and amount of precipitation impacted as a result of land cover change within the region. Climatic parameters and their variations with the land cover change should be considered for the future land use planning of the Marmara Region.

I conclude that;

- Model land cover data is not up-to-date and accurate for some land cover types especially for urban and forest areas,
- Remote sensing and GIS technology can be used to create new land cover data sets for past and present. Accurate geometric correction of satellite images and selection of common coordinate system for each data set is a prerequiste to conduct precise land cover change quantification, collect different source of data in GIS and introduce land cover data to regional climate modeling system,
- Landsat images can be succefully used to create improved land cover data for regional climate modeling, these new land cover data improved the climate simulation results especially for minimum, maximum and average temperatures and emphasized the importance of accurate land cover for regional climate modeling,
- Surface roughness and albedo are represeted better with new land cover data which leads change in the Bowen ratio, and therefore partitioning of latent

and sensible heat flux, and better simulation results for temperature and wind patterns,

- The results of this work are evidence that anthropogenic land cover change has impacted several aspects of the regional climate of the Marmara Region, including warming of 2m air temperatures and the strength and orientation of the sea breezes. Urbanization increase in Istanbul, Bursa and Adapazarı resulted in statistically significant changes in urban climatology of the region. Changes in temperature and wind patterns due to land cover changes depend on the type of land cover conversion. The perturbations introduced to the climate system through anthropogenic land cover change are physically and socioeconomically significant.
- Land surface is an important part of the climate system and must be represented correctly. Misrepresentations in land cover data will lead to poor simulation of current climate. Moreover, to find out land cover change impact on climate both past and present land cover must be created accurately. Without complete knowledge of past and present land cover it is not possible to correctly simulate land cover change impact on climate. Also, predicting future climate changes as a result of future land cover activities require accurate representation of past and present land cover data. Usage of remote sensing and GIS technologies accommodate better understanding of atmosphere and land surface interactions.

Suggestions for future studies

Different satellite sensor images and different digital image processing techniques can be used to derive new land cover datasets. Landsat images are alternative source of creating land cover data for finer scales and smaller regions. Since a Landsat frame constitutes 180 km x 180 km area, it is hard to work with many Landsat images if the experiments will be conducted in a country basis. In this case, new generation satellite images with high spectral and moderate spatial resolution like MODIS and MERIS can be used.

New vegetation indices can be derived using satellite images and remote sensing techniques and these products can be implemented into regional climate modeling to investigate if new NDVI data sets can improve the simulation results.

To better assess land cover change effects on hydrological variables like precipitation, a better description of the water table and ground water processes is needed. Usage of a coupled climate model including complete hydrology would be beneficial to derive precise results. Land cover change impact on water resources can be investigated using a coupled climate model.

Different study regions encountered with different types of land cover change can be studied to simulate the impacts of different land cover changes on climate.

Land transformation models and different scenarios can be used to project future land cover data using past and present land cover data. Then, this land cover data can be implemented to a regional climate model to evaluate how local climate might be affected and how large these local effects can be as a result of future land cover activities.

In order to asses how the land atmosphere feedbacks behave in seasonal timeframe, new experiments can be designed to be conducted for longer periods and for different years.

Different initial and boundary condition data like ECMWF can be used to find out the sensitivity of simulations to initial and boundary conditions and if this new data can improve the results.

REFERENCES

Adler, R.F., G.J. Huffman, A. Chang, R. Ferraro, P. Xie, J. Janowiak, B. Rudolf, U. Schneider, S. Curtis, D. Bolvin, A. Gruber, J. Susskind, and P. Arkin, 2003. The Version 2 Global Precipitation Climatology Project (GPCP) Monthly Precipitation Analysis (1979-Present). *J. Hydrometeorology*, **4,** 1147-1167.

Armstrong, M., 1998. Basic Linear Geostatistics. Springer. Germany.

Baidya Roy, S., G.C. Hurtt, C.P. Weaver, and S.W. Pacala, 2003. Impact of historical land-use/land-cover change on the July climate of the United States. *Journal of Geophysical Research,* **108**, 4793, doi:10.1029/2003JD003565.

Belward, A.S., 1996, The IGBP-DIS global 1 km land cover data set (DISCover)-proposal and implementation plans: IGBP-DIS Working Paper No. 13, Toulouse, France, 61 p.

Bolle, H. J., 1991. Land surface transformation processes, Report of the Earth Observation User Consultation Meeting, The Netherlands, 1143, 181-192.

Bozkurt, D., Sen, O.L, 2007. Sensitivity of Turkish precipitation to sea surface temperature variability in the surrounding seas. European Geosciences Union General Assembly 2007, Vienna, Austria, 15 – 20 April 2007.

Brivio, P. A. , Colombo, R., Maggi, M. ve Tomasoni, R., 2002. Integration of remote sensing data and GIS for accurate mapping of flooded areas, *International Journal of Remote Sensing*, **23 (3),** 429–441.

Campbell, J. B., 1996. Introduction to Remote Sensing (2nd ed.). Taylor and Francis. London.

Canters, F., 1997. Evaluating the uncertainty of area estimates derived from fuzzy land-cover classification, *Photogrammetric Engineering and Remote Sensing,* **63,** 403–414.

Chen, F., and J. Dudhia, 2001. Coupling an advanced land-surface/ hydrology model with the Penn State/ NCAR MM5 modeling system. Part I: Model description and implementation. *Monthly Weather Review*, **129,** 569–585.

Climate Change and A Global City: An Assessment of The Metropolitan East Coast Region web page, November 2005, http://Metroeast_Climate.Ciesin.Columbia.Edu/İndex.Html

Congalton, R. G., and Green, K., 1999. Assessing the accuracy of remotely sensed data: principles and practices. Boca Raton: Lewis Publishers.

Cosgrove, Brian A., Dag Lohmann, Kenneth E. Mitchell, Paul R. Houser, Eric F. Wood, John Schaake, Alan Robock, Curtis Marshall, Justin Sheffield, Lifeng Luo, Qingyun Duan, Rachel T. Pinker, J. Dan Tarpley, R. Wayne Higgins, and Jesse Meng, 2003. Realtime and retrospective forcing in the North American Land Data Assimilation Systems (NLDAS) project. *J. Geophys. Res.,* **108 (D22),** 8842, doi:10.1029/2002JD003118.

Cosgrove, Brian A., Dag Lohmann, Kenneth E. Mitchell, Paul R. Houser, Eric F. Wood, John C. Schaake, Alan Robock, Justin Sheffield, Qingyun Duan, Lifeng Luo, R. Wayne Higgins, Rachel T. Pinker, and J. Dan Tarpley, 2003: Land surface model spinup behavior in the North American Land Data Assimilation System (NLDAS). *J. Geophys. Res.*, **108 (D22)**, 8845, doi:10.1029/2002JD003119.

Cotton, W., R. and Pielke, R., A.,1995. Human Impacts on Weather and Climate, Cambridge University Press, U.S.A.

Curran, P. J., and Atkinson, P. M., 1998. Geostatistics and remote sensing, *Progress in Physical Geography*, **22**, 1, 61-78.

Curran, P. J., 1988. The semi-variogram in remote sensing: an introduction. *Remote Sensing of Environment,* **24,** 493-507.

Demirel, H., Sertel, E., Kaya, S., and Seker,D. Z., 2007. Exploring impacts of road transportation on environment: A spatial approach, *Desalination,* (in press).

Dickinson, R.E., Henderson-Sellers, A., Kennedy, P.J., and Wilson, M.F., 1986, Biosphere-atmosphere transfer scheme (BATS) for the NCAR community climate model: NCAR Technical Note NCAR/TN275+STR, Boulder, CO. 69 .

Dingman, S. L, 2002. Physical Hydrology, Orentice Hall, New Jersey, USA.

Ek, M. B., K. E. Mitchell, Y. Lin, E. Rogers, P. Grummann, V. Koren, G. Gayno, and J. D. Tarpley, Ekstrand, S., 1994. Assessment of forest damage with Landsat TM: correction for varying forest stand characteristics. *Remote Sens. Environ.,* **47,** 291–302.

Erinç, S., 1996. Klimatoloji ve Metodları, Alfa Basım, İstanbul.

Ezber, Y., Sen,O,L, Kindap, T and Karaca, M, 2007. Climatic effects of urbanization in İstanbul: a statistical and modeling analysis, *Int. J. Climatol.*, **27**,667–679.

Fan, Y., Miguez-Macho, G., Weaver, C., Walko, R. And Robock, A., 2007. Incorporating water table dynamics in climate modeling: 1. Water table observations and the equilibrium water table. *J. Geophys. Res.*, **112**, D10125, doi:10.1029/2006JD008111.

Foody, **G.M.,** 2002. Status of land cover classification accuracy assessment, *Remote Sensing of Environment,* **80,** 185–201.

Friedl, M. A., McIver, D.K., Hodges, J.C.F., Zhang, X.Y., Muchoney, D., Strahler, A.H., Woodcock, C. E., Gopal, S., Schneider, A., Cooper, A., Baccini, A., Gao, A., Schaaf, C., 2002. Global land cover mapping from MODIS: Algorithms and early results, *Remote Sens. Environ.*, **83,** 287– 302.

Ge, J., J. Qi, B. M. Lofgren, N. Moore, N. Torbick, and J. M. Olson, 2007. Impacts of land use/cover classification accuracy on regional climate simulations, *Journal Geophysical Research*, **112**, D05107, doi:10.1029/2006JD007404.

Goovaerts, P., 1999. Geostatistics in soil science: state-of-the-art and perspectives, *Geoderma*, **89,** 1–45.

Hall, F. G. and Badhwar, G. D.,1987. Signature-Extendable Technology: Global Space-Based Crop Recognition, *IEEE Transactions on Geoscience and Remote Sensing*, **25,** 93-103.

Hall, F., G., Townshed, J. R. and Engman, E. T., 1995. Status of Remote Sensing Algorithms for Estimation of Land Surface State Parameters, *Remote Sensing of Environment*, **51**, 138-156.

Hansen, M., R. DeFries, J.R.G. Townshend, and R. Sohlberg, 2000. Global land cover classification at 1km resolution using a decision tree classifier, *International Journal of Remote Sensing,* **21,** 1331-1365.

Hartmann, D. L., 1994. Global Physical Climatology, Academic Press, USA.

Howard, L., 1833. The Climate of London, Vols. I– III. London: Harvey And Dorton.

Huffman, G.J., R.F. Adler, M. Morrissey, D.T. Bolvin, S. Curtis, R. Joyce, B McGavock, J. Susskind, 2001: Global Precipitation at One-Degree Daily Resolution from Multi-Satellite Observations. *J. Hydrometeor.*, **2**, 36-50.

IPCC, 1996b. Climate Change 1995, Impacts, Adaptations and mitigation of Climate Change: Scientific-Technical Analyses. Contribution of Working Group II to the Second Assessment Report of the Intergovernmental Panel on Climate Change, Watson R, T., *et al*., Eds., WMO/UNEP. Cambridge University Press, New York.

IPCC, 2001. Climate Change 2001: The Scientific Basis. Contribution of Working Group I to the Third Assessment Report of the Intergovernmental Panel on Climate Change [Houghton, J.T.,Y. Ding, D.J. Griggs, M. Noguer, P.J. van der Linden, X. Dai, K. Maskell, and C.A. Johnson (eds.)]. Cambridge University Press, Cambridge, United Kingdom and New York, NY, USA, 881pp.

IPCC, 2007. Climate Change 2007, The Physical Science Basis, Contribution of Working Group I to the Fourth Assessment Report of the

Intergovernmental Panel on Climate Change [Edt. Solomon, S., Qin, M., Manning, M., Marquis, M., Averyt, K., Tignor, M. M. B., Miller, H. L., chen, Z.]

Jensen, J. R., 1996. Introductory Digital Image Processing, A Remote Sensing Perspective, Prentice-Hall, Englewood Cliffs, NJ.

Jin, M. and Shepherd, J., M., 2005. Inclusion of Urban Landscape in Climate Model. How Can Satellite Data Help?, American Meteorological Society, 681-689.

Kanamitsu, M., Ebisuzaki, W., Woollen, J., Yang, S-K, Hnilo, J.J., Fiorino, M. and Potter, G. L. , 2002. NCEP-DEO AMIP-II Reanalysis (R-2), *Bul. of the Atmos. Met. Soc.,*1631-1643,

Karaca M, Tayanc M, Toros H.,1995a. The effects of urbanization on climate of İstanbul and Ankara: a first study. *Atmospheric Environment Part B-Urban Atmosphere,* **29**, 3411–3421.

Karaca M, Anteplioglu U, Karsan H., 1995b. Detection of urban heat island in İstanbul, Turkey. *Il Nuovo Cimento*, **18,** 19-55.

Karaca, M., Deniz, A. and Tayanc, M., 2000. Cyclone track variability over turkey in association with regional climate, *Int. J. Climatol*., **20,** 1225–1236

Kato, S. and Yamaguchi, Y., 2005. Analysis of Urban Heat Island effect using ASTER and ETM+ Data: Separation of anthropogenic heat discharge and natural heat radiation from sensible heat flux, *Remote Sensing of Environment,* **99,** 44 – 54.

Kaya Ş., 2007. Multitemporal Analysis of Rapid Urban Growth in İstanbul Using Remotely Sensing Data*, Environmental Engineering Science*, **24,** 228-233.

Kaya, S. and Curran, P.J., 2006. Monitoring urban growth on the European side of the İstanbul metropolitan area: a case study. *International Journal of Applied Earth Observation and Geoinformation*, **8,** 18-25.

Kaya, S., Sertel, E., Seker, D. Z., and Tanik, A., 2007. Multi-temporal analysis and mapping of coastal erosion caused by open mining areas, *Environmental Forensics*, (in press).

Kaya, Ş., Sertel, E, 2006. Semivariogram Model of Remotely Sensed Data . Uzaktan Algilama-CBS Çaliştay ve Paneli-2006, İstanbul Teknik Universitesi, Eylül 2006.

Koukoulas, S., and Blackburn, G. A., 2001. Introducing new indices for accuracy evaluation of classified images representing semi-natural woodland environments. *Photogrammetric Engineering and Remote Sensing*, **67,** 499– 510.

Landsat program web page, June 2007. http://landsat.gsfc.nasa.gov/

Lathrop, R. G., 1988. The integration of remote sensing and geographic information systems for Great Lakes water quality monitoring, Ph D Thesis, University of Wisconsin, USA.

Liang, S., 2004. Quantitative Remote Sensing of Land Surfaces, John Wiley and Sons, New Jersey, USA.

Liang, S., 2001. Atmospheric Correction of Landsat ETM+ Land Surface Imagery—Part I: Methods, *IEEE Transactions On Geoscience And Remote Sensing,* **39 (11).**

Loveland, T.R., Reed, B.C., Brown, J.F., Ohlen, D.O., Zhu, J, Yang, L., and Merchant, J.W., 2000. Development of a Global Land Cover Characteristics Database and IGBP DISCover from 1-km AVHRR Data: *International Journal of Remote Sensing* , **21,** 1303-1330.

Matthews, E., 1983. Global vegetation and land use: New high resolution data bases for climate studies, *J. Clim. Appl. Meteorol*., **22,** 474–487.

McGuffie, K., and Henderson-Sellers, A., 2001. Forty Years of Numerical Climate Modelling, *International Journal of Climatology*, **21**, 1067-1109.

Miguez-Macho, G., Fan, Y., Weaver, C., Walko, R., and Robock, A., 2007. Incorporating water table dynamics in climate modeling: 2. Formulation, validation, and soil moisture simulation. *J. Geophys. Res.*, **112**, D13108, doi:10.1029/2006JD008112.

Miguez-Macho, G., Stenchikov, G. L., and Robock, A., 2005. Regional climate simulations over North America: Interaction of local processes with improved large-scale flow. *J. Climate*, **18**, 1227-1246

Miguez-Macho, G., Stenchikov, G. L., and Robock, A., 2004. Spectral nudging to eliminate the effects of domain position and geometry in regional climate model simulations. *J. Geophys. Res*., **109**, D13104, doi:10.1029/2003JD004495.

Miller, A., Thompson, J. C., Peterson, R. E, 1983. Elements of Meteorology, Merrill Pub Co; 4th edition.

Min, s., Legutke, S., Hense, A., Cubasch, U., Kwon, W., Oh, J. and schlese, U., 2006**.** East Asian climate change in the 21st century as simulated by the coupled climate model ECHO-G under IPCC SRES scenarios, *Journal of the Meteorological Society of Japan,* **84,** 1-26

Mitchell, K and Ek, M., 2006. A Description and Example Output of the WRF-NMM land surface and radiation packages used at NCEP, WRF-NMM Tutorial, 8-11 August 2006, Boulder, CO.

Musaoglu, N., Seker, D.Z., Kabdasli, S., Kaya, S. and Duran, Z., 2004. Using remote sensing and GIS for the assessment of visual attributes; case study of the south coastal zone of Turkey. *Fresenius Environmental Bulletin*, **13,** 854-859.

Ninyerola, M., Pons, X. ve Roure, M. J., 2000. A Methodological Approach of Climatological Modelling of Air Temprature And Precipitation Through GIS Techniques, *International Journal Of Climatology*, **20**, 1823-1841.

Oke, T.R., 1982. The energetic basis of urban heat island. *Journal of the Royal Meteorological Society,* **108**, 1-24.

Okyar, Z. and Aktaç, N., 1999. Trakya B.lgesi Geometridae T.rlerinin Taksonomik ve Faunistik Yonden Arastirilmasi. *Tr. J. of Zoology*. **23,** 99-132.

Ostır, K., Veljanovskı, T., Podobnıkar, T. and Stancıc, Z., 2002. Application of Satellite Remote Sensing in Natural Hazard Management: The Mount Mangart Landslide Case Study, *International Journal Of Remote Sensing*, **24 (20),** 3983–4002.

Olson, J.S., 1994a, Global ecosystem framework-definitions: USGS EROS Data Center Internal Report, Sioux Falls, SD, 37 p.

Olson, J.S., 1994b, Global ecosystem framework-translation strategy: USGS EROS Data Center Internal Report, Sioux Falls, SD, 39 p.

Örmeci, C.,1987. Uzaktan Algılama (Temel Esaslar Ve Algılama Sistemleri), İ.T.Ü Matbaası, İstanbul.

Ormeci, C., Ekercin, S., 2007. An assessment of water reserve change in the Salt Lake, Turkey through multitemporal Landsat imagery and real-time ground surveys. *Hydrological Processes*, **21**, 1424-1435, DOI: 10.1002/hyp.6355

Pennsylvania State University / National Center for Atmospheric Research numerical model web page, May 2006. http://www.mmm.ucar.edu/mm5/

Pielke, R. A., 2001. Influence of the Spatial Distribution of Vegetation and Soils on the Prediction of Vegetation and Soils on the Prediction of Cumulus Connective Rainfall, *Rev. Geophys* , **39,** 151-177.

Pielke, R. A., Sr., Adegoke, J., Beltran-Przekurat, A., Hiemstra, C. A., Lin, J., Nair, U. S., Niyogi, D., and Nobis, T. E, 2007. An overview of regional land-use and land-cover impacts on rainfall, *Tellus,* **59B,** 587–590.

Pielke, R. A., Sr., R. L. Walko, L. T. Steyaert, P. L. Vidale, G. E. Liston, W. A. Lyons, and T. N. Chase, 1999. The influence of anthropogenic landscape changes on weather in south Florida, *Mon. Weather Rev.,* **127,** 1663–1673.

Piper, S. E., 1983. The evaluation of the spatial accuracy of computer classification. In: Proceedings of the 1983 Machine Processing of Remotely Sensed Data Symposium (pp. 303 – 310). West Lafayette: Purdue University.

Pitman, A. J., 2003. The Evolution of, and Revolution in, Land Surface Schemes Designed for Climate Models, *International Journal of Climatology*, **23,** 479-510.

Potter, C. S. ve Brooks, V., 1998. Global Analysis of emprical Relations Between Annual Climate Andseasonality of NDVI, *International Journal of Remote Sensing*, **19**, 2921-2948.

Quattrochi, D., Luvall, J., Rickman, D., Estes, M., Laymon, C., Howell, B., 2000. A decision support information system for urban landscape management using thermal infrared data. *Photogrammetric Engineering and Remote Sensing*, **66,** 1195-1207.

Reynolds, R. W. and T. M. Smith, 1994. Improved global sea surface temperature analyses using optimum interpolation. *J. Climate*, **7,** 929-948.

Richardson, L. F., 1922. Weather Prediction by Numerical Process, Cambridge University Press: Cambridge.

Robock, A., 1985: An updated climate feedback diagram. *Bull. Amer. Met. Soc.*, **66**, 786-787.

Robock, A., Konstantin Y. Vinnikov, Govindarajalu Srinivasan, Jared K. Entin, Steven E. Hollinger, Nina A. Speranskaya, Suxia Liu, and A. Namkhai, 2000. The Global Soil Moisture Data Bank. *Bull. Amer. Meteorol. Soc.*, **81,** 1281-1299.

Robock, A., Lifeng Luo, Eric F. Wood, Fenghua Wen, Kenneth E. Mitchell, Paul R. Houser, John C. Schaake, Dag Lohmann, Brian Cosgrove, Justin Sheffield, Qingyun Duan, R. Wayne Higgins, Rachel T. Pinker, J. Dan Tarpley, Jeffrey B. Basara, and Kenneth C. Crawford, 2003, Evaluation of the North American Land Data Assimilation System over the Southern Great Plains during the warm season. *J. Geophys. Res.*, **108 (D22)**, 8846, doi:10.1029/ 2002JD003245.

Robock, A., 2007, Physical Climatology Lecture Notes, http://www.envsci.rutgers.edu/~robock/.

Robinson, P. J. and Henderson-Sellers, A, 1999. Contemporary Climatology,Pearson, Malaysia.

Roy, S. S., Mahmood, R., Niyogi, d., lei, M., Foster, S., Hubbard, K., Douglas, e. and Pielke, R., 2007. Impacts of the agricultural Green Revolution–induced land use changes on air temperatures in India, *Journal Of Geophysical Research,* **112**, D21108, doi:10.1029/2007JD008834.

Running, S.W., Loveland, T.R., and Pierce, L.L., 1994. A Vegetation Classification Logic Based on Remote Sensing for Use in Global Biogeochemical Models, *Ambio* , **23**, 77-81.

Saroğlu, E., 2004. Farklı Çözünürlükteki Uydu Görüntülerinin Geometrik Dönüşümü ve Dönüşüm Sonucunda Elde Edilen Görüntülerin Dış Doğruluğunun Araştırılması. *Yüksek Lisans Tezi*, İTÜ Fen Bilimleri Enstitüsü, İstanbul

Saroglu, E., Kaya, S., and Ormeci, C., 2005. Analysis of geometric accuracy of Landsat 5 TM and IRS 1D data by means of DGPS and Map data. 25th EARSeL (European Association of Remote Sensing Laboratories) Symposium. Global Developments in Environmental Earth Observation from Space. 6-11 June, 2005, Porto, Portugal.

Saroglu, **E., Yasa, F., Akcay, O., Abali, H., and Musaoglu, N.**, 2003. Coastal and erosion risk analysis using remote sensing and GIS: A case study in Sile and Agva towns.Proceedings , 23th Earsel Conference, Remote Sensing in Transition, 2-5 June, Belgium. p.p.349-352.

Schroeder, T. A., Cohen, W. B., Song, C., Canty, M. J. and Yang , Z., 2006. Radiometric correction of multi-temporal Landsat data for characterization of early successional forest patterns in western Oregon. *Remote Sensing of Environment*, **103,** 16-26

Schweiger, E. W., Bolgrien, D. W., Angradi, T. R. ve Kelly, J., R. 2005. Environmental Monitoring and Assessment of A Great River Ecosystem: The Upper Missouri River Pilot. *Environmental Monitoring and Assessment*, **103**, 21–40.

Seker, D.Z., Goksel, C., Kabdasli, S., Musaoglu, N., Kaya, S., 2003. Investigation of coastal morphological changes due to river basin characteristics by means of remote sensing and GIS techniques, *Water Science and Technology*, **48,** 135-142.

Seker, D.Z., Kaya, S., Kabdasli, S., Musaoglu, N., Yuasa, A. and Duran, Z., 2005. Investigation of meandering in filyos river by means of satellite sensor data. *Hydrological Process,* **19,** 1497-.1508.

Sellers, P. J., Los, O., L., Tucker, C. J., Justice, C. O., Dazlich, D., A., Collatz, G. J. ve Randall, D. A., 1996. A Revised Land Surface Parameterization (Sib2) for Atmospheric Gcms. Part II: The Generation of Global Fields of Terrestrial Biophysical Parameters From Satellite Data. *Journal of Climate*, **9,** 706-737.

Sellers, P. J., ve Schimel, D., 1993. Remote Sensing of the Land Biosphere And Biogeochemistry in the EOS Ers: Science Priorities, Methods and İmplimentation- EOS Land Biosphere and Biogeochemical Cycles Panels, *Global and Planetery Change,* **7,** 279-297.

Sellers, P. J., D. A. Randall, G. J. Collatz, J. A. Berry, C. B. Field, D. A. Dazlich, C. Zhang, G. D. Collelo, and L. Bounoua, 1996a. A revised land surface parameterization (SiB2) for atmospheric GCMs. part 1: Model formulation, *Journal of Climate,* **9,** 676– 705.

Sellers, P. J., S. O. Los, C. J. Tucker, C. O. Justice, D. A. Dazlich, G. J. Collatz, and D. A. Randall, 1996b. A revised land surface parameterization (SiB2) for atmospheric GCMs. part 2: The generation of global fields of terrestrial biophysical parameters from satellite data*, Journal of Climate,* **9,** 706– 737.

Sellers, P.J., Mintz, Y., Sud, Y.C., and Dalcher A., 1986, A simple biosphere model (SiB) for use within general circulation models: *Journal of Atmospheric Science* , **43,** 505-531

Seker, D.Z., Tanik, A., Gurel, M., Ekdal, A., Erturk, A., Kabdasli, S., Aydingakko, A., 2004. An Overview of Integrated and Interdisciplinary Studies on Conservation of a Lagoon System in Turkey, Management of Environmental Quality, *An International Journal,* **15,** 364-379.

Sertel, E., Findik, N., Kaya, S., Seker, D. Z., and Samsunlu, A, 2008. Assessment of landscape changes in the Kizilirmak Delta, Turkey using remotely sensed data and GIS, *Environmental Engineering Science*, (in press).

Sertel, E., Kaya, S. and Curran, P. J., 2007. Use of semi-variograms to identify earthquake damage in an urban area, *IEEE Transactions on Geoscience and Remote Sensing*, 45, 6, 1590-1594.

Sertel, E., Kutoglu, S. H., Kaya, S, 2007. Geometric correction accuracy of different satellite sensor images: application of figure condition, *International Journal of Remote Sensing,* DOI: 10.1080/01431160701592452.

Sertel, E, Cigizoglu, H. K., and Sanli, D. U, 2008. Estimating daily mean sea level heights using artificial neural networks, *Journal of Coastal Research,* DOI: 10.2112/06-742.1.

Steinecke K. 1999. Urban climatological studies in the Reykjav´ik subarctic environment, Iceland. *Atmospheric Environment,* **33**, 4157–4162.

Shabanov, N., V., Zhaou, L., Knyazikhin, Y., Myheni, R., B. ve Tucker, C., J., 2002. Analysis of International Chnages in Northern Vegetation Activity Observed in AVHRR Data From 1981 To 1994. *IEEE Transactions on Gescience And Remote Sensing*, **40**, 115-132.

Skamarock, W. C, Klemp, J. P, Dudhia, J, Gill, D. O., Barker, D. M., Wang, W, and Powers, J. 2005. A Description of the Advanced Research WRF Version 2. National Center for Atmospheric Research, Boulder, Colorado, USA

Skole, D. and Tucker, C. J., 1993. Tropical deforestration habitat fragmentation in Theamazon: Satellite data from 1978 to 1988, *Science,* **260,** 1905-1910.

Song, C., Woodcock, C. E., Seto, K. C., Lenney, M. P., and Macomber, S. A., 2001. Classification and change detection Using Landsat TM data: When and how to correct atmospheric effects? *Remote Sensing of Environment***, 75,** 230-244.

Spanner, M. A., Pierce, L. L., Peterson, D. L., and Running, S. W., 1990. Remote sensing of temperate coniferous forest *Vegetation, Modeling and Climatic Change Effects*, *Int. J. Remote Sens.,* **11(1),** 95–111.

Streutker, D., R., 2003.Satellite-Measured growth of the Urban Heat Island of Houston, Texas. *Remote Sensing of Environment*, **85**, 282–289.

Suzukia, R., Tanakab, S. ve Yasunaria, T., 2000. Relationships Between Meridional Profiles of Satellite-Derıved Vegetation Index (NDVI) and

Climate Over Siberia, *International Journal of Climatology,* **20,** 955-967.

Tapper, N. J. 1990. Urban influences on boundary layer temperature and humidity: results from Christchurch, New Zealand. *Atmospheric Environment B* **24**, 19–27.

Tayanc, M., Im, U., Dogruel, M. and Karaca, M. 2007. Climate change in turkey for the last half century, submitted to Climatic Change.

Tayanç, M., Dalfes, N., Karaca, M. and Yenigün, O., 1998. A comparative assessment of different methods for detecting inhomogeneities in Turkish temperature data set, *Int. J. Climatol.*, **18**, 561–578.

Tayanç, M. and Toros, H., 1997. Urbanization effects on regional climate change in the case of four large cities of Turkey, *Climatic Change,* **35,** 501-524.

T. C Basın Yayın ve Enformasyon Genel Müdürlüğü web page, June 2006. http://www.byegm.gov.tr/

Teilet, P. M., 1986. Image correction for radiometric effects in remote sensing, *International Journal of Remote Sensing***, 7:12,** 1637 – 1651.

Unwin DJ. 1980. The synoptic climatology of Birmingham's heat island. *Weather,* **35**, 43–50.

Vitousek, P. M., Money, H., A., Lubchenco, J., ve Melillo, J.,M., 1997. Human Domination of Earth' S Ecosystems, *Science*, **125,** 2401-2426.

Voogta, J.A. ve Oke T.R., 2003. Thermal Remote Sensing of Urban Climates. *Remote Sensing of Environment*, **86,** 370–384.

Walko, R. L., et al., 2000. Coupled atmosphere-biophysics-hydrology models for environmental modeling, *J. Appl. Meteorol.,* **39,** 931–944.

Wang, W, Barker, D, Bray, J., Bruyere, C., Duda, M., Dudhia, J., Michalakes, J. and Gill, D. 2006. ARW Version 2 Modeling System User's Guide.

Wang, H., Shi ,W., and Chen ,X.., 2006. The statistical significance test of regional climate change caused by land use and land cover variation in West China, *Advances in Atmospheric Sciences*, 23, 355–364

Washington, W. M. and Parkinson, C. L, 2005. An introduction to three-dimensional climate modeling. Univesity Science Books, USA.

Weaver, C.P., and R. Avissar, 2001. Atmospheric disturbances caused by human modification of the landscape. *Bull. Amer. Meteorol. Soc*., **82,** 269-*281.*

Wichansky, P.S., L.T. Steyaert, R.L. Walko, and C.P. Weaver, 2007. Evaluating the effects of historical land cover change on summertime weather and climate in New Jersey: Part I: Land cover and surface energy budget changes. *J. Geophys. Res.*, in press.

Weng, Q., 2001. Modeling urban growth effects on surface runoff with the integration of remote sensing and GIS. Environmental Management, **28,** 737-.

Woodcock, C. E., Strahler, A. H., and Jupp, D. L. B., 1988. The use of semi-variograms in remote sensing I: Scene models and simulated images. *Remote Sensing of Environment,* **25,** 323-348.

- **Elif SERTEL**

Department of Environmental Sciences
Rutgers University
14 College Farm Road
New Brunswick, NJ 08901-8551

Phone: (732) 425-1127
E-mail: esertel@envsci.rutgers.edu
WWW: http://envsci.rutgers.edu/~esertel

İstanbul Technical University
Civil Engineering Faculty
Remote Sensing Department
34469, Maslak-İstanbul/TURKEY.

Phone: +90(212) 285-6110
E-mail: elifsertel@ins.itu.edu.tr
WWW: http://www.ins.itu.edu.tr/esertel

- ***Education***

B.A. in Geodesy and Photogrammetry Engineering, 2002
İstanbul Technical University, Turkey

M.Sc. in Geomatic Engineering, 2004
İstanbul Technical University, Turkey
Thesis: Accuracy assesment for rectification of multisensor satellite images
Advisor: Prof. Cankut Ormeci

Ph.D. in Geomatic Engineering, 2008
İstanbul Technical University, Turkey
Thesis: Investigation of land cover change impact on climate
Advisor: Prof. Cankut Ormeci

- ***Professional Work Experience***

08.2006-	Rutgers University Department of Environmental Sciences Visiting Fulbright Researcher
10.2002-	İstanbul Technical University Geodesy and Photogrammetry Department Remote Sensing Division Research and Teaching Assistant

- ***Grants and Awards***

Fulbright Ph.D. Scholarship (2006-2008)

Rutgers University, Deparment of Environmental Sciences, NSF project scholar (June 2007-June 2008)

NSF Grant to attend Detecting the Atmospheric Response to the Changing Face of the Earth: A Focus on Human-Caused Regional Climate Forcings, Land-Cover/Land-Use Change, and Data Monitoring Workshop (August 2007).

National Center for Atmospheric Research (NCAR) , Access to Computing Resources. Investigation the impacts of land cover change on climate. Lead User (2006-2008).

TUBITAK (The Scientific & Research Council of Turkey) National Ph. D. Scholarship (2005-2008)

The first student among the 2002 Geodesy and Photogrammetry Engineering graduates, June 2002, given by İstanbul Technical University Rectorate.

Rize Foundation (Rize Vakfı) Undergraduate Scholarship (2000-2001)

Refereed Journal Articles

E. Sertel, S. Kaya, P. J. Curran, 2007. Use of semi-variograms to identify earthquake damage in an urban area, *IEEE Transactions on Geoscience and Remote Sensing*, 45, 6, 1590-1594.

E. Sertel, S. H. Kutoglu, S. Kaya. Geometric correction accuracy of different satellite sensor images: application of figure condition, *International Journal of Remote Sensing,* 28, 20, 4685 – 4692, DOI: 10.1080/01431160701592452.

E.Sertel, H. K. Cigizoglu and D. U. Sanli, 2007. Estimating daily mean sea level heights using artificial neural networks, *Journal of Coastal Research,* DOI: 10.2112/06-742.1.

H. Demirel, **E. Sertel**, S. Kaya, and D.Z. Seker**,** 2008**.** Exploring impacts of road transportation on environment: A spatial approach, *Desalination,* 226, 279-288.

S. Kaya, **E. Sertel**, D. Z. Seker, and A. Tanik, 2008. Multi-temporal analysis and mapping of coastal erosion caused by open mining areas, *Environmental Forensics*, (in press).

E. Sertel, N. Findik, S. Kaya, D. Z. Seker and A. Samsunlu. Assessment of landscape changes in the Kizilirmak Delta, Turkey using remotely sensed data and GIS, *Environmental Engineering Science*, (in press, March 2008).

C. Ormeci, **E. Sertel**, O. Sarikaya. Determination of Chlorophyll-A Amount in Golden Horn, İstanbul, Turkey Using Ikonos and In Situ Data, submitted to Water Reseach.

Presentations

E. Sertel and A. Robock. Regional Climate Modeling over the Marmara Region, Turkey, with Improved Land Cover Data, AGU Fall Meeting, 10–14 December 2007, San Francisco, CA, USA.

E. Sertel and A. Robock. Introducing land cover data into a climate model, Detecting the Atmospheric Response to the Changing Face of the Earth: A Focus on Human-Caused Regional Climate Forcings, Land-Cover/Land-Use Change, and Data Monitoring, 27-29 August 2007, Boulder, CO, USA.

E. Sertel, S. Kaya, P.J. Curran. The use of geostatistical methods to identify severe earthquake damage in an urban area, Urban Remote Sensing Joint Event 2007, 11-13 April 2007, Paris, France (Invited).

E. Saroglu, S. Kaya & C. Ormeci, 2005. Analysis of geometric accuracy of Landsat 5 TM and IRS 1D data by means of DGPS and Map data. 25th EARSeL Symposium. Global Developments in Environmental Earth Observation from Space. 6-11 June, 2005, Porto, Portugal.

S. Kaya, F. Bektas, C. Goksel & **E. Saroglu,** 2004. Analyses of Izmit Earthquake by Means of Remotely Sensed Data: A Case Study, Yalova City, ECPPM 2004, e-work and ebusiness in Architecture, 8–10 September 2004, İstanbul, Turkey.

E. Saroglu, F.Bektas, N. Musaoglu & C. Göksel, 2004. Fusion of multisensor remote sensing data: assessing the quality of resulting images. International Society for Photogrammetry and Remote Sensing XX. Congress, 15-23 July, İstanbulInternational Society for Photogrammetry and Remote Sensing (ISPRS) XX. Congress, 15-23 July, İstanbul.

Other Publications

E. Sertel, H. Demirel and S. Kaya. Predictive Mapping of Air Pollutants: A GIS framework, 5th International Symposium on Spatial Data Quality, 13-15 June 2007, Enschede, The Netherlands.

E. Sertel, S. Kaya, P.J. Curran. The use of geostatistical methods to identify severe earthquake damage in an urban area, Urban Remote Sensing Joint Event 2007, 11-13 April 2007, Paris, France.

F. Bektas Balcik and **E. Sertel**, Wavelet-based image fusion of Landsat ETM images: A case study for different landscape categories of İstanbul. Conference on Information Extraction from SAR and Optical Data, with Emphasis on Developing Countries, 16-18 May 2007, İstanbul, Turkey.

E. Sertel, H. Demirel, S.Kaya, 2007. Geostatistical Approach for Sapatial Analysis, Türkiye Ulusal Fotogrametri ve Uzaktan Algilama Birliği IV. Sempozyumu, 5-7 Haziran 2007, İstanbul Teknik Üniversitesi, İstanbul (in Turkish).

Ş. Kaya, **E. Sertel**, 2006. Semivariogram Model of Remotely Sensed Data . Uzaktan Algilama-CBS Çaliştay ve Paneli-2006, İstanbul Teknik Universitesi, İstanbul (in Turkish).

N. Musaoglu, C. Goksel, **E. Saroglu,** F. Bektas Balcik, 2005. Evaluating Urban Expansion in Asian Part of İstanbul by Using Multitemporal Satellite Image Data, 3rd International Conference on Ecological Protection of the Planet Earth. 10-11June 2005, İstanbul, Turkey.

E. Saroglu, F. Bektas, A.O. Dogru, C. Ormeci, N. Musaoglu, S. Kaya, 2005. Environmental Impact Analyses of Quarries Located on the Asian Side of İstanbul Using Remotely Sensed Data. XXIInd International Cartographic Conference, 9-16 July, A Coruna, Spain (CD ROM).

E. Saroglu, S. Kaya & C. Ormeci, 2005. Analysis of geometric accuracy of Landsat 5 TM and IRS 1D data by means of DGPS and Map data. Global Developments in Environmental Earth Observation from Space, Millpress,

N. Musaoglu, **E. Saroglu,** F. Bektas, C. Goksel, S. Kaya, 2006**.** Assesment of forest degradation by means of remotely sensed data, Global Developments in Environmental Earth Observation from Space, Millpress, 413-418.

F. Bektas Balcik,, **E. Saroglu,** C. Goksel, N. Musaoglu, 2006. High resolution mapping land cover classification of the Elmali water basin, Global Developments in Environmental Earth Observation from Space, Millpress, 437-441.

S. Kaya, **E. Saroglu ,** N. Musaoglu, 2006**.** Analyses of earthquake induced damage in urban areas by means of remotely sensed data, Global Developments in Environmental Earth Observation from Space, Millpress, 207-213.

E. Saroglu, S. Kaya, 2005. Determination of the earthquake induced heavy damages using remotely sensed data and semivariograms, Modern Methods in Science Symposium, 16-18 November, Kocaeli, Turkey (in Turkish).

E. Saroglu, S. Kaya & C. Ormeci, 2005. Geometric transformation of multisensor remotely sensed data, 10th Map Meeting, 28 March-1 April, Ankara, Turkey.(in Turkish)

E. Saroglu, 2004, Rectification and outer accuracy analysis of remotely sensed data which have different spatial resolutions, Master Thesis, ITU Institute of Science and Technology, İstanbul.

E. Saroglu, F.Bektas, N. Musaoglu & C. Göksel, 2004. Fusion of multisensor remote sensing data: assessing the quality of resulting images. International Society for Photogrammetry and Remote Sensing XX. Congress, 15-23 July, İstanbul, p.p.575-579.

S. Kaya, F. Bektas, C. Goksel & **E. Saroglu,** 2004. Analyses of Izmit Earthquake by Means of Remotely Sensed Data: A Case Study, Yalova City, ECPPM 2004, e-work and ebusiness in Architecture, Engineering and Construction, Taylor and Francis, Netherlands, p.p.603-608.

M. Coşkun, F. Bektaş & **E. Saroğlu,** 2004. Fuzzy K Means and ISODATA Classification of Landsat ETM+ images, Akıllı Sistemlerde Yenilikler ve Uygulamaları Sempozyumu, 23-25 Haziran, İstanbul. p.p. 183-186. (in Turkish)

N. Musaoglu, Bektas, F., **Saroglu, E.,** Kaya, S. & C. Goksel, Use of Corona, Landsat TM, Spot 5 images to assess 40 years of land use/cover changes in Cavusbasi, 24. EARSeL Symposium 25-27 May 2004, Dubrovnik, Croita, 2004.

E. Saroglu, F. Yasa, O. Akcay, H. Abali & N. Musaoglu, 2003. Coastal and erosion risk analysis using remote sensing and GIS: A case study in Sile and Agva towns.Proceedings , 23th Earsel Conference, Remote Sensing in Transition, 2-5 June, Belgium. p.p.349-